UPPSALA
UNIVERSITET

Digital Comprehensive Summaries of Uppsala Dissertations from the Faculty of Science and Technology 1693

Synchrotron Radiation Studies of Molecular Building Blocks for Functional Materials

TENG ZHANG

ACTA
UNIVERSITATIS
UPSALIENSIS
UPPSALA
2018

ISSN 1651-6214
ISBN 978-91-513-0383-3
urn:nbn:se:uu:diva-354766

Dissertation presented at Uppsala University to be publicly examined in Häggsalen, Ångström Laboratory, Lägerhyddsvägen 1, Uppsala, Friday, 7 September 2018 at 10:15 for the degree of Doctor of Philosophy. The examination will be conducted in English. Faculty examiner: Dr. Albano Cossaro (CNR-IOM Laboratorio TASC, Italy).

Abstract

Zhang, T. 2018. Synchrotron Radiation Studies of Molecular Building Blocks for Functional Materials. *Digital Comprehensive Summaries of Uppsala Dissertations from the Faculty of Science and Technology* 1693. 97 pp. Uppsala: Acta Universitatis Upsaliensis. ISBN 978-91-513-0383-3.

The research on new materials is a primary driving force for progress in human society. One of the most significant research topic nowadays is the development of new functional materials for technological applications, like perovskite implemented in solar cells, and graphene as a representative for the new 2D materials family. It is then crucial to fully understand the functionality of such materials from a fundamental point of view, as a complementary and useful guide to develop/design new devices of improved performance and energy efficiency.

In the thesis, comprehensive characterizations of molecular building blocks used in i) novel energy conversion devices (CoPc, TPA, DPTA and m-MTDATA), and ii) in 2D materials (biphenylene and melamine) have been performed by PhotoElectron Spectroscopy (PES), and Near Edge X-ray Absorption Fine Structure (NEXAFS) spectroscopy carried out at synchrotron radiation facilities, representing effective, powerful light source dedicated to the front-line materials research of great value in both science and industry. PES and NEXAFS spectroscopy, in combination with Density Functional Theory (DFT) calculations have provided a deep understanding of the electronic structure of the investigated systems in relation to their functionality. The investigations always included the combination and comparison between experimental and theoretical results. The studied molecules were characterized as free and adsorbed on surfaces, from the simple building blocks to more complex molecular systems. The characterizations allowed us to identify the electronic structure modifications due to substitutions (Paper III), increasing complexity of the molecules (Paper V), molecule-substrate interactions (Paper I, II, IV, V) and intra-molecular H-bonding interactions (Paper VI).

Keywords: Synchrotron radiation study, Functional materials, Molecular building blocks, Electron donor, 2D material, Gas-phase, Organic thin film, Electronic structure, Molecule-molecule interaction, Molecule-substrate interaction, Photoelectron spectroscopy, PES, XPS, Near edge X-ray absorption fine structure, NEXAFS, X-ray Absorption Spectroscopy, XAS, Au(111), Cu(111), Surface, Interface, Electronic structure, H-bonding, Cobalt phthalocyanine, CoPc, Triphenylamine, TPA, DPTA, m-MTDATA, Melamine, Biphenylene, Carbon nitride, Graphenylene, Density functional theory, DFT

Teng Zhang, Department of Physics and Astronomy, Molecular and Condensed Matter Physics, Box 516, Uppsala University, SE-751 20 Uppsala, Sweden.

ISSN 1651-6214
ISBN 978-91-513-0383-3
urn:nbn:se:uu:diva-354766 (http://urn.kb.se/resolve?urn=urn:nbn:se:uu:diva-354766)

To my family

致我的家人

List of papers

This thesis is based on the following papers, which are referred to in the text by their Roman numerals.

I **Conclusively Addressing the CoPc Electronic Structure: A Joint Gas-Phase and Solid-State Photoemission and Absorption Spectroscopy Study**
Teng Zhang, Iulia E. Brumboiu, Valeria Lanzilotto, Johann Lüder, Cesare Grazioli, Erika Giangrisostomi, Ruslan Ovsyannikov, Yasmine Sassa, Ieva Bidermane, Matija Stupar, Monica de Simone, Marcello Coreno, Barbara Ressel, Maddalena Pedio, Petra Rudolf, Barbara Brena and Carla Pulia
The Journal of Physical Chemistry C, **121**, 27372 (2017)

II **Electronic Structure Investigations of Biphenylene Films**
Roberta Totani, Cesare Grazioli, Teng Zhang, Ieva Bidermane, Johann Lüder, Monica de Simone, Marcello Coreno, Barbara Brena, Luca Lozzi and Carla Pulia
The Journal of Chemical Physics, **146**, 054705 (2017)

III **Lone Pair Delocalization Effect within Electron Donor Molecules: The Case of Triphenylamine (TPA) and Its Thiophene-Analog (DPTA)**
Teng Zhang, Iulia E. Brumboiu, Cesare Grazioli, Ambra Guarnaccio, Marcello Coreno, Monica de Simone, Antonio Santagata, Håkan Rensmo, Barbara Brena, Valeria Lanzilotto and Carla Puglia
Submitted to The Journal of Physical Chemistry C

IV **X-ray Spectroscopy Investigations of TPA/Au(111): Charge Redistribution via Core Excitation?**
Teng Zhang, Iulia E. Brumboiu, Valeria Lanzilotto, Cesare Grazioli, Ambra Guarnaccio, Fredrik Johansson, Klára Ševčíková, Marcello Coreno, Monica de Simone, Antonio Santagata, Barbara Brena, and Carla Puglia
Manuscript

V **Electronic Structure Study of Free and Adsorbed m-MTDATA**
Teng Zhang, Iulia E. Brumboiu, Valeria Lanzilotto, Cesare Grazioli, Ambra Guarnaccio, Fredrik Johansson, Klára Ševčíková, Marcello

Coreno, Monica de Simone, Antonio Santagata, Barbara Brena, and Carla Puglia
Manuscript

VI **Spectroscopic Fingerprints of Carbon Nitride Functional Groups Locked-up in Intermolecular H-bonding Interactions**
Valeria Lanzilotto, Jose Luis Silva, Teng Zhang, Matuš Stredansky, Cesare Grazioli, Konstantin Simonov, Erika Giangrisostomi, Ruslan Ovsyannikov, Monica de Simone, Marcello Coreno, Carlos Moyses Araujo, Barbara Brena and Carla Puglia
Submitted to Chemistry - A European Journal

Reprints were included with the permission from the publishers.

Comments on my own participation

The studies presented in the thesis are the result of collaborations between experimentalists and theoreticians. The research work got contribution from all of the authors, experts either in experiment or theory.

Our experiments were carried out at three synchrotron radiation facilities: ELETTRA (Italy), BESSY II (Germany) and MAX IV (Sweden). The articles presented in the thesis summarize data of several hardworking beamtimes. As known in the field, the data taken at synchrotron radiation facilities are usually result of good teamwork.

I have taken part in all the experimental work, and been the responsible person for performing experiments reported in Papers I, III, IV, V.

Our theoretical calculations have been mainly performed by our collaborators of the Materials Theory Division of our department, Uppsala University, whereas I have contributed with the valence level calculations in Papers III and V.

I have been in charge of the data analysis and manuscript writing for Papers I, III, IV, V, while I have involved in the data treatment and manuscript discussion of Papers II and VI.

Extended bibliography

I also participated in the following project, which are not included in the thesis, as they are falling out of the main scope of the thesis and due to the extent of my contributions.

1. **Low Dose Photoelectron Spectroscopy at BESSY II: Electronic Structure of Matter in Its Native State**
   Erika Giangrisostomi, Ruslan Ovsyannikov, Florian Sorgenfrei, Teng Zhang, Andreas Lindblad, Yasmine Sassa, Ute B. Cappel, Torsten Leitner, Rolf Mitzner, Svante Svensson, Nils Mårtensson and Alexander Föhlisch,
   Journal of Electron Spectroscopy and Related Phenomena, **224**, 68 (2018)

2. **Electronic Properties and Charge Transfer Mechanisms of the Interfaces Between CuPc:C60 Blend Films and Graphene**
   R. Totani, F. Perrozzi, L. D'Ortenzi, F. Bisti, I. Bidermane, T. Zhang, M. Stupar, B. Ressel, P. Lacovig, S. Lizzit, L. Bignardi, S. Santucci, C. Puglia, L. Lozzi
   Manuscript

3. **A Combined Theoretical and Experimental Study of the Valence and Rydberg States of Iodopentafluorobenzene**
   M. H. Palmer, S. V. Hoffmann, N. C. Jones, M. Coreno, M. de Simone, C. Grazioli, K. A. Peterson, A. Baiardi, T. Zhang and M. Biczysko
   The Journal of Chemical Physics, **146**, (17), 174301, 2017

4. **A Combined Theoretical and Experimental Study of the Ionic States of Iodopentafluorobenzene**
   M. H. Palmer, M.Coreno, M. De Simone, S. V. Hoffmann, N. C. Jones, C. Grazioli, K. A. Peterson, A. Baiardi, T. Zhang and M. Biczysko
   The Journal of Chemical Physics, **146**, (8), 084302, 2017

5. **Combined Theoretical and Experimental Study of the Valence, Rydberg and Ionic States of Fluorobenzene**
   M. H. Palmer, T. Ridley, S. V. Hoffmann, N. C. Jones, M.Coreno, M. de Simone, C. Grazioli, T. Zhang, M. Biczysko, A. Baiardi and K. A. Peterson
   The Journal of Chemical Physics, **144** (20), 204305, 2016

6. **Combined Theoretical and Experimental Study of the Valence, Rydberg, and Ionic states of Chlorobenzene**
   M. H. Palmer, T. Ridley, S. V. Hoffmann, N. C. Jones, M. Coreno, M. de Simone, C. Grazioli, T. Zhang, M. Biczysko, A. Baiardi and K. A. Peterson
   The Journal of Chemical Physics, **144**, (12), 124302, 2016

7. **Interpretation of the Photoelectron, Ultraviolet, and Vacuum Ultraviolet Photoabsorption Spectra of Bromobenzene by *ab initio* Configuration Interaction and DFT Computations**
   M. H. Palmer, T. Ridley, S. V. Hoffmann, N. C. Jones, M. Coreno, M. de Simone, C. Grazioli, T. Zhang, M. Biczysko, A. Baiardi and K. A. Peterson
   The Journal of Chemical Physics, **143**, (16), 164303, 2015

Contents

1. Introduction

From ancient era, the development of human society has begun by making tools from natural materials. These are still vital for sustaining human society, for example, oil and gas exploitation for energy purpose, production of high purity monocrystalline silicon for semiconductor device which is extensively demanded in information technology industry, *etc*.

The future world will rely on new developments for energy production and for information technology (IT). We are all aware of the limitation of the existing materials and of the needs of new technology for future energy production and IT. For example, from 2016, many countries, including Norway, United Kingdom, France, Netherlands, India, China, *etc.*, decided to ban passenger vehicles powered by fossil fuel, aiming to reduce pollution and to reduce health risks. The fossil fuel transportations are supposed to be replaced by the electric vehicles. However, the development of electric cars is limited by the battery which still have characteristics (energy density, charge/discharge rate and the lifetime) far below the ideal needed. For this reason, electric transportation media still lack competitiveness compared to standard fossil fuel vehicles. On the other hand, to be truly environmentally friendly, the power to the electric cars should also come from clean energy, produced from renewable energy sources. Despite the clean secondary solar energy like wind and hydropower, a solar cell can convert the solar energy of light directly into electricity, and thus potentially have the highest energy utilization rate. However, in 2015, the energy produced by the photovoltaics represented only 1.05% of total global power generation [1], which is, to a large extent, still limited by the lack of appropriate energy-conversion materials and/or their costs.

The innovation of the IT has also reshaped our society on using and processing large-scale of data and surrounded by more and more smart devices. The ability of data-processing and storage largely depends on the semiconductor industry. Silicon has played a key role in the semiconductor industry since 1940 when Russell Ohl discovered the p-n junction and the photovoltaic effects in silicon. But now, after more than half century of development for improving capacity and performance, the production of silicon-based devices is reaching its limit: in April 2018, TSMC$^{\text{TM}}$ announced high volume production of 7 nm chips. Transistors smaller than 7 nm will experience strong quantum tunnelling effect through the gate oxide layer and interfere with the normal operation of the chips. Then the need of new 2D materials (like graphene) rises, attracting the interest of researchers for the possibilities to design/make faster, smaller, cheaper and more efficient electronic devices.

In the thesis, I focused on the study of the electronic structure of two groups of molecular building blocks implemented in i) energy-conversion materials, namely CoPc, TPA, DPTA and m-MTDATA, and ii) 2D materials, namely biphenylene and melamine. My studies are aimed to understand the functionality of such building blocks from a fundamental point of view, as a complementary and useful guide to develop/design new materials. The characterizations were performed by PhotoElectron Spectroscopy (PES), and Near Edge X-ray Absorption Fine Structure (NEXAFS) spectroscopy carried out at synchrotron radiation facilities, representing effective, powerful light source dedicated to the front-line materials research of great value in both science and industry.

My thesis includes gas-phase and adsorbate studies. Firstly, gas-phase experiments of the molecules were performed. The experimental results were usually compared with results from DFT calculations. Through this approach, we got a detailed and comprehensive description of the electronic structures of the free molecules. The comparison of the results of molecules of increasing complexity enlightened the changes of the electronic structure when passing from the simplest building blocks to the more complex molecules (for example TPA and m-MTDATA).

To optimize the surface/interface property as well as to minimise the size of a device, functional materials are now processed and studied down to the nanoscale. At such scale, the behaviour of a material is often completely different and dominated by the surface and interface properties, with crucial implications when implemented in applications such as heterogeneous catalysis, semiconductor device fabrication, solar cells, fuel cells, and molecular devices built by bottom-up self-assembly processes.

Therefore, as second aspect investigated in my research work, was the interactions between adsorbates and surfaces. Thin films of molecular building blocks and more complex molecules used in energy-conversion and 2D materials, grown in a carefully controlled way, were studied. By comparing the electronic structure characterizations of free molecules and adsorbate samples we could also identify the modifications of the molecular electronic structure due to the interaction with the surface.

About the cover art

The cover art is an illustration by Zilian LIU of the triphenylamine (TPA) molecule studied in the thesis, in a Chinese painting style. It also shows the mechanism affecting the binding energy of the C 1s core level photoemission line of TPA, an important result described in Paper III of the thesis, presented in an artistic way.

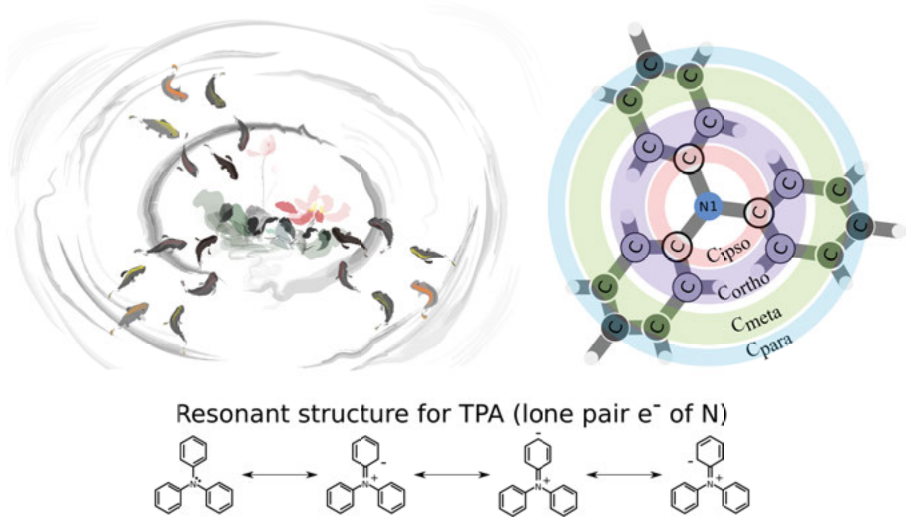

Figure 1.1. The cover art: an illustration of the TPA molecule, presenting the chemically non-equivalent carbon atoms. It also shows the mechanism affecting the binding energy of the C 1s photoemission line of TPA, namely the electronegativity and lone pair electron delocalization effect of the central nitrogen.

Figure 1.1 helps to understand the painting. In fact, the lotus in the center represents the central nitrogen of the TPA molecule, while the 18 Chinese koi fishes represent the carbon atoms in the three phenyl rings. As can be seen, the fishes are divided into 4 colors: black, light grey, yellow and orange. They can be interpreted as the *ipso*, *ortho*, *meta* and *para* kinds of carbon atoms, respectively, explained by the molecular structure on the right side of Figure 1.1. As will be shown later in the thesis, the C 1s binding energies of these carbons are affected by N atom electronegativity, which increases their binding energy. This is visualised by the fishes swimming towards the lotus. Nevertheless, the delocalization of the lone pair electrons of the N (see the resonant structure for TPA in Figure 1.1) will give especially the *ortho* and *para* atoms extra density of charge and reduce their binding energy. This is displayed by waves spreading only onto the (light grey) (*ortho*) and orange koi fishes (*para*).

2. Molecules and substrates

As mentioned in the previous chapter, the research on new materials is a primary driving force for progress in human society. One of the most significant research topic nowadays is the developing of new functional materials for technological applications like perovskite in solar cells for energy-conversion, and graphene as a representative for the new 2D materials family. It is then crucial to fully understand the functionality of such materials from a fundamental point of view. In this thesis, I concentrate on the characterization of molecular building block molecules used in i) novel energy conversion devices (Section 2.1), and ii) in 2D materials (Section 2.2), for getting a deeper understanding of their functionality/properties.

Then, Section 2.1 is dedicated to the molecular building blocks for energy-conversion materials, namely CoPc, TPA, DPTA, and m-MTDATA.

In Section 2.2 instead, the molecular units for building 2D materials, namely biphenylene and melamine, are introduced. Such molecular building blocks forms 2D network, by bottom-up self-assembly interactions on surfaces. However, it is worth mentioning that the molecules presented here are usually multi-functional: for example, CoPc is also regarded as a good candidate for single-molecule magnets, and melamine has the property to catalyze water splitting. How these molecules are grouped in the thesis is only one of many possible ways.

The electronic structure of the organic thin films prepared by adsorbing these molecules on a solid surface is largely affected by the substrate-adsorbate interaction.

A short introduction of the substrates used in the thesis, *i.e.* Au(111) and Cu(111) substrates, are given in Section 2.3.

2.1 Molecular building blocks for energy-conversion materials

2.1.1 Cobalt Phthalocyanine (CoPc)

The Phthalocyanines (Pc's), discovered accidentally in 1907 by Braun and Tcherniac, are macrocyclic compounds of intense blue-green color. They are similar to porphyrins, which are essential in nature for participating in processes and reactions in living organisms, being for example in the active sites of many different enzymes, in hemoglobin, and in chlorophyll. Pc's are instead synthetic organic planar aromatic macrocycles formed by four isoindole units linked together by four bridging nitrogen atoms. In Figure 2.1, a metal-free Pc, H_2Pc (with a molecular formula $C_{32}H_{18}N_8$) (a) is shown beside a metal Pc (MPc) (b), where the two hydrogen atoms at the center of the metal-free Pc are replaced by a metal atom, as Co in Figure 2.1 (b). The Pc central ring can host almost all types of metal atoms and a variety of substituents on the ligands can also be used to modify the Pc's, tuning their electronic and optical properties.

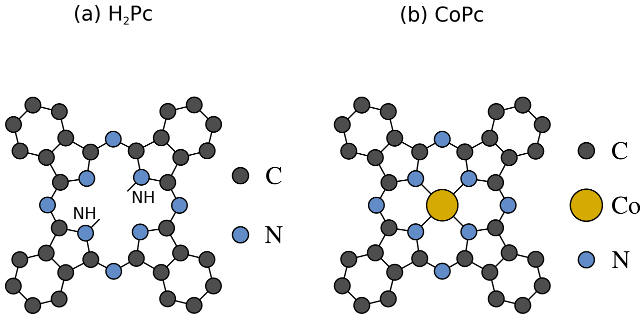

Figure 2.1. Molecular structure of (a) metal-free phthalocyanine (H_2Pc) and (b) cobalt phthalocyanine (CoPc).

Nowadays Pc's are commonly used as industrial pigment being dyes of very high thermal stability and low cost. However, they have also been implemented in a variety of different technological applications, such as in opto-electronics (OLEDs for example) and solar cells, in catalysis [2, 3, 4], in fuel cells [5] and as sensing materials (organic field effect transistors used as gas sensors [6]). Pc's are perfect candidates for these kinds of applications due to their photochromic properties, thermal and chemical stability, together with their molecular structure which readily form supramolecular self-assembled thin films. In films and bulk materials, the Pc's form molecular stackings where the orientation of the molecules results in different crystalline phases (for example α and β phases). Moreover, the stacking orientation with respect to the surface often varies with the thickness of the deposited film leading to slightly different electronic structures/property of the material [7].

In this thesis, CoPc has been studied (Paper I). There is an emerging interest in transition metal Pc's (TMPc's, with a transition metal, like Co, Fe, and Mn in the molecular center), considered by recent studies as a model for single-molecule magnets [8].

In Paper I, we addressed two still open questions regarding the electronic structure of CoPc: i) the atomic character of the highest occupied molecular orbital (HOMO), and ii) the electronic configuration of the molecular ground state. The atomic character of the HOMO of CoPc has been investigated by performing valence level PhotoEmission Spectroscopy (PES) experiments of both gas-phase CoPc and film samples, varying the photon energies used as excitation. Together with DFT calculations, our results clearly show that the HOMO is only formed by the organic ligand, with leading contributions from the carbon atoms and slightly from the nitrogen atoms.

Moreover, a comparison between our experimental results and new DFT simulations performed by our colleagues, confirms that the molecular ground state is correctly described by only $^2A_{1g}$ electronic configuration.

2.1.2 TPA, DPTA and m-MTDATA: electron donors

An electron donor molecule has the property to easily give (*i.e.* "donate") electrons to the surroundings or just to another part of the same molecular complex. The "electron-donating process" has a key role in optoelectronic devices such as light emission in Organic Light-Emitting Diodes (OLEDs) and charge generation in Organic Photovoltaics (OPVs).

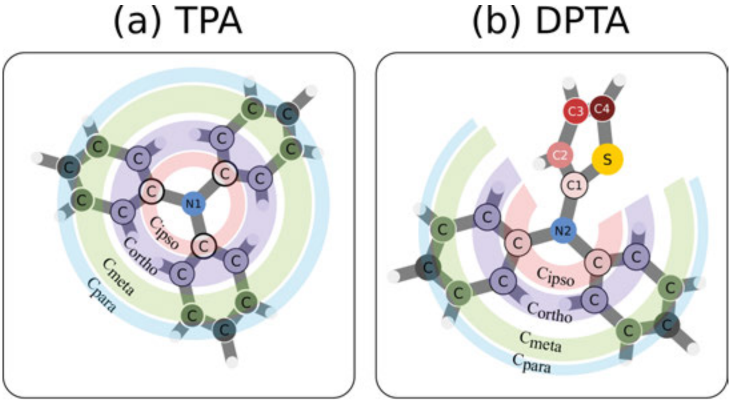

Figure 2.2. Molecular structure of (a) TPA and (b) DPTA simulated from our DFT calculation. For TPA, following the nomenclature of benzene-derived compounds, the carbon atoms directly bound to the N atom are denoted as C_{ipso}. The carbon atoms binding to the C_{ipso} are indicated as C_{ortho}, whereas those opposite to the C_{ipso} are named as C_{para}. The carbon atoms binding the C_{para} are labelled as C_{meta}. For DPTA, the carbon atoms within the phenyl ring are named accordingly, while the four carbon atoms in the thiophene ring are named C1, C2, C3 and C4.

In this thesis, we studied three electron donating molecules, TPA, DPTA, and m-MTDATA used in high-efficiency devices [9]. The characterizations included both studies of free molecules and solid-state measurements. The gas-phase investigations are fundamental for the understanding of the electronic structure of the electron donors helping then in recognizing their pristine properties. The acquired knowledge is then important for the design of new compounds for devices of improved performance. Notice that the studies of electron donors presented in the thesis are only one part of our bigger collaboration project aiming to understand the functionality of donor-acceptor molecular systems already used in real optoelectronic devices.

Triphenylamine (TPA)

Triphenylamine (TPA, $(C_6H_5)_3N$) was first synthesized by Merz and Weith in 1873 [10]. Since then the structure of TPA has been studied profoundly. The molecular structure of TPA is shown in Figure 2.2 (a). The central N binds three phenyl rings forming three co-planar N-C bonds via a sp^2-hybridization, which leaves a valence lone pair of electrons on the N $2p_z$ orbital. However, in TPA (and DPTA), the lone pair electrons are delocalized within the molecule, as shown in Figure 2.3 (a).

(a) Resonant structure for TPA (lone pair e⁻ of N)

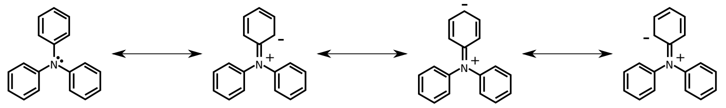

(b) Resonant structure for DPTA (lone pair e⁻ of S)

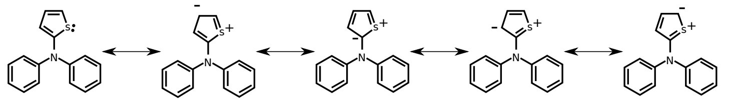

(c) Resonant structure for DPTA (lone pair e⁻ of N)

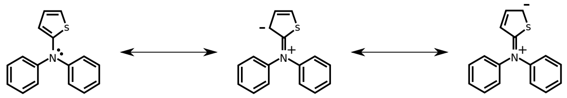

Figure 2.3. (a) The resonant electronic structures for the N lone pair electrons of TPA: the lone pair electron can delocalize to *ortho* and *para* positions of the phenyl ring. The delocalization shown in (a) can equally involve all 3 phenyl rings of TPA. (a) is also valid for the two phenyl rings of DPTA, whereas DPTA has two additional resonances, (b) - (c), associated to the thiophene ring. (b) Resonant electronic structures of S p_z lone pair electrons of DPTA: the S lone pair electron can delocalize to all positions in the thiophene ring of DPTA. (c) The resonant electronic structures for the N lone pair of DPTA to the thiophene ring. According to (c), the C3-carbon cannot accept the N lone pair electrons.

The phenyl groups are not on the same plane defined by the three C-N bonds, but are twisted, giving the molecule a "propeller-like shape" [9]. This non-planar molecular structure prevents the intermolecular aggregation, promoting instead the formation of isotropic homogeneous amorphous films [11], good as hole transport materials, important for improving the performance and stability of optoelectronic devices [12] and dye-sensitized solar cells [13, 11, 9, 14, 15, 16].

During the last decade, TPA and its derivatives have become recurring moieties implemented into Donor-π-Acceptor (D-π-A) molecules [17, 18, 19]. In this kind of systems, the HOMO and the Lowest Unoccupied Molecular Orbital (LUMO) are localized on two different portions of the molecule (the donor and the acceptor moieties, respectively) connected through a π-conjugated bridge. The D-π-A design provides the advantage to generate long-living charge separated states. TPA-based dyes are considered very promising and implemented in highly efficient DSSCs [15], with a validated efficiency over 11% for metal-free organic dyes [18].

In Paper III, the electronic structure of gas-phase TPA and DPTA are studied by PES and Near Edge X-ray Fine Structure (NEXAFS), together with Density Functional Theory (DFT). Our investigations provide a detailed and comprehensive understanding of the delocalization effect of the lone pair electrons of TPA. The electron-donating property of TPA is explained by the significant lone pair electron (N $2p_z$) contribution to the HOMO.

Moreover, to understand the electron-donating property of TPA when adsorbed, we performed the study of monolayer coverage of TPA on an Au(111) surface (Paper IV). Compared to the free TPA, the electronic structure of the monolayer is found clearly affected by the interaction between the molecule and gold substrate.

N,N-Diphenyl-2-thiophenamine (DPTA)

N,N-Diphenyl-2-thiophenamine ($C_{16}H_{13}NS$, DPTA) has very similar molecular structures to TPA, but in DPTA a phenyl is replaced by a thiophene ring, as shown in Figure 2.2 (b). Also DPTA has a propeller-like shape, making it a good candidate for isotropic amorphous materials. Similar to TPA, DPTA is also a recurring moiety implemented into Donor-π-Acceptor (D-π-A) molecules.

As shown in Figure 2.3 (c) and (d), DPTA shows almost equivalent N lone pair electron delocalization properties as TPA, but at the same time, it joins an important functionality in the thiophene ring. The use of thiophene-based donors as π-conjugated linkers in D-π-A system, usually facilitates the π-electron delocalization by maintaining the π-conjugation over the whole molecular back-bone, facilitating the charge separation from the donor to the acceptor moiety of the compound. Indeed, DPTA is found in a very promising donor-acceptor-acceptor molecular complex/system called DTDCTB. In DTDCTB, DPTA acts as an electron-donating moiety, that through the thiophene ring directly binds a benzothiadiazol unit which, in turn, is bonded to a dicyanovinylene electron-acceptor group [19, 20, 21].

In Paper II, the DPTA is studied in gas-phase. In addition to the similar N lone pair electron delocalization observed for TPA, we also found that the thiophene substitution does not affect the HOMO energy, but contributes significantly to the unoccupied density of states, introducing a slightly more acceptor character with respect to TPA. This also confirms why DPTA is better in promoting charge separation when it is implemented in D-π-A systems.

m-MTDATA

The m-MTDATA (4,4',4"-Tris[(3-methylphenyl)phenylamino]triphenylamine, $C_{57}H_{48}N_4$) belongs to the so-called "starburst π-conjugated molecules" with triphenylamine (TPA) as its building block (Figure 2.4). Synthesized and characterized for the first time by Shirota *et al.* in 1989 [22], m-MTDATA was soon found to be a good candidate for amorphous molecular materials of excellent processability (as they can be easily prepared by solution-processing techniques), transparency, isotropic and homogeneous morphology with absence of grain boundaries [9]. For these properties m-MTDATA is implemented in many novel photo- and electro-active devices.

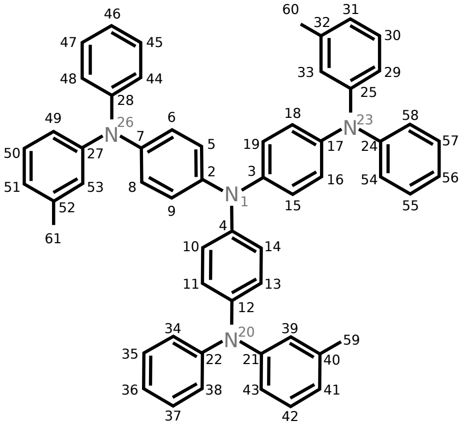

Figure 2.4. Molecular structure of m-MTDATA molecule.

The TPA moieties within these starburst molecules usually keep good electron-donating and charge-transfer properties just as pristine TPA molecule. Also, the design of the starburst molecule improves the functionality by, for example being more thermally stable and forming steadier amorphous glassy phases. The starburst structure also influences the optical absorption causing a red-shift from 299 nm (TPA) to 342 nm (m-MTDATA).

In Paper V, the m-MTDATA is studied both in gas-phase and adsorbed on an Au(111) surface by PES and NEXAFS. The investigations revealed the modification of the molecular electronic structure due to the interaction with the surface. The results are also compared with those of TPA, elucidating the electronic structure changes due to the increased complexity of the molecular structure.

2.2 Molecular building blocks for 2D materials

2.2.1 Biphenylene: molecular building block for graphenylene

Biphenylene (first synthesized by Lothrop in 1941 [23]), is a pale yellowish powder with melting temperature of about 110 °C. As shown in Figure 2.5, it is a cyclic hydrocarbon with chemical formula $C_{12}H_8$, formed by two benzene rings and a cyclobutadiene ring in between. J. Waser et al. first calculated the crystal structure of biphenylene in 1944 proposing a planar structure for the biphenylene molecule [24].

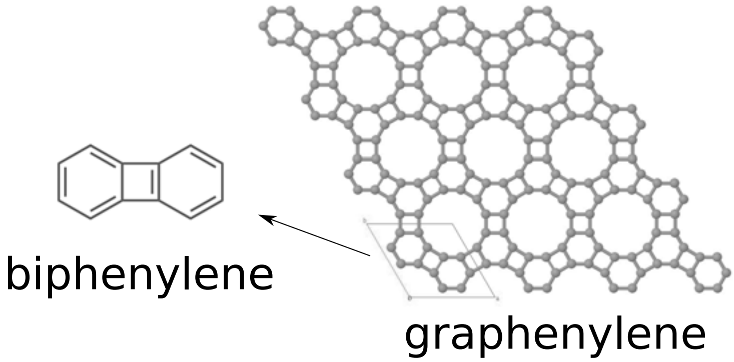

Figure 2.5. Structure of graphenylene and its building block, biphenylene. Figure adapted from Ref. [25].

Novel two dimensional (2D) functional materials, like graphene or boron-nitride, are considered to be prospective candidates for the next-generation electronic and optical devices [26] [27]. In this respect, also biphenylene becomes interesting being the precursor of a 2D porous graphene-like molecular network called graphenylene (also called biphenylene carbon, Figure 2.5). This new material would be characterized by a delocalized band with good dispersion and gap separation [28]. In previous studies, it has been shown that the most promising surfaces to grow this kind of covalently-bonded carbon-materials are the coinage metal surfaces, *i.e.* Au, Ag, Cu, Ni. In fact, these types of surfaces are able to promote a 2D molecular ordering when the building blocks are functionalized by halide ions [29] [25].

However, our research is more fundamental and starts with the characterization of biphenylene, molecular building blocks of such 2D network. In Paper II, a Cu (111) crystal has been used to grow biphenylene films of different thicknesses. A comparison with the previous gas-phase results allowed to characterize the electronic structure modifications induced by the molecule-substrate interactions for low molecular coverages, and the molecular arrangement within films of different thicknesses.

2.2.2 Melamine: molecular building block for $g-C_3N_4$

In the last few years, graphitic carbon nitride ($g-C_3N_4$) 2D nanosheets have attracted enormous interest due to their photocatalytic properties, being capable to split water into hydrogen and oxygen under visible light [30]. $g-C_3N_4$ is a 2D material consisting of sp^2-hybridized carbon and nitrogen atoms in an alternating fashion (Figure 2.6 b). Compared to graphene, the $g-C_3N_4$ is a semiconductor with a suitable band gap between 1.6 and 2.0 eV, similar to Si (1.11 eV), GaAs (1.43 eV), and GaP (2.26 eV), as confirmed by UV-visible measurements, DFT and PES investigations [31].

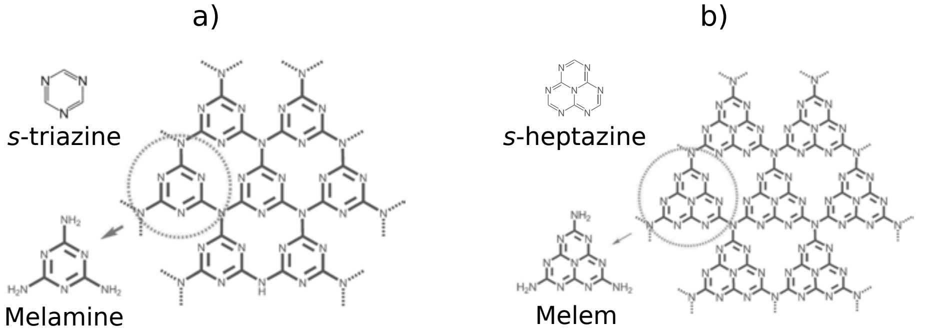

Figure 2.6. Postulated binary CN materials based on the building blocks melamine a) and melem b). Structures of *s*-triazine and *s*-heptazine are also shown. Figure adapted from ref. [32]

Different compounds are usually modeled as binary carbon-nitrogen (CN) sheets based on *s*-triazine or *s*-heptazine units connected through tertiary amino-groups N-C_3 (see Figure 2.6 a, b). Equivalently, triamino-*s*-triazine (melamine) and triamino-*s*-heptazine (melem) can be considered as the corresponding building blocks.

In Paper VI, we performed investigations by PES and NEXAFS on the melamine molecule, both in gas-phase and adsorbed on an Au(111) surface. According to previous theoretical studies of ideal binary CN sheets [33, 34] or *s*-heptazine unit [35], the H-boding formation between the lone pair of the aromatic N would be the active site for the water-splitting mechanism. For this reason, the aim of our study was to identify the spectroscopic evidence of the electronic structure modification induced by the intermolecular H-bonding between the amino functional groups of one melamine and the pyridine-like N (*i.e.* in the ring) of the adjacent molecule.

In details, Paper VI compares PES and NEXAFS investigations of free melamine with the characterization of the adsorbed molecule on an Au(111) surface. Our results reveal that the H-bonds mainly affect the N 1s level of the amino group, leaving almost unperturbed the N inside the aromatic ring. With the help of DFT calculations, the study gives a detailed description of the modification of the electronic structure of the melamine molecule induced by the adsorption on the surface and by the H bond interaction among the molecules.

2.3 Substrates

2.3.1 Au(111)

Gold (Au) is a noble metal. Its conductivity, stability and the fact that it is not reacting much with the adsorbate, make it a common substrate for the PES measurement in UHV conditions. It is easy to clean in UHV condition by Ar^+ and annealing cycles and can stay clean for quite a long time, *i.e.* for several hours in 10^{-10} mbar.

Being rather inert, Au(111) surface is more often used for studying the molecular electronic structure of adsorbates in presence of a quite moderate adsorbate-surface interaction. We used the Au(111) surface for our experiments in Paper I, IV, V and VI.

2.3.2 Cu(111)

Compared to Au, Cu (copper) is chemically more reactive. The Cu(111) surface can induce stronger surface-adsorbate interaction. For biphenylene functionalized by halide atoms, such interaction would promote the molecular covalent self-assembly, resulting in a graphenylene 2D sheet [29]. Moreover, the higher sticking coefficient of Cu(111) with respect to Au(111) allowed the study of biphenylene films of different thicknesses deposited on Cu(111). The results are presented in Paper II.

3. Photoelectron spectroscopy (PES)

PhotoElectron Spectroscopy (PES) is based on the photoelectric effect, a phenomenon first detected by Heinrich Hertz in 1887 and also known as the Hertz Effect [36]. Hertz discovered that the irradiation of ultraviolet light to a metal electrode would help to generate electric sparks.

However, only 18 years later, in 1905 Albert Einstein could theoretically explain the photoelectric effect by introducing a description of *light quanta* [37]. For this work Einstein was awarded the Nobel Prize in Physics in 1921, *"... for his services to theoretical physics, and especially for his discovery of the law of the photoelectric effect ..."* [38]. The photoelectric effect, stating and demonstrating that the energy of electronic orbitals is not continuous (*i.e.* quantized), was an important basic proof for the quantum mechanics at that time.

According to the photoelectric effect, electrons are emitted from their original electronic orbitals to the vacuum level when the material interacts with photons of sufficiently high energy.

3.1 Photoemission process

A schematic description of the photoemission process is presented in Figure 3.1. If the energy of the incoming photon is larger than the binding energy of the electron, the electron gets ejected from its original orbital in an atom. This process is called photoemission. Losing the electron, the atom is therefore positively charged, *i.e.* ionized. The kinetic energy (E_k) of the outgoing electron depends on the photon energy ($h\nu$), and the binding energy (E_B) of the electron (*i.e.* the energy required to remove the electron from the atom) is given by:

$$E_k = h\nu - E_B \tag{3.1}$$

The binding energy is the minimum energy required to remove the electron from its original orbital. As will be discussed later, for core level electrons, each chemical element has its own, unique set of binding energies.

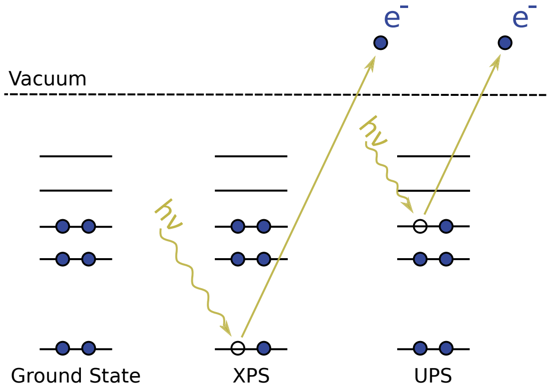

Figure 3.1. A schematic illustration describing the photoemission process examined by the PES technique, namely XPS and UPS. In both cases, an electron is removed from its original orbital by the interaction of the incoming photon ($h\nu$) which leaves the atom with a charge of +1. During the XPS process, electrons as deep as from the core level can be emitted after the excitation by the incoming photon $h\nu$. In a UPS experiment, only electrons from the valence level are emitted.

Generally, depending on the photon energy of the incoming light, X-ray or UltraViolet (UV) light, a core or valence level electron can be ejected. In both cases, an electron is removed from its original orbital by the interaction of the incoming photons ($h\nu$) and leaves the atom with a charge of +1. For core level photoemission, X-ray photons are usually used, and for this reason, the technique is also called X-ray Photoelectron Spectroscopy (XPS). On the other hand, Ultraviolet Photoelectron Spectroscopy (UPS) indicates photoemission investigations of valence levels using UltraViolet (UV) light (Figure 3.1).

3.2 PES for solid samples: three-step model

Besides gas-phase experiments, PES is more often applied to solid samples. When the sample is exposed to X-ray or UV light, electrons are ejected to vacuum from the sample by the interaction of the incoming photons, leading to the appearance of a positive surface charge induced by photoelectron emission. To avoid sample charging, which will shift the kinetic energy of the ejected electrons, samples are usually grounded and in good electric contact with the electron analyzer. Therefore, the favourable sample substrate for PES studies are metals, often single crystals as for example the Au(111) surface used in Paper I.

The Fermi level is the energy of the highest occupied single particle state in a metal at absolute zero temperature. By definition, when the metal system is in its ground state at absolute zero, no electron will be above the Fermi level, leading to a Fermi edge cut-off for such a system. At higher temperature, the

Fermi edge stays approximately at the same position, but it gets broader because of the thermal energy of the electrons. Since the sample is grounded, the Fermi level of the sample will be aligned with the Fermi level of the manipulator as well as the electron analyzer. The Fermi level is different from the vacuum level. The difference is the work function Φ.

For solid samples, the whole photoemission process can be explained and divided into three steps (Figure 3.2):

1) photoemission process (as in atomic case): locally the photons are absorbed, and photoelectrons are excited;
2) photoelectrons transport to the surface: the photoelectrons transport through the sample towards the surface. During the transport, the photoelectrons will experience energy loss processes, for example, inelastic scattering which creates secondary electrons; and
3) photoelectrons escape to vacuum: the photoelectrons, as well as the secondary electrons, escape to vacuum with kinetic energy E_k, and are finally detected by the electron analyzer. Note that only the electrons that overcome the work function Φ can escape from the sample to the vacuum.

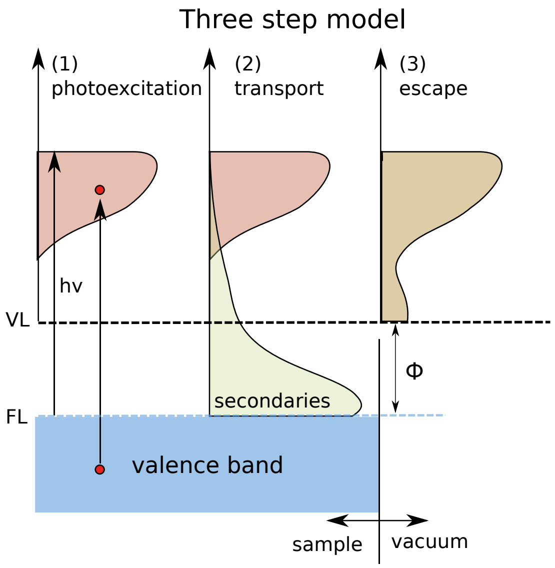

Figure 3.2. Illustration of the three step model. The whole photoemission process can be divided into three steps: 1) photoemission, 2) photoelectrons transport to the surface, and 3) photoelectrons escape to vacuum. The abbreviation VL denotes “vacuum level” and FL means “Fermi level”. Φ is the sample work function. The sketch is readapted from [38].

3.3 Photoionisation cross-section

The probability of photoemission is not constant. It is related to the photoionization cross-section, which depends on the photon energy and varies strongly between different elements being excited [39]. As a result, different photon energies can be used, for example, to distinguish contributions from different elements to molecular valence spectra. This is a valid strategy for disentangling the atomic character of different valence state as already shown in previous studies [40] [41] [42].

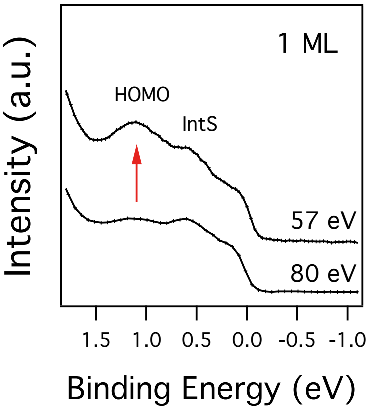

Figure 3.3. Comparison of valence-band photoemission spectra of the 1 ML CoPc/Au(111) sample taken with photon energies of 57 and 80 eV. The spectra were normalized and calibrated at the Fermi edges. The features due to the molecular HOMO and to the interface state (IntS), formed between the Co 3d out-of-plane orbital (a_{1g}) and the gold valence states, are indicated in the figure.

Photoemission Cross Section		
Photon energy	C 2p	Co 3d
57 eV	0.909	8.966
80 eV	0.328	7.154

Table 3.1. Comparison between cross section of C 2p and Co 3d at 57 eV and 80 eV, respectively.

The technique is called *variable photon energy photoelectron spectroscopy* and is applied in Paper I. Figure 3.3 shows spectra for CoPc/Au(111) recorded with photon energies of 80 eV to 57 eV. The enhancement of the CoPc HOMO *vs* the interface state (IntS) feature is due to the cross-section change between C 2p and Co 3d. As shown in Table 3.1, from 80 eV to 57 eV, the cross-section of C 2p is greatly enhanced from about 0.3 to 0.9, while the Co 3d does not change much. As a result, we can conclude that the CoPc HOMO is dominated by the organic ligand while the IntS is due to the Co-Au interface interaction.

In fact, the HOMO/IntS intensity ratios measured at the two different photon energies can correlate with the corresponding C 2p/Co 3d cross section ratio.

Resonant photoemission

As shown in Figure 3.4, in resonant photoemission, the photon energy is scanned over an absorption edge while measuring the valence region for each photon energy. One possibility is that a core electron is excited to an unoccupied valence level and decays by the so-called "participator decay". If a valence orbital has a high population localized on the same atom of the core-hole for a timescale longer or comparable to the core-hole lifetime, the valence state can be enhanced, because the non-resonant (PES in Figure 3.4) and resonant photoemission have the same initial and final states. The resonant photoemission is useful to get projections of the valence orbitals to the individual atoms, to know the character of the orbital.

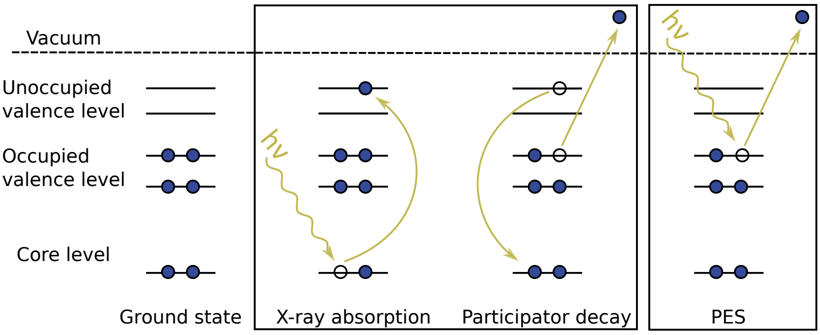

Figure 3.4. A schematic illustration comparing the resonant photoemission (X-ray absorption and then followed by the participator decay) and the normal photoemission process (PES). It is clear that the resonant photoemission (with participator decay) shares the same initial and final state as normal photoemission.

For example, for an organic-metal system like CoPc, some valence state is less hybridized with the organic ligand and has a large cobalt character. Therefore with the core excitation locally on the Co site during the resonance, *i.e.* when a core electron is excited to an unoccupied valence level, a valence state which is mainly localized on the Co atom will have a larger cross-section due to the previously mentioned participator decay. Therefore, this technique will enhance features in the valence region originating from the element carrying the core-hole, allowing (to some extent) an "element character" analysis of the valence band.

3.4 PES set-up

A typical surface experimental set-up of PES is shown in Figure 3.5. After the photoemission process, the kinetic energy of the photoelectron, E_k, is measured by the electron analyzer. Then, considering the energy conservation, knowing the excitation energy ($h\nu$) and measuring the kinetic energy E_k of the photoemitted electrons, the binding energies can be determined according to the formula:

$$E_B = h\nu - E_k - \phi_{sample} \tag{3.2}$$

where ϕ_{sample} is the work function of the sample, with the value of the energy difference between the Fermi level and the vacuum level of the sample.

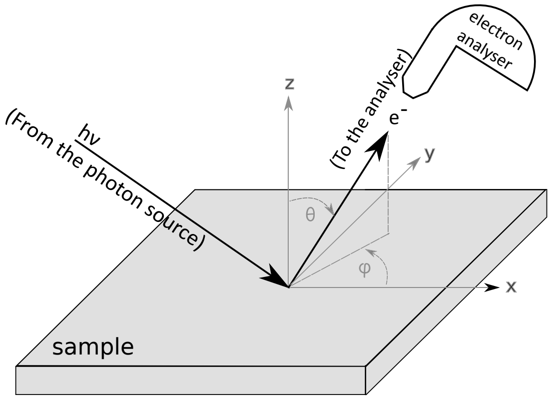

Figure 3.5. Experimental set-up of a Photoelectron Spectroscopy (PES) experiment. A photon impinges on a sample, and an electron is excited, escaping into the vacuum and finally detected by an electron analyzer. Polar (θ) and azimuthal (φ) angles of the photoelectron with respect to the normal to the surface (z-axis) and to the plane (x-axis), respectively, are displayed.

However, when the spectrum is taken with an analyzer, we have to take into account the work function of the analyzer, ϕ_{spec}, which is in principle different from the ϕ_{sample}. Usually, the sample and the spectrometer are in good electric contact, and then their Fermi levels are aligned. Obviously, there will be a difference/misalignment of the vacuum levels ($E_k = 0$) of the spectrometer and of the sample, due to their different work functions, $\Delta\phi = \phi_{sample} - \phi_{spec}$, where ϕ_{spec} is the spectrometer work function. Therefore, the measured E_k finally becomes:

$$\begin{aligned} E_k &= h\nu - E_B - \phi_{sample} + \Delta\phi \\ &= h\nu - E_B - \phi_{sample} + (\phi_{sample} - \phi_{spec}) \\ &= h\nu - E_B - \phi_{spec} \end{aligned} \tag{3.3}$$

Each chemical element has its own, unique set of binding energies, whereby PES can be used as a powerful method for chemical analysis. For this reason, PES is also called Electron Spectroscopy for Chemical Analysis (ESCA) [43, 44].

Usually, PES requires a good vacuum in order to prolong the mean free path of the outcoming photoelectrons [38]. PES requires a sufficiently monochromatized photon source to give accurate information. The kinetic energies (E_k) of photoemitted electrons, as well as the total electron counts, are measured by the electron energy analyzer. The PES result is usually shown in an energy spectrum where the integration of electron counts *vs* electron kinetic energies is given.

Electron energy analyser

An electron spectrometer in the PES set-up is used to analyze the kinetic energy of the photoemitted electrons. The electron kinetic energies (E_k) are measured either by deflecting the emitted electrons with a Lorentz force using magnetic or electrostatic fields (e.g. in a hemispherical analyser) or by applying a drift tube and measuring the time-of-flight of the electrons, *i.e.* velocities (for example the ARTOF spectrometer used in some of the experiments reported in this thesis).

Hemispherical analyser

A picture of SES200 hemispherical electron analyzer, which we used in our gas-phase experiments, is shown in Figure 3.6. The basic principle of hemispherical type electron analyzer is based on applying a Lorentz force to deflect the photo-emitted electrons. The Lorentz force **F** can be generated either by using magnetic or electrostatic fields:

$$\mathbf{F} = q \cdot \mathbf{E} + q \cdot (\mathbf{v} \times \mathbf{B}), \tag{3.4}$$

where **E** and **B** are the electric and the magnetic field, respectively. As a result, electrons of different kinetic energy E_k can be deflected spatially. Most of electron energy analyzers use ONLY electrostatic fields to deflect electron trajectories. Therefore, in order to get precision measurements, the electron analysers need to be carefully magnetically isolated from the surroundings. Usually, at least the analysis chamber and the electron analyser should have μ-metal shields to prevent stray magnetic fields from deflecting the photoelectrons. At the exit of the hemispherical analyzer, there is a combination of a multichannel plate and a fluorescent screen with CCD camera, where the number of electrons (intensity) *vs* E_k can be recorded.

To improve the stability and resolution of the hemispherical electron analyser, the electrostatic fields within the analyser usually only works in several pass energy (E_p) modes. In this mode, the functionality of the analyser is optimised, *i.e.* the analyser only allows electrons of given $E_p \pm \Delta E$ energy to arrive at the detector. As a result, a pre-lens electron optics unit is added before the electron entering the hemispherical analyzer. By setting voltages for the pre-lens system, the electrons of the required initial energy that we want to analyze will be focused and retarded so that their kinetic energy after passing through the pre-lenses matches the pass energy of the hemispherical analyzer. The pre-lens must scan the voltages to record a spectrum over a range of initial E_k energies. The energy resolution for a hemispherical analyzer is

$$\Delta E = \frac{E_p S}{2R} \tag{3.5}$$

where S is the entrance slit and R is the mean radius of the analyzer.

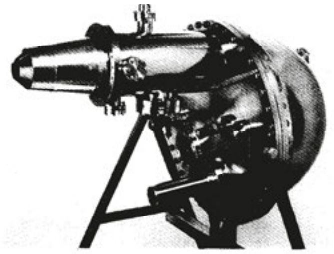

Figure 3.6. Photograph of SES-200 hemispherical electron analyser, from Ref. [45].

The Scienta$^{\text{TM}}$ analyser (for example SES-200) can run in two modes: Pulse Counting mode, in which individual pulses are counted, and the Analog to Digital Converter mode (ADC) in which the integrated CCD charge is recorded. The Pulse Counting mode is more often used in low count rate experiment before the signal is saturated. For example, we used the Pulse Counting mode for the CoPc gas-phase measurement (Paper I).

Angle-Resolved Time-Of-Flight spectrometer (ARTOF)

As described above, the normal PES detects the kinetic energy of the photoemitted electrons. In Angle-Resolved PhotoEmission Spectroscopy (ARPES), the emission angles of the emitted electron, θ and φ, are also registered (see Figure 3.5). Thus, since electrons with different momenta escape at different angles from the surface of the sample, ARPES measurements allow determining the electron momentum, as it can be calculated from the emission angles of electrons with respect to the sample surface.

The relationship between the kinetic energy (E_k^{vacuum} which can be measured by the electron analyzer) and the momentum (k^{vacuum}) of the photoelectron is:

$$E_k^{vacuum} = \frac{(k^{vacuum})^2}{2m}, \tag{3.6}$$

and we know the parallel component of the k-vector is conserved:

$$\hbar k_{\parallel}^{sample} = \hbar k_{\parallel}^{vacuum}, \tag{3.7}$$

where the $k_{\parallel}^{sample}$ is the momentum of the photoelectron in the plane of the sample.

With the basic geometry of an ARPES measurement shown in Figure 3.5, we get:

$$\hbar k_{\parallel}^{sample} = \hbar k_{\parallel}^{vacuum} = \sqrt{2mE_k}\sin\theta. \tag{3.8}$$

In summary, ARPES is a powerful tool to get simultaneously information about the energy and the momentum of an electron emitted from the sample surface by the photoionization process. Specifically, by locating the crossings of the bands with the Fermi level, the Fermi surfaces can be obtained. ARPES is one of the most direct methods of studying the electronic structure of surfaces and solids.

Angle-Resolved Time-Of-Flight (ARTOF) spectrometer is a new type of analyzer for ARPES. An ARTOF spectrometer measures at the same time energy and momentum of the electrons with high transmission and high resolution. The construction of the new ARTOF spectrometer dates back to 2004 [46]. The fundamental principle of the ARTOF is to use time-of-flight measurement to determine the electron velocities and thus the electron kinetic energies. An advanced electron lens system makes it possible to simultaneously determine the emission angles of the electrons. Using the time-of-flight concept, ARTOF needs pulsed sources for the excitations with maximum repetition rate below 3 MHz. Thus ARTOF needs a synchrotron radiation facility of a special kind or a pulsed laser source. In the thesis, all the experiments carried out with ARTOF analyzer were done at the LowDosePES endstation at PM4 beamline at the BESSY II synchrotron located in Berlin, Germany [47].

3.5 Electron mean free path

If the sample is in a condensed phase, after the photoemission process, the ejected electron will be transported to the surface according to the second step of the three-step model (Figure 3.2). During the transport, the ejected electron may experience collisions that cause it to lose energy. The mean free path here denotes the average distance traveled by an ejected electron between particle interactions. It is clear that the mean free path is depending on the kinetic energy of the electron. Figure 3.7 shows the so-called "universal curve". From about 20 eV up to about 500 eV we have the mean free path $\lambda < 10$ Å which usually equals to only about three molecular layers. The small mean free path makes PES technique a powerful surface analytical tool.

In the PES experiments, neglecting elastic scattering events, the electron inelastic mean free path λ can be used to estimate an adsorbate layer thickness (d) according to the so-called effective attenuation length (EAL) method. For the substrate signal I_s we have:

$$I_s = I_s^0 exp(-\frac{d}{\lambda} \cdot \frac{1}{cos\theta}). \tag{3.9}$$

Then we have:

$$d = -\lambda \cdot ln(\frac{I_s}{I_s^0}) \cdot \cos\theta, \tag{3.10}$$

where d is the adsorbate overlayer thickness, θ is the angle at which the electrons are detected with respect to the surface normal, λ is the mean free path in the adsorbate (which we usually took from the "universal curve"), I_s^0 is the signal from the clean substrate and I_s is the same signal but measured with adsorbate on top of the substrate. From Equation 3.10, the measured photoemission signal before and after the film deposition can be used to determine the adsorbate layer thickness d. Along with instrumental influences, elastic scattering effects will give a non-exponential decay curve and makes it difficult to determinate the layer thickness accurately. However, the method is still important to estimate the film thickness [48].

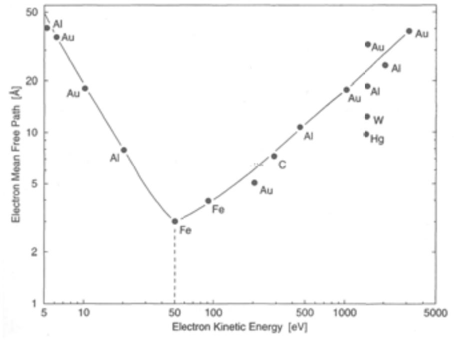

Figure 3.7. "Universal curve", *i.e.* mean free path λ *vs* kinetic energy (E_k) for various metals. The minimum is found of 2 - 5 Å for E_k of 50 - 100 eV [38].

According to Equation 3.10, with normal emission geometry ($\theta = 0$), the I_s/I_s^0 *vs* d is plotted in Figure 3.8. If we integrate the intensity over all depths, the whole signal will be equal to 100%. However, at $d = 1\lambda$, the signal is already reaching 63% of the total signal, meaning that more than half of the detected signal comes from a surface layer of depth less than 1λ. Furthermore, it is 87% at $d = 2\lambda$, while at 3 λ depth, it will generate 95% of detected electrons. Therefore, the 3λ is often refer to as the so-called "sampling depth".

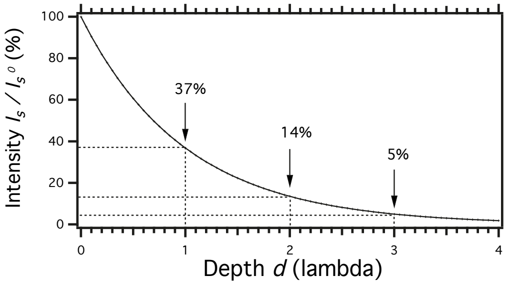

Figure 3.8. A plot of Equation 3.10 at normal emission geometry ($\theta = 0$). By the area integration we know that 95% of the PE signal detected by the electron analyzer comes below the "sampling depth" 3λ.

It is possible to obtain a more surface sensitivity by changing the emission geometry of θ. As shown in Figure 3.9, the depth z, where 95% of the PE signal generate, is reduced to half by changing the geometry from normal emission to 60° emission. In summary, the surface sensitivity will be enhanced if we use a more grazing emission geometry.

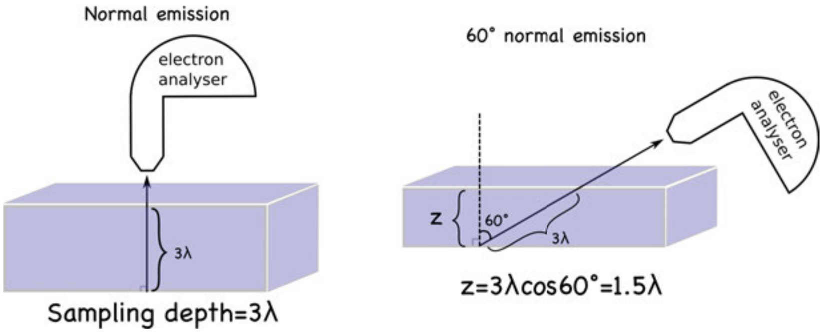

Figure 3.9. Comparison of the depth z, where 95% of the PE signal generate, between the normal emission (left) and 60° normal emission geometry (right).

3.6 Energy reference

For the researchers of the field, different reference levels are default for gas-phase measurements (free atoms and/or molecules) and for solids. I will clarify this issue in this section as sometimes it is misleading.

In gas-phase PES measurements, the binding energies are calibrated referring to the vacuum level. In this case, a reference gas, with spectroscopic lines of known binding energy (with reference to vacuum level), is introduced and measured simultaneously with the sample to calibrate the binding energy.

However, when studying surfaces and adsorbates, the sample and the spectrometer are usually in electrical contact so that their Fermi levels get in good alignment. For these experiments, the binding energies are referred to the Fermi level, since the Fermi edge can be used as an internal calibration point.

Due to, among other things, the different references used for the binding energy scales, comparing film and gas-phase measurements requires a shift to align the corresponding spectral features. In this case, sometimes the work function ϕ_{sample} of the film needs to be taken into account for film *vs* gas-phase comparison.

3.7 X-ray Photoelectron Spectroscopy (XPS)

As already mentioned, X-ray Photoelectron Spectroscopy (XPS), as shown in Figure 3.1, also known as Electron Spectroscopy for Chemical Analysis (ESCA), is a quantitative technique using high energy photons for the excitation (typically in the range from 200 eV to 10 keV). Because of the relatively high energy used (compare to UPS, which will be discussed later), XPS is often used to study core level electronic structure.

The XPS technique was developed by Professor Kai Siegbahn from Uppsala and his collaborators. The technique was quickly applied in the field of surface science, and it is still considered as one of the most powerful techniques for material characterization, being essentially non-destructive to most materials.

3.7.1 Core level binding energy

The energy of the system before and after the photoemission process will be conserved:

$$E_G(N) + h\nu = E_{ion}(N-1) + E_k, \tag{3.11}$$

where $E_G(N)$ is the total energy of the atom in its ground state with N electrons, while $E_{ion}(N-1)$ is the total energy of the excited ion with the removal of one electron.

The core level binding energy is defined as the difference before and after the photoemission:

$$E_B = E_{ion}(N-1) - E_G(N) = h\nu - E_k. \tag{3.12}$$

Hartree-Fock approach

The Hartree-Fock approach gives an approximation to solve the Schrödinger equation, which states that each electron moves in the average electrostatic field of the nuclei and the other electrons. This approach supposes the wavefunctions of Slater-type orbitals. The solution of the Hartree-Fock equation gives eigenfunctions called Hartree-Fock orbitals and eigenvalues.

Koopman's approximation
If we assume that after the electron emission the orbitals remain the same, the binding energy E_B can be approximated by the Koopman's theorem, which states that the binding energy can be approximated by the negative of the Hartree-Fock (HF) orbital energy, $\varepsilon(H)$, from which the electron is emitted, *i.e.*,

$$E_B = -\varepsilon(H) = E_{ion}(N-1)^{KT} - E_G(N). \tag{3.13}$$

For bound-state orbitals $\varepsilon(H)$ is negative which means that the binding energy E_B has a positive sign.

From the theorem, it is easy to understand the error of the approximation mainly comes from the "frozen orbital approximation" because the remaining N-1 electrons have a different set of Hartree-Fock orbital energies. For a real system, the changes of the orbitals due to the ejecting of an electron need to be considered. In fact, usually $E_{ion}(N-1) < E_{ion}(N-1)^{KT}$ and result in $E_B < -\varepsilon(H)$.

Δ SCF approach
In the Δ SCF approach, one determines the difference between two self-consistent field calculations, *i.e.* the binding energy E_B is obtained as a total energy difference between the ground state and the selected core-excited state. The Δ SCF approach has been successful because most of the error brought by Hartree-Fock approach has been cancelled out.

Electron correlation: full calculation
As shown before, the Hartree-Fock approach is based on mean field approximation and uses a single Slater determinant to approximate the wave function.

To account for electron correlation effect especially for the final state case (excited state), configuration interaction (CI) method and other more advanced theoretical methods can be used. The CI method uses a linear combination of possible n-electron Slater determinants to express more exact ground-state or excited-state wavefunctions. The coefficient of every Slater determinant is optimized to find the minimum ground/excited state energy.

The ground state energy found by the CI is lower than the Hartree-Fock approach and closer to the exact ground state energy.

3.7.2 Core level line shapes

The core level line shape is determined by several effects. The most important factor inducing the intrinsic core level broadening is due to the lifetime of the final state.

Core-hole lifetime
The photoemission process will, to a first approximation, generate a sharp line (a Dirac δ function). However, in quantum mechanics, we have the uncer-

tainty relation between energy and time. If we observe a quantum state with a lifetime τ, the energy of the level cannot be known with accuracy:

$$\Delta E \cdot \tau \geq \frac{\hbar}{2} \tag{3.14}$$

Therefore the finite lifetime of the hole state defines the minimum intrinsic line width, which is called lifetime broadening. The lifetime of the core-hole is of the order of femtoseconds (fs, 10^{-15} s). Through Equation 3.14, a lifetime of 1 fs implies roughly a lifetime broadening of 0.1 eV. The lifetime broadening has a Lorentzian shape.

Other factors affecting the line shapes

Besides the lifetime broadening, there are also important contributions to the core level line shapes, such as:

- Doppler broadening: the atoms or molecules detected by PES are always in thermal motion with a distribution of velocities, which end up with different Doppler shifts. The collective effect of all different Doppler shifts results in a Doppler broadening, which has a Gaussian line shape.
- Shake-ups: as will be discussed later in Section 3.7.4, the shake-ups can generate satellites in photoemission. For example, it can give rise to characteristic core line asymmetries for the metals.
- Extrinsic broadening: as shown in the three-step model (Figure 3.2) of the solid samples, when the photoelectron travels to the surface, the interaction between the particles will expand the energy distribution of the photoelectron.
- And finally there is the broadening due to the instrumental resolution, which usually can be approximately regarded as a Gaussian filter. As a result, the final shape of the spectrum is a convolution of all above features with a Gaussian shape instrumental broadening.

3.7.3 Chemical shifts

XPS measures the binding energies of the atoms in the sample, and it is an element-specific method. However, the position of the binding energy of a specific element and the line profile of a spectral feature can vary as a result of the chemical environment of the atom or molecule. For core levels, we can observe a chemical shift giving more detailed information about the bonding and the interaction of the atom with the surroundings. To a first approximation, in molecular systems, the BE shift can be correlated to the charge state of the atom. Through a careful analysis of the chemical shift, we can study changes in the electronic structure of a system. Often, chemical shifts are regarded as initial state effect.

In addition, for an adsorbate we can, for instance, characterize the interaction and bonding with the surface or with other atoms/molecules. The shifts may also be sensitive to the orientation of the adsorbates and their adsorption sites.

The most famous example establishing the chemical shift is by the C1s PE spectrum of ethyl trifluoroacetate ($CF_3 - CO - O - CH_2 - CH_3$), which is also known as the "ESCA molecule" (inset of Figure 3.10) [49]. In the spectrum, it is evident that the BEs of the four C atoms within the molecule are well separated due to the chemically non-equivalent character, well reflecting the electronegativities of the substituents on each carbon atom. Similar BE shifts in C 1s spectra are also observed and discussed in Paper III.

Figure 3.10. A photo of an exhibition of ESCA at Ågström laboratory, Uppsala University in memory of Prof. Kai Siegbahn, who developed ESCA. The coil system of the 1^{st} mordern electron detector of the magnetic iron-free double focusing type (1955) is seen in the left corner (pointed by red arrow). The chemical shifts of the so-called "ESCA molecule" is found on the right side, pointed by a white arrow and also enlarged in the inset.

Binding energy shift due to the screening effect

The core-hole effect will usually reduce the kinetic energy E_k of the ejected photo-emitted electron because the electron is attracted by the core-hole. By the electron clouds screening of the core-hole, the ejected electrons "*feel less*" the core-hole, therefore have higher kinetic energy E_k, *i.e.* lower binding energy E_B.

The screening can be *intra*-molecular, *i.e.* within the molecule itself. For example, the comparison of S 2p core level spectra between DPTA and thiophene is shown in Figure 3.11. The comparison shows a shift of about 0.52 eV to lower BE of the spectrum of DPTA, attributed to the more effective *intra*-molecular screening due to the increasing molecular size of DTPA compared to thiophene, as discussed and observed in previous studies for other molecules like linear alkanes and C60 [50, 51].

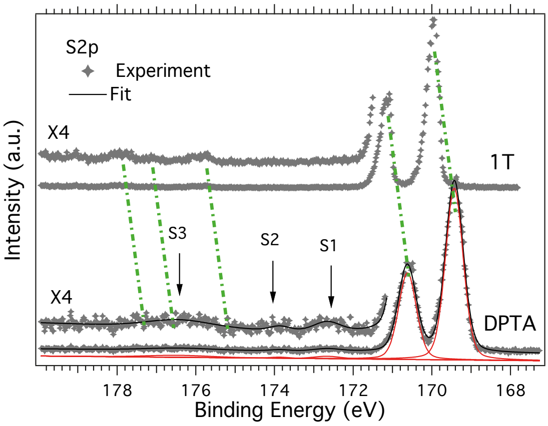

Figure 3.11. Comparison of S 2p PE spectra of gas-phase DPTA and thiophene measured with 260 eV photon energy, as in Paper III. The S 2p peaks of DPTA are shifted about 0.52 eV to lower BE with respect to those of thiophene (1T) due to the intra-molecular screening.

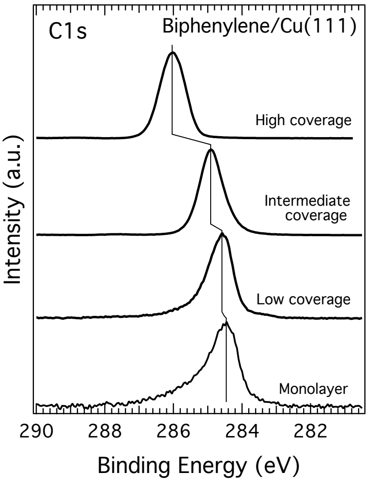

Figure 3.12. C1s PE spectra of a biphenylene film of high (100 Å), intermediate (30 Å), low (7 Å) and monolayer (3 Å) coverages acquired with $h\nu$ = 400 eV. Adapted from Paper II.

The screening can also be due to the surroundings, as often observed in solid-state measurements. Figure 7.4, adapted from Paper II, shows the C1s spectra of biphenylene deposited on Cu(111) at the given molecular thicknesses, taken with a photon energy of 400 eV. It is evidence that the C1s is shifting to higher binding energy with increasing molecular coverage on the Cu(111) substrate. For lower molecular coverage, the core-hole screening is very effective, resulting in lower binding energy. This screening is due to the metal Cu(111) surface, where the conduction electrons can move freely. However with increasing molecular coverage, the screening of the core-hole by the Cu (111) substrate is less effective and the BE of the C1s increases, which gives a $\Delta E = 1.5$ eV for the high coverage biphenylene with respect to the monolayer sample.

Core level in gas-phase *vs* in solid-state measurements

As discussed in Chapter 3.6, if we refer the core level measured in the gas-phase and in solid to the same reference level, for example, the vacuum level, still some shift will be observed. The most important energy shift between a core level measured in the gas-phase and the solid-state is ascribed to the additional screening in the solid-state.

In addition, the charge redistribution due to the substrate lattice will lead to a broadening of the peaks and new shake-up features. There will be additional local shake-up confined to the adsorbate-substrate excitations and non-local shake-up attributed to the excitations in the substrate due to the long-range screening.

3.7.4 Satellites

As shown in Chapter 3.7.1, the "frozen orbital approximation" cannot describe the real electronic orbitals after the photoexcitation process. The core ionization will lead to complicated modifications of the electronic structure, such as orbital relaxation and correlation. The perturbations will give rise to the satellites features in addition to the main line. In a simple picture, the satellites may be viewed as excitations in the core-ionized final state. For excitations to bound states we use the term shake-up, and for excitations to continuum states, we use the term shake-off.

In gas-phase measurements, the shake-up consists of some discrete transitions from occupied to unoccupied molecular orbitals. After the photoionization, the creation of a core-hole can also affect the energy potential curve for the molecule, such that the equilibrium bond distance will be changed. Such modifications give rise to extra collective excitation of vibrational motion and the intra-molecular vibrational excitations can be described by the Franck-Condon principle. In molecules the vibrational states are discrete. There are also extrinsic losses related to the environment surrounding the core-hole. For example, in gas-phase measurements, the intensities of some satellite lines will vary depending on the pressure of the sample gas. Such satellites are then attributed to extrinsic losses.

For solid samples, it is common to distinguish several types of shake-up processes. In metals, the core-electron lines are always asymmetric, known as the Doniach-Sunjic profile [52], due to the transitions from occupied states up to Fermi level to unoccupied states just above the Fermi level (for example the C1s of monolayer biphenylene/Cu(111), shown in Paper II). For the adsorbates, the vibrationally excited states are known as phonons and they form continua due to the continuous band structure in solids. The phonon peaks often have Gaussian shapes. Other shake-up includes plasmon excitations, interband transitions, *etc*. [53]. According to the three-step model, after the photoemission process, the electron will transport to the surface and lose energy (Figure 3.2 (2)), which will also generate extra extrinsic losses satellites.

The shake-up features carry information on the multi-electron system. Detailed information such as the atomic chemical environment, HOMO-LUMO gap for free and adsorbed molecular systems can also be obtained by studying the shake-ups.

3.8 Ultraviolet Photoelectron Spectroscopy (UPS)

Ultraviolet Photoelectron Spectroscopy (UPS) is a technique developed by David W. Turner at 1960's for valence photoelectron studies of free molecules in the gas-phase. UPS uses photon energies ranging from few eV to hundred eV, *i.e.* low photon energy which allows a detailed investigation of the valence orbitals as shown in Figure 3.1. In the thesis, UPS has been used to study both molecular vapour (gas-phase) and solid films.

Unlike core-level PE spectrum that is atomic like, the valence PE spectrum shows highly hybridized molecular orbitals. However, to understand the valence PE spectrum is important since the valence electrons are significantly involved in the chemical reactions and are responsible for the electronic property of the materials. For example, in the thesis, the nitrogen lone pair electron contribution to HOMO was found the key reason for the electron-donating property of TPA, DPTA and m-MTDATA (Paper III, V).

Because of the complexity of the valence spectra, it is difficult to accomplish the detailed information with experimental results alone. Therefore in the thesis, the experimental valence PE spectra are compared with theoretical results from quantum chemistry (DFT in our case). The results give a reliable assignment of the molecular orbitals of the valence level and give a comprehensive description of the electronic structure.

4. Photoabsorption spectroscopy

Photoabsorption spectroscopy is another important spectroscopic technique. In the photoemission process, photoelectrons are ejected from the system, while in the main processes of photoabsorption, the system remains neutral.

Depending on the photon energy of the incoming light, the method to detect the absorption and what kind of information we want to draw from the absorption data, photoabsorption spectroscopy can be further divided into many techniques, like: Ultraviolet-Visible Spectroscopy (UV-Vis), Near Edge X-ray Absorption Fine Structure (NEXAFS), Extended X-ray Absorption Fine Structure (EXAFS), *etc.* In the following, we will focus on the UV-Vis and NEXAFS techniques.

4.1 Ultraviolet-Visible Spectroscopy (UV-Vis)

The photon source used for UV-Vis is light with continuum wavelength from ultraviolet to visible, roughly in the range between 190 - 750 nm, *i.e.* from 1.65 to 6.52 eV. The light absorption in such energy region plays a key role in the photovoltaic applications. Therefore, it is vital to measure the UV-Vis to characterize the performance of solar cells.

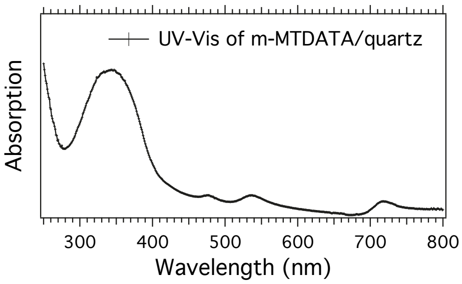

Figure 4.1. UV-Vis result of m-MTDATA thin film on top of quartz glass, showing a broad absorption ranging from 300 to 400 nm.

During the measurement, the sample is exposed to monochromatized light and the wavelength is scanned from near-infrared wavelengths to UV region utilising the UV-Vis continuum source. The transmitted light intensity is registered for each scanned wavelength. Then the absorbance A can be calculated through:

$$A = log(I_0/I_{sample}), \tag{4.1}$$

where I_0 is the intensity measured for the background (no sample, clean substrate or solution) and I_{sample} is the intensity measured with the sample. A UV-Vis result of m-MTDATA thin film on quartz glass is shown in Figure 4.1. It shows a broad absorption in the wavelength range of 300-400 nm.

From molecular electronic structure view, the UV-Vis is also important. The typical energy range of UV-Vis, about 1.65 to 6.52 eV as mentioned before, corresponds to the transition from the outermost occupied molecular valence levels to the lowest lying unoccupied levels. By a more careful analysis, we can get a detailed information about the HOMO-LUMO gap.

4.2 Near Edge X-ray Absorption Fine Structure (NEXAFS)

As illustrated in Figure 4.2, during the X-ray absorption process, a core electron is excited to an unoccupied valence orbital. The intensity of the absorption varies as a function of the incoming photon energy. After the X-ray absorption process, the system will decay within 10^{-15} s (femtosecond range). For low-Z elements, such as N or C, the Auger decay is more probable while for high-Z element fluorescence decay dominates.

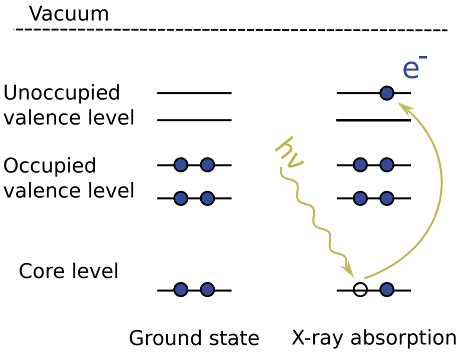

Figure 4.2. A schematic illustration of the absorption process.

A NEXAFS spectrum is measured by irradiating the sample with a tunable X-ray source to excite core electrons into unoccupied valence levels. One usually records NEXAFS spectra either by measuring the absorbance in transmission mode or by monitoring the amount of decay processes, *e.g.*, through emission of photons (fluorescent decay) or electrons (electron yield).

When measuring the electron yield, NEXAFS can be recorded in the following modes: total, partial, or Auger electron yield by a multi-channel plate or by an electron spectrometer. For measuring the Auger electron yield by the electron analyzer, we usually choose kinetic energy window of the Auger electron transitions of the target decay channel.

The width of XAS features relates to:

1. the broadening due to the lifetime of the core-hole (Lorentzian lineshape);
2. the resolution of the instrument (Gaussian lineshape); and
3. the vibrational motion of the molecule often leading to an asymmetrical broadening [54].

Unlike PES that probes the occupied electronic structure, NEXAFS probes the unoccupied atomic/molecular valence electronic states in the presence of a core-hole. The excitation in the XAS process is governed by the dipole selection rule, namely, the excitation (de-excitation) can only occur with $\Delta L = \pm 1$ [55]. Relating to the core excitation process, NEXAFS is also an element-specific technique.

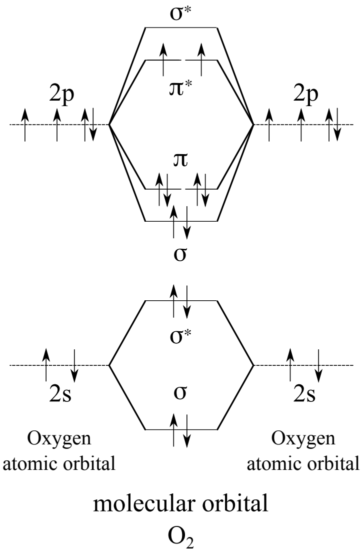

Figure 4.3. Molecular orbital diagram of O_2.

We will now discuss the general case of a symmetric diatomic molecule as an example. Figure 4.3 shows an energy level diagram of O_2. This diagram is true for the heavier main group elements (for example, F_2), but not valid for lighter elements like N_2 because of the s-p hybridization. The π bonds are usually weaker than the σ bonds because the orbital overlap is smaller. As a result, a π orbital is usually lower in binding energy, while σ orbital is lying deeper (with higher binding energy). Since the σ bonds have larger overlap than π bonds, the σ and σ^* orbitals are more energy splitted than the π and π^* orbitals. As a result, the π^* resonance is usually the 1^{st} resonance observed at lower energy, while σ^* orbitals are higher in energy and are often found in the continuum. Therefore, the π^* resonances have a smaller line-width, due to a longer lifetime of the π^* excited state.

Instead, σ^* resonances are much broader because they are usually at higher energies above the threshold and overlaps with the continuum, increasing the probability of the decay into the continuum of the excited electron. At the σ^* resonant energy, the vibronic broadening can be also significant. The asymmetric lineshape of σ^* resonances is therefore due to a combination of lifetime broadening and molecular vibration along the bond direction.

As illustrated in Figure 4.2, in general, a NEXAFS spectrum reflects the dependence of the photoabsorption cross section *vs* the photon energy near the absorption edge, *i.e.* from just below the ionization threshold up to around 50 eV above it [54]. In the case of linearly polarized light, the X-ray absorption cross section can be calculated from Fermi's Golden Rule where we expand the Hamiltonian as follows [38]:

$$\sigma_{XAS} \propto |\langle f|\mathbf{e}\cdot\mathbf{p}|i\rangle|^2 \delta\left(E_f - E_i - h\nu\right)\rho_f(E), \tag{4.2}$$

where σ_{XAS} is the X-ray absorption cross section, **e** the unit electric field vector, **p** the dipole transition operator and $\rho_f(E)$ is the density of final states.

From Equation 4.2 we see that the transition intensities depend on the orientation of the electric field vector relative to the orientation of the molecule. In this way NEXAFS makes it possible to monitor/determine real space orientation of the molecules adsorbed on a surface. For a K-edge spectrum, the intensity will be proportional to the direction of the final state orbital according to [55]:

$$I \propto |\mathbf{e}\langle f|\mathbf{p}|i_{1s}\rangle|^2 \propto cos^2\delta, \tag{4.3}$$

with δ being the angle between the electric field vector **e** of the incoming light, and the direction of the final state orbital. In the case of O_2 molecules adsorbed flat on a surface, the direction of maximum π^* orbital amplitude is pointing out-of-plane. See Figure 4.4. Therefore, if we use grazing incidence of the synchrotron radiation, the δ in Equation 4.3 is about 0°, and result in $cos^2\delta = 1$, giving a strong enhancement intensity. On the other hand, for the Normal Incident (NI) case $\delta = 90°$, which lead to $cos^2\delta = 0$ and strongly reduced π^* state intensity. The transition to σ^* states behaves in the opposite way. We can thus study the geometry of the adsorbate molecules on the surface using NEXAFS.

The Rydberg states of a molecule are electronically excited states with energies that follow the Rydberg formula. Transitions to Rydberg orbitals generate sharp but weak resonances. If the resolution is high enough, the Rydberg states of a free molecule can be observed between the π^* resonance and the ionization potential. However in the condensed phase or for strongly chemisorbed molecules, pure Rydberg resonances are quenched because of the large spatial extent of the orbitals, which have most of their orbital density at the periphery of the molecule [54].

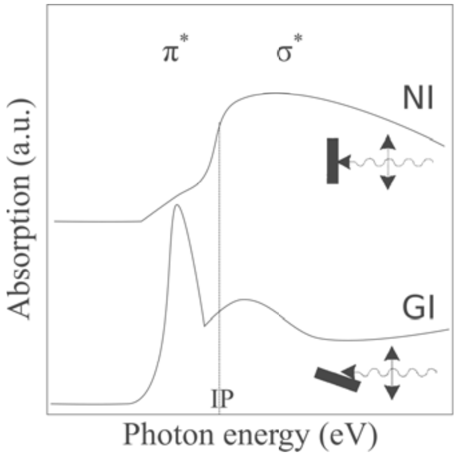

Figure 4.4. An illustration of angular dependent NEXAFS of O_2 molecular adsorbed flat on a surface. NI and GI denote normal incident and grazing incident angle, respectively. IP marks the ionization potential.

5. Density Functional Theory (DFT)

I have performed electronic structure calculations based on Density Functional Theory (DFT) for Papers III & V in the thesis. In this chapter I will illustrate my computational work.

5.1 A short introduction to DFT

DFT is one of the most widely used methods for the computation of the electronic structure of multielectron systems like molecules and solids. Beside the electronic structure of a system, it can provide a great variety of chemical and physical properties, such as molecular structures, vibrational frequencies, atomization energies, ionisation energies, electric and magnetic properties, reaction paths, *etc.* [56]. DFT has been very popular since its appearing in the 1970s, and the number of scientific publications based on it is still increasing significantly, as shown in Figure 5.1. Due to its high relevance and achievements in materials science, the Nobel Prize in Chemistry in 1998 was awarded to Walter Kohn, *"for his development of the density functional theory"*, and John Pople, *"for his development of computational methods in quantum chemistry"*.

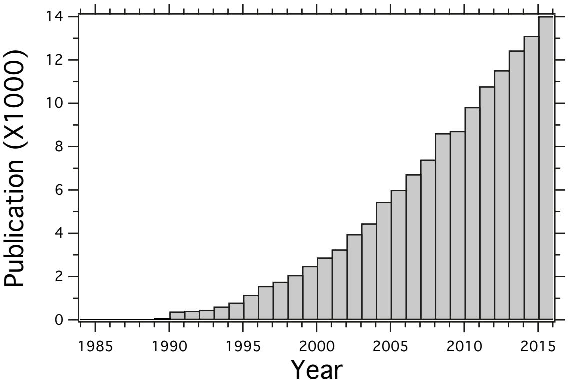

Figure 5.1. Publication number with the topic of "Density Functional Theory" from the years 1985 to 2016. A result from *Web of Science*.

The core of DFT is that the ground state properties of a system of N electrons like, for example, molecules, solids or liquids, can be known if the related electronic density is known. However, in general, we do not know the expression of the electronic density. In practice, in most cases the calculations are performed using the Kohn-Sham formalism, where a real (interacting) system is replaced by a reference system (non-interacting) that has exactly the same ground state density $\rho(\mathbf{r})$. The electrons are subject to an effective potential, $\hat{v}_{eff}$, which is expressed by:

$$\hat{v}_{eff}(\mathbf{r}) = v_{ext}(\mathbf{r}) + e^2 \int \frac{\rho(\mathbf{r}')}{|\mathbf{r}-\mathbf{r}'|} d\mathbf{r}' + v_{xc}(\mathbf{r}) \tag{5.1}$$

where $\hat{v}_{ext}(\mathbf{r})$ is the external potential (for example the electron-nuclei interaction), the second term denotes the Coulomb potential where $\rho(\mathbf{r})$ is the density of states, and the last term $v_{xc}(\mathbf{r})$ is the exchange-correlation potential and equals to $\frac{\delta E_{xc}(\rho)}{\delta(\mathbf{r})}$. This term is unknown in the Kohn-Sham approach and large efforts have been and are still being devoted to find exchange-correlation potentials, in order to describe the most important characteristics of various types of materials. For example the Local Density Approximation (LDA) and the Generalized Gradient Approximation (GGA). Currently, one of the most popular and successful approaches for the treatment of molecular systems is the hybrid functional B3LYP, which results from a parametrised mixing of GGA and Hartree Fock functionals [57].

5.2 Details of the performed simulations

Due to the massive load, DFT calculations are running on supercomputers. I personally used the supercomputers named Abisko at High-Performance Computing Centre North (HPC2N), which is a Swedish national centre for Scientific and Parallel Computing.

I performed the calculations using the mentioned B3LYP functional within the Gaussian 16 program [58]. The Gaussian software is one of the most popular and widely used packages in computational quantum chemistry.

The 6-31G(d,p) basis set [59] was applied for H, C, N and S of each molecule studied in the works presented in this thesis. A basis set in DFT is a set of mathematical functions used to represent the electronic wave function. A larger basis set usually gives better approximation of the real wave function, but on the other hand the calculation becomes more time consuming. Therefore to choose the basis set requires a balance between calculation load and the required accuracy. 6-31G(d,p) (or 6-31G**) are popular basis sets developed by John Pople and used in the Gaussian program.

5.2.1 Geometry optimization

In the geometry optimization procedure, the structure of the materials (*i.e.*, the spatial coordinates of the nuclei) is adjusted in successive steps for which the total energy is calculated. The process stops when a required accuracy, for example in the order of 10^{-6} eV, is reached, and in that case the calculation is considered to be *"converged"*, *i.e.* when successive geometry steps give total energies differing by no more than the desired accuracy. A good starting point is often necessary to reach an energy minimum to define the ground state of the system. It is important to know that the geometry optimization can lead to a local minimum, and therefore different starting points, and if available, the experimental data need to be checked.

5.2.2 HOMO-LUMO analysis

Using the geometry obtained in the minimization procedure, one can calculate the electronic structure of the molecules, and the energy of each molecular orbital. Among the most important results, we have the energy of the Highest Occupied Molecular Orbital (HOMO) and of the Lowest Unoccupied Molecular Orbital (LUMO).

I will take benzene and thiophene as examples. The HOMO and LUMO molecular orbitals and their energy positions for benzene and thiophene, are shown in Figure 5.2. The orbitals were visualized with the MOLDEN^{TM} program [60]. The benzene HOMO is a B_{2g} orbital and the LUMO is a B_{3u} orbital, while the HOMO-LUMO gap for benzene is 6.79 eV. For thiophene, the sulphur does not take part in the HOMO but contributes to the LUMO. The HOMO-LUMO gap of thiophene is 6.16 eV, smaller than benzene.

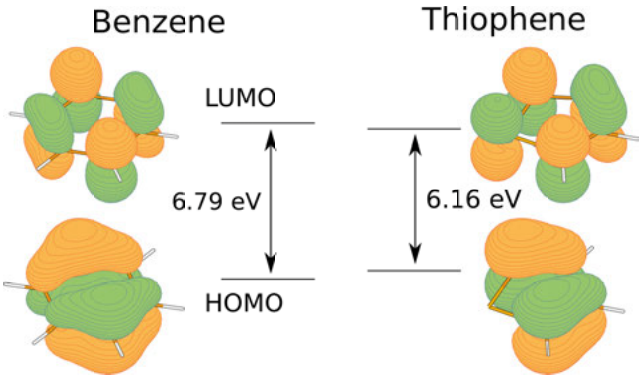

Figure 5.2. Electron density of HOMO and LUMO of benzene and thiophene and their HOMO-LUMO gap, calculated through Gaussian 16, with B3LYP and 6-31G(d,p).

5.2.3 Valence levels from DFT calculations

After the geometry optimisation is properly completed, the ground state electronic structure of the system can be obtained from the output file, *i.e.*, the eigenvalues of each molecular orbital, shown as bars in Figure 5.3. By convoluting each eigenvalue with a Gaussian function and summing up the intensities, we get an intensity *vs* energy spectrum, as the black curve (Cal.) in Figure 5.3, where the calculated valence levels of TPA are convoluted by Gaussian function FWHM of 0.3 eV.

The simulation can be compared to the experimental valence photoelectron spectrum. Figure 5.3 shows the experimental spectrum of gas-phase TPA measured at 100 eV photon energy taken at the ELETTRA synchrotron (black line with marker), compared to the calculated valence results by DFT calculation (black curve). The simulated spectrum is shifted +2.36 eV in order to align with the experimental results for an easy comparison. The theoretical and experimental spectra are in very good agreement, well showing the accuracy of the DFT ground state calculation.

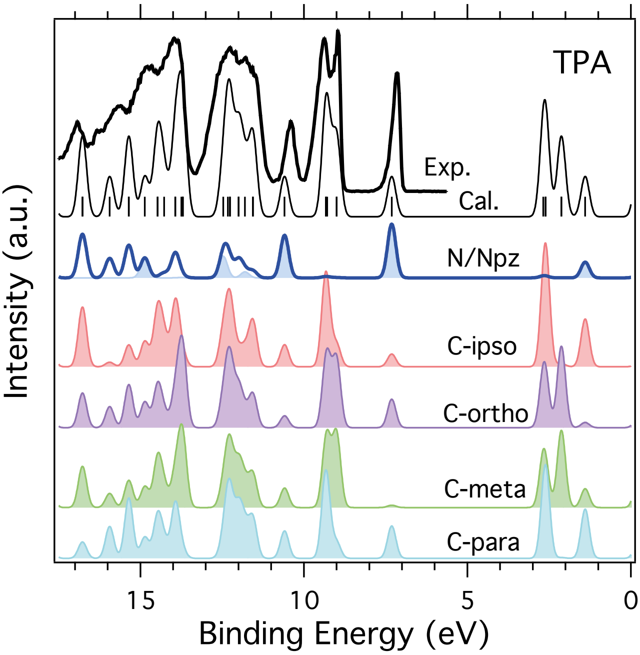

Figure 5.3. Valence PE spectrum of TPA measured with 100 eV photon energy in comparison with the corresponding DFT calculated spectra. The partial density of states (PDOS) of individual C (C-*ipso*, C-*ortho*, C-*meta*, C-*para*) and N (blue lines for N PDOS and light blue filled for N p_z) are also presented. The theoretical spectra of the different C atoms are normalized to the numbers of corresponding type of carbons present in the molecule. Figure adapted from Paper III.

5.2.4 Partial Density Of States (PDOS)

My goal was to use the DFT calculations to interpret the experimental results. With the DFT we can further resolve the Density Of States (DOS) in element and orbital components, obtaining the so called Partial Density Of States (PDOS). This means that we can obtain the site-projected DOS, where the information about the different element contributions to various molecular orbitals can be visualized. We can further decompose the elemental contributions into the orbital contributions.

In Figure 5.3, we resolved the DOS according to the different element and different orbital, namely C (C-*ipso*, C-*ortho*, C-*meta*, C-*para*) and N (blue lines for N PDOS and filled light blue for N p_z) of TPA molecule. With the help of the PDOS from DFT, we can understand better the valence photoelectron spectra of DPTA and TPA, and how this could be related to the electronic property of the molecule. For example, the electron-donating property of both TPA and DPTA molecules and the reason of the improved performance of D-π-A molecules which include a DPTA moiety are studied and understood by the PDOS calculations in Paper III.

6. Experiments

6.1 Gas-phase measurements

6.1.1 GasPhase beamline, Elettra

GasPhase is a beamline at the Elettra synchrotron radiation facility in Trieste, Italy, characterized by high resolution and high photon flux and devoted to research on gaseous systems. It is an undulator-based beamline with a monochromator consisting of a plane mirror and five spherical gratings. The beamline provides a photon energy range from 13 eV up to 900 eV and a photon spot size of around 200 μm at the target. The base pressure of the experimental chamber is in the 10^{-9} mbar range. However, when measuring a gas-phase sample, the pressure in the chamber can reach 10^{-5} mbar but, thanks to the differential pumping system, the pressure in the electron analyzer is kept within a safe working range. To get a better base pressure, a cryo-trap, cooled by liquid nitrogen, can be used during the experiments.

During our characterizations, the experimental chamber was equipped with a home-built effusive molecular oven nozzle [61] and a VG Scienta SES200 spectrometer mounted at the magic angle (54.7°) with respect to the beam of the linearly polarized incident light.

6.1.2 Gas-phase measurement set-up

Our gas-phase measurements were performed at the GasPhase photoemission beamline at the Elettra. A gas-phase photoemission experiment in general needs a constant gas flow in the analysis chamber. This task is not straight forward when dealing with big molecules such as phthalocyanines due to the difficulty to keep a steady molecular vapor flux at high temperature (ranging from 320°C to 435°C) for days, when acquiring data.

As a consequence, compared to the abundant Photoelectron Spectroscopy (PES) and Near Edge X-ray Absorption Fine Structure (NEXAFS) studies of thin films of phthalocyanines, only very few gas-phase measurements have been carried out. However, such experiments are important since they contribute significantly to the understanding of the electronic structure of the molecules and also for identifying the modification induced by the adsorption when the molecules are deposited on surfaces. Considering CoPc, its gas-phase characterizations could give insights into the molecular ground state configuration as isolated molecules. In the case of biphenylene instead, such studies enabled us to identify the influence of the molecular-substrate interaction to the molecular electronic structure when adsorbed at low coverage or as thin films. For TPA, DPTA and m-MTDATA, we could get a fundamental understanding of their electron-donating property.

As mentioned, the experimental chamber at the GasPhase beamline was equipped with a home built effusive molecular oven nozzle to heat and evaporate the molecules. Depending on the molecules, it is possible to choose a proper nozzle diameter to obtain the preferable molecular evaporation rate.

Compared to the small molecules such as biphenylene or TPA/DPTA, it is always difficult to evaporate molecules with high molecular weight, as CoPc's or m-MTDATA, since, despite the high evaporation temperature, one gets only a low evaporation rate. Moreover, phthalocyanines are often clogging the nozzle and requiring its replacement. We found that the best evaporation condition for CoPc was to use the largest size of the nozzle, i.e. removing the nozzle cap, resulting in an aperture size of about 1 cm in diameter. This led to a reduced sample density but we still gained in experimental time by preventing the nozzle from clogging, avoiding time-consuming changes of the CoPc sample and necessary cleaning procedures.

To further purify the samples from water, CO_2 as well as molecular residues from the synthesis, the sample powder was heated by gradually raising the temperature up to the evaporation temperature in the experimental chamber. This purification procedure always takes several hours before the experiments. We had to warm up the oven carefully, avoiding big temperature steps and preventing the cooling of the molecular flux which would condense at the nozzle clogging it (especially for phthalocyanine molecules). The cleanness of the molecular sample was usually checked by valence PES until no peaks due to contaminants, such as H_2O, CO_2 or other residues, could be seen in the spectrum. To have a constant flux, the count rate was also checked and compared each time by measuring the intensity of the valence peaks.

Especially during the CoPc gas-phase experiment, a cryo-trap cooled by liquid nitrogen was used during the measuring to improve the vacuum in the chamber,

6.2 Adsorption measurements

6.2.1 End-stations at synchrotrons

The I311 beamline at MAX IV laboratory

Biphenylene films were characterized at the photoemission branch of beamline I311 at MAX IV laboratory, the Swedish synchrotron radiation facility, in Lund [62]. I-311 was an undulator-based soft X-ray beamline (30 – 1500 eV), equipped with a modified Zeiss SX-700 monochromator. The spectroscopy end-station was equipped with a hemispherical electron energy analyzer (Scienta SES200) for high-resolution PES and NEXAFS. The manipulator in the analysis chamber was equipped with resistive heating and a cold finger which allowed to reach a temperature of about 70 K on the sample cooling with liquid nitrogen.

A heating band wrapped around a glass tube containing the biphenylene powder was used to deposit the molecules onto the surface by sublimation. The pressure in the analysis chamber and the preparation chamber, during the experiments, was kept in the low 10^{-10} mbar range.

With the permanent shut down of the MAX I, II and III accelerators on December 13, 2015, in preparation for the new MAX IV facility, I-311 is now in the history.

Materials Science beamline at Elettra

Materials Science beamline is a bending magnet beamline with a single grating monochromator similar in design to an SX-700 and located at the Elettra synchrotron (Italy). A bending magnet beamline is quite suitable for studies of organic molecules, for avoiding beam damage which would be caused by a too high beam flux. At this beamline, the light is mostly linearly polarized, with photon energy ranging from 22 to 1000 eV, allowing to investigate the geometric arrangement of molecules adsorbed on surfaces by angle-dependent NEXAFS. The spot size on the sample has a diameter of about 100 μm.

The experimental end-station includes a sample preparation chamber with a fast-entry load-lock and an analysis chamber. The sample transfer between these two chambers is done with the help of a long sample transfer arm. The sample holder has a special design allowing heating and temperature reading in the analysis chamber.

The sample preparation chamber is designed for preparing sample *in-situ*. It allows mounting different evaporators like for our experiment, when up to 3 evaporators were mounted to the preparation chamber. The base pressure of this chamber is usually in low 10^{-9} mbar range.

The analysis chamber is equipped with a Specs Phoibos 150 hemispherical electron analyzer; it is designed for surface science studies by PES and X-ray absorption spectroscopy. The angle between the incident light and the analyzer entrance is 60°. The chamber is equipped with a manipulator with X, Y and Z linear axis movements and polar angle rotations. The cleaning procedures of the samples, *i.e.* Ar^+ sputtering and annealing, are also done in the analysis chamber. The base pressure of the main chamber is usually in low 10^{-10} mbar range.

LowDosePES endstation at PM4 beamline at BESSY II

The LowDosePES is a permanent experimental station located at the PM4 dipole beamline at BESSY II synchrotron in Berlin, Germany. It is equipped with an Angle-Resolved Time-Of-Flight (ARTOF) spectrometer as well as a VG Scienta SES100 hemispherical analyzer.

For excitation, the ARTOF needs a pulsed source with a maximum repetition rate of few MHz. The BESSY II ring works in three modes, Standard Fill Pattern (Multi Bunch Hybrid), Single Bunch Operation and Low-alpha Multi Bunch Hybrid Mode. In Single Bunch Operation only one bucket with a bunch current of 13 mA is populated with electrons. The photon pulse train derived from this bunch has a frequency of 1.25 MHz. Single bunch operation is the most suitable operation mode for ARTOF experiments. However, only two weeks of single bunch operation twice a year are provided. For the other two hybrid operational modes, LowDosePES uses a chopper [63], *i.e.* a rotating wheel to achieve pseudo single bunch conditions. This wheel is installed at the intermediate focus of the beamline, allowing only one pulse per turn out of the 400 possible X-ray flashes at BESSY II storage ring, to fulfill the repetition rate of the pulsed source that ARTOF needs.

In our experiments, as shown in Figure 6.1, the end-station consisted of a fast-entry load-lock chamber (D), a radial distribution chambers transfer system ((E), also called “UFO”), a lateral preparation chamber (C), also called (“Racoon”), a vertical preparation chamber ((B), also called “top chamber”) equipped with LEED and the main experimental chamber (A) for spectroscopic experiments. The system is equipped with a manipulator with x, y modules, a z translation, a polar angle rotary platform and with a Janis cryostat which can reach a temperature as low as -269 °C (4 K) with liquid Helium cooling.

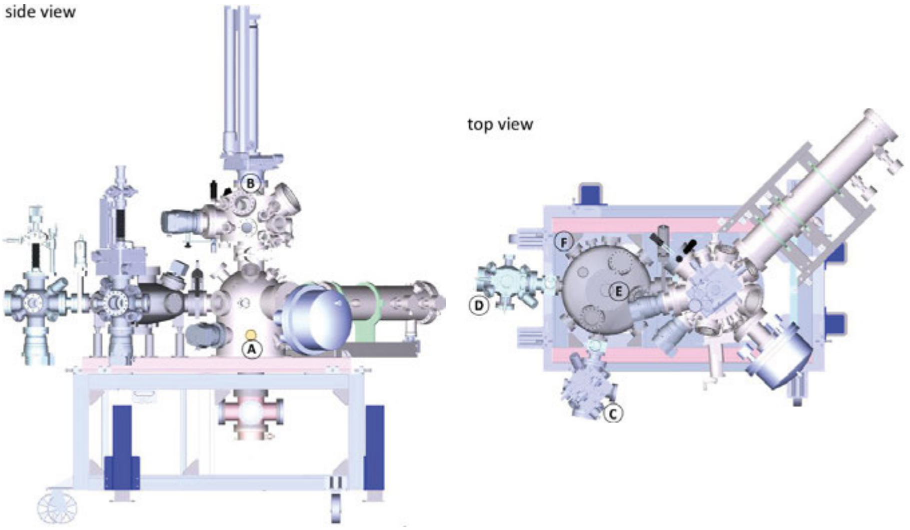

Figure 6.1. Sketch of the LowDosePES end-station: (A) Main experimental chamber equipped with ArTOF and hemispherical electron analyzers; (B, C) clean sample preparation chambers; (D) organic sample preparation chamber and load-lock; (E) transfer chamber with free ports for additional preparation chambers (F). Figure adapted from Ref. [47].

During our experiments, the base pressure in the Racoon chamber (after baking) was in low 10^{-9} mbar range. The base pressure in the main chamber was also in low 10^{-9} mbar range with sample (and manipulator) at room temperature or in low 10^{-10} range with helium cooling during the experiment. The thermal evaporator used in our experiments for depositing CoPc and melamine films was brought from Uppsala. For deposition of CoPc, the evaporator was mounted on the Racoon chamber while for melamine film it was mounted on the top chamber. The Racoon chamber was used to prepare the clean Au (111) surface by sputtering and annealing cycles.

6.2.2 Substrate preparations

Au (111)

The Au(111) single crystal, used in CoPc and melamine film experiments (Paper I, VI and VII in this thesis), was bought from MaTecK. The crystal was mounted on a molybdenum Omicron standard sample plate, used at Low-DosePES beamline at BESSY II. The crystal was fixed by a tantalum wire (diameter 0.3 mm) which was spot welded to the sample plate.

On the other hand, the Au(111) used for TPA and m-MTDATA (Paper IV and V) was from the Materials Science beamline and mounted in a special design to allow heating and temperature reading in the analysis chamber.

The Au (111) surface was prepared with standard Ar^+ sputtering and annealing (up to 500 °C) cycles. Usually, two cycles were needed, one cycle with the sample facing the sputter gun and the other cycle at 45 ° with respect to the sputter gun.

For the sputtering, the parameters were: Argon gas pressure in 10^{-6} mbar range, 1 kV, 10 mA emission current, usually for 20 minutes were usually used. The temperature for the annealing after the sputtering was read by both a pyrometer and/or a thermocouple located near the sample plate. The base pressure in the preparation chamber was always better than low 10^{-9} mbar range.

The cleanness of the Au (111) surface was then checked with the PES until the Au surface state was seen in the band dispersion spectra (with ArTOF) or no contaminants (for example no C1s signal) were seen in the spectra.

Cu (111)

The Cu (111) was used as the substrate for biphenylene films (Paper II in this thesis) investigated at I311 in Lund. The surface was prepared with the standard procedure of Ar^+ sputtering (1 kV, 20 minutes) and annealing (547 °C, 20 minutes) to clean and reconstruct the Cu (111) crystal surface. The surface cleanness was checked with PES until no signal from contaminations was detected.

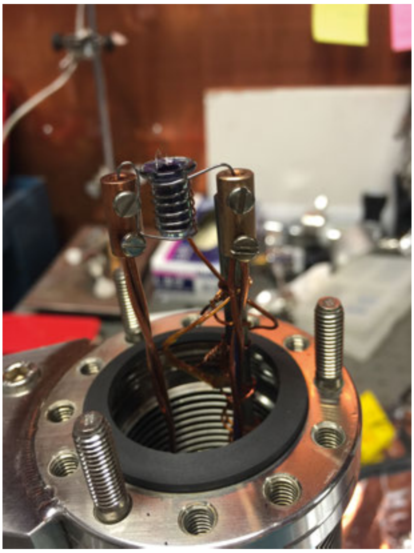

Figure 6.2. The evaporator used for CoPc deposition. Similar evaporator set-up was also applied to m-MTDATA and melamine depositions.

6.2.3 Molecular film prepared by evaporators

A thermal evaporator as shown in Figure 6.2 was used in this thesis for depositing thin films of CoPc, m-MTDATA and melamine, all molecules with high melting point (melting point above 120°). A filament made from a tantalum wire (diameter 0.5 mm) was wrapped around a quartz crucible (6 rounds). A molybdenum sheet was wrapped and inserted into the crucible to keep the temperature stable. A thermocouple wire was dipped into the crucible between the crucible and the molybdenum sheet. Finally, the molecule powder was filled into the crucible. We have found that the evaporation rate was quite reproducible with the used settings, *i.e.* even if we changed the filament and/or molecular sample, we could get almost same evaporation temperature at same filament current. Therefore, knowing the temperature we wanted to reach, the set-up allowed us saving sample preparation time since we did not need to find the filament current each time.

With this set-up, the evaporator could be mounted directly on the sample preparation chamber and baked together with the chamber before the experiment, resulting in a very good base pressure. With the evaporator on the chamber and pointing to the sample at a preferred short distance, a directional stable high-flux molecular beam towards sample can be achieved. This allowed a reproducible evaporation rate.

Cobalt Phthalocyanine (CoPc)

CoPc by Sigma-Aldrich (purity 97 %) was used of our experiments.

CoPc films of different thicknesses were grown on the Au (111) surface at Low-Dose endstation, BESSY II (Paper I) with the thermal evaporator as shown in Figure 6.2. The pressure in the Racoon chamber (preparation chamber) during deposition was in the high 10^{-9} mbar range.

m-MTDATA
m-MTDATA (powder, purity 98%, Sigma Aldrich) thin films were prepared *in-situ* on Au(111) by thermal deposition at Materials Science beamline, Elettra (Paper V). During the deposition, the quartz crucible was resistively heated to 190 °C. The thickness of the m-MTDATA films was controlled by the evaporation time and was also estimated by the attenuation of the PES Au 4f signal.

Melamine
Melamine powder was also purchased from Sigma Aldrich with a purity of 99%. Melamine films were characterized at the LowDose PES end-station, BESSY II (Paper VI and VII). During the deposition, the quartz crucible was resistively heated to about 120 °C. The monolayer sample was prepared by desorbing a thick film deposited at liquid nitrogen temperature. The corresponding N 1s / Au 3d intensity ratio was used to estimate the coverage of the 1.2 ML sample, which was further confirmed by fitting the corresponding N 1s level.

6.2.4 Molecular film prepared by glass tube

For the characterization of adsorbed biphenylene, and TPA, both molecules of low melting point molecules (melting $T < 120°$), a glass tube was used instead of the evaporator since it could not be mounted onto the chamber and properly baked without damaging the molecules. A glass tube instead was connected to the preparation chamber through a leak valve and pumped separately by a dedicated pumping system. A heating band wrapped around the glass tube containing the molecular powder was used to rise the temperature of the molecular sample. The molecular sample (in the tube) was usually degassed by heating the molecule up to the evaporation temperature and pumping them away by the separate pump system for 3 to 5 times. During the deposition instead, the glass tube was heated to the evaporation temperature leaving the leak valve fully open, allowing the molecule to flow into the chamber. Compared to the evaporator, the deposition via the glass tube produced a non directional molecular beam, which was also farther away from the sample, resulting in a low evaporation rate.

Biphenylene
The biphenylene powder (99% purity) was bought from Sigma-Aldrich.

Before the deposition, the biphenylene was outgassed at the temperature around 100 °C for 3 to 5 times. The same temperature was used to evaporate and deposit biphenylene on the freshly prepared Cu (111) crystal (Paper II). It is known that at room temperature biphenylene only forms a monolayer. We needed to cool the Cu (111) crystal down to -183 °C with liquid nitrogen for increasing the sticking coefficient of biphenylene and getting molecular films of different thicknesses.

The monolayer coverage was obtained by increasing the temperature up to -53 °C to desorb the thick biphenylene multi-layer. The similarity of the monolayer as deposited and desorbed was also checked afterwards.

The pressure in the preparation chamber during the depositions was in the low 10^{-8} mbar range.

Triphenylamine (TPA)

The characterization of adsorbed TPA on an Au(111) substrate was performed at Materials Science beamline, Elettra (Paper IV). Similar to biphenylene, TPA did not adsorb in more than one monolayer on Au(111) at room temperature. For TPA we used an evaporation temperature of about 95°C, resulting in a pressure in the low 10^{-7} range in the preparation chamber.

7. Summary of papers

For a full characterization of the electronic structure of the different investigated molecules and films presented in this thesis, I used a combination of a variety of experimental techniques along with DFT calculations. We were interested in identifying the modification of the electronic structures of the studied systems by, for example, combining/comparing the results of:

- gas-phase experiments (PES and NEXAFS) *vs* single molecule DFT calculations (Paper I, III, V, VI);
- solid-state experiments (PES and NEXAFS) *vs* DFT calculations on adsorbed systems (Paper VI);
- gas-phase *vs* solid-state experiments (PES and NEXAFS) (Paper I, II, IV, V, VI);
- building-blocks *vs* complex molecules (Paper III, V).

The combination and comparison of the experimental and theoretical results of free and adsorbed molecule allowed us to study the electronic structure modifications of the studied system due to:

- substitutions (Paper III);
- increasing complexity of the molecules (Paper V);
- molecule-substrate interactions (Paper I, II, IV, V);
- intra-molecular H-bonding interactions (Paper VI).

These electronic structure modifications (compared to the pristine, simple, free molecules) may bring new insights into molecular properties which can be relevant for tuning the functionality of novel materials.

7.1 Electronic structure of CoPc (Paper I)

7.1.1 Gas-phase measurements *vs* DFT calculations: CoPc electronic ground state configuration and atomic character of HOMO

As mentioned in previous chapters, only few gas-phase measurements have been done on phthalocyanines (Pc's), likely due to the difficulties to obtain a stable Pc molecular flux at high temperature for a long time [64]. However, with this kind of experiments, we could significantly contribute to the debate about the electronic structure of CoPc. In fact, we could address (in Paper I) the molecular ground state configuration and the Highest Occupied Molecular Orbital (HOMO) character of CoPc, for a long time under discussion.

Previous experimental and theoretical studies have provided controversial results, suggesting the electronic ground-state configuration of CoPc to be either $^2A_{1g}$ [65] or a mixture of $^2A_{1g}$ and ^2E_g, where ^2E_g would be the first excited state at slightly higher energy [66, 67, 68]. Other studies have proposed instead the ^2E_g configuration with a 3d hole in the e_g state as the ground state of CoPc [69].

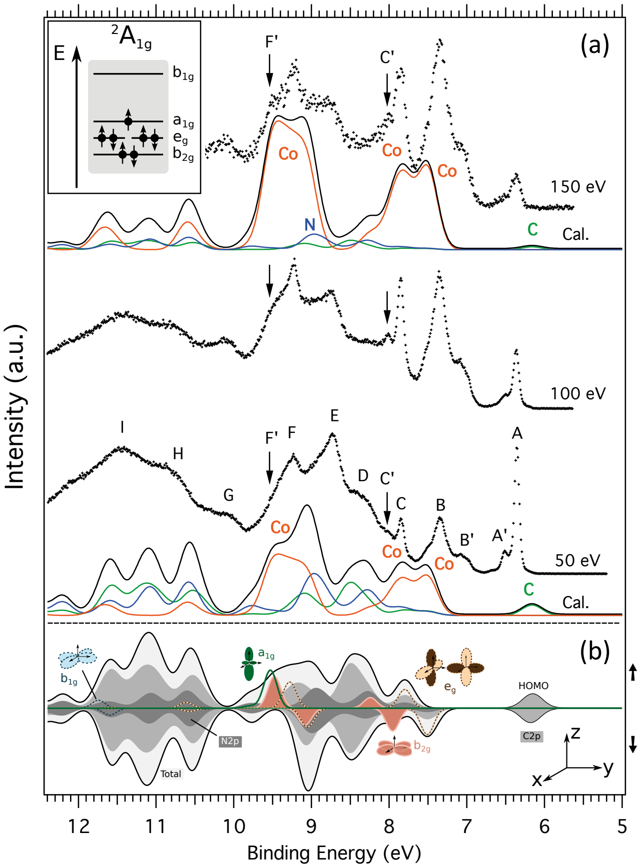

Figure 7.1. (a) Experimental valence-state photoemission spectra of CoPc in the gas-phase with the cross-section corrected DFT calculation results. (b) Calculated valence electronic structure with orbital- and spin-resolved atomic contributions. Inset: simplified Co *3d* electronic configuration corresponding to the $^2A_{1g}$ found by our DFT calculation to be the ground state of CoPc, and applied in the shown calculations. Figure adapted from Paper I.

As shown in Figure 7.1, our DFT calculations, performed considering the $^2A_{1g}$ configuration to describe the ground state of CoPc, are in very good agreement with the experimental results, confirming that this configuration can correctly describe the molecular ground state. This result is further proved by the good agreement between the experimental and theoretical Co $L_{2,3}$-edge NEXAFS as shown, in more details, in Paper I.

Also, the character of the highest occupied molecular orbital (HOMO) of CoPc molecules has been under debate for a long time. This orbital has been suggested either to be of a metal 3d-like character and localized on the central Co atom [69, 70] or to originate from the organic ring of the molecule [71, 72]. In Paper I, we addressed this aspect too, by comparing valence photon energy dependent photoemission measurements of CoPc in gas-phase with DFT calculations. The DFT results predict the HOMO feature at 6.12 eV, which is in good agreement with the measured HOMO binding energy at 6.38 eV as shown in Figure 7.1. The DFT calculations also distinguish the atomic character of the peaks in the valence spectrum (from A to H) as related to molecular states of C, N and Co atomic character. Especially, the calculations indicated that the HOMO fully originates from the C 2p states related to the a_{1u} molecular orbital, coming from the C-C hybridization of π type orbitals.

These theoretical results are confirmed by the gas-phase photon energy dependent spectra shown in Figure 7.1 (a), measured by taking advantage of the different photoemission cross-sections that C and N atoms have with respect to the Co metal [39], (details see Section 3.3). In Figure 7.1, we can clearly discern the HOMO (at about 6.38 eV) decreasing in intensity with increasing photon energy. Considering that the cross-sections of C and N decrease dramatically for photon energies varying from 50 eV to 150 eV, we can conclude that the HOMO is mostly due to the contributions from the organic ligand of the molecule. On the other hand, peaks B, B', C, C', F, and F' have significant Co 3d contributions, also in agreement with the theoretical results.

7.1.2 CoPc HOMO characterization: gas-phase *vs* solid-state measurements

Even if our gas-phase measurements and DFT calculations have indicated the ligand character of the CoPc HOMO, we performed a more careful study to identify if any metal character could be hidden underneath the HOMO intensity. Then we deposited CoPc films of different coverages on an Au (111) surface to get a further confirmation of our conclusions from solid-state results.

Figure 7.2 shows the comparison between the valence photoemission results of CoPc in gas-phase and of a thick film deposited on Au (111). Apart from an overall broadening, the spectrum of the film has a quite similar appearance as the gas-phase results, indicating that the CoPc film maintains a molecular-like character, as already observed for other metal Pc's films [40]. The molecular character of the CoPc film makes it possible to study the HOMO origin through an investigation of CoPc adsorbed on a surface.

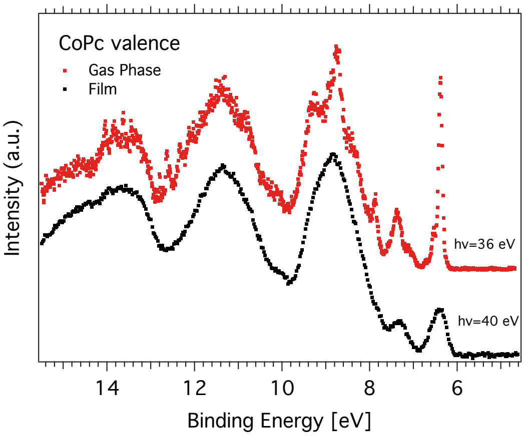

Figure 7.2. Comparison between the valence photoelectron spectra of gas-phase CoPc, taken with photon energy of 36 eV (red) and of a CoPc thick film absorbed on Au (111), measured with 40 eV (black). The spectrum of the film is shifted and aligned to the gas-phase spectrum with the HOMO at 6.38 eV. Figure taken from Paper I.

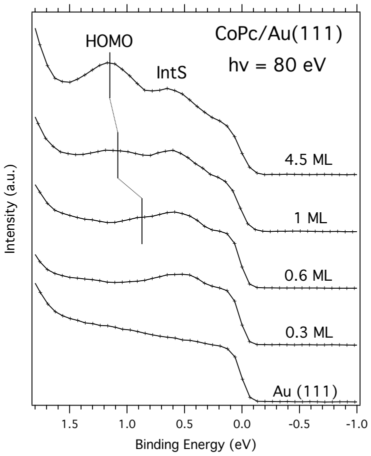

Figure 7.3. Valence photoelectron spectra of CoPc deposited on Au(111) at the given molecular thicknesses, taken with a photon energy of 80 eV. The binding energy is calibrated to the Fermi level of the Au(111) substrate. Figure taken from Paper I.

Figure 7.3 shows valence PE spectra of CoPc films of different thickness adsorbed on Au(111). Compared to the thick film in Figure 7.2, the CoPc thin films show, already at very low molecular coverage (0.3 ML), a new peak at lower BE than the HOMO (at 0.55 eV) while the HOMO is clear visible at 1.15 eV for higher molecular thickness. The new peak at 0.55 eV is the so-called “Interface State” (IntS) ascribed, in previous studies, to a new state of fully metallic character [73, 74]. It would originate from the interaction between the Co 3d out-of-plane orbitals and the delocalized states of the Au (111) surface.

Then we performed a photon energy-dependent valence photoemission investigations following the intensity variation of the HOMO and of the IntS, the latter known to be purely metallic. The results, already described in Section 3.3, give a further confirmation about the organic ligand character for the HOMO of CoPc and purely metallic character for the IntS, *i.e.* in agreement with our gas-phase and DFT results as well as with previous assignments of the IntS [71] [74] [73].

7.2 Biphenylene films (Paper II)

7.2.1 Biphenylene/Cu(111): interface interaction

The C 1s photoelectron spectra of biphenylene films of high (100 Å), intermediate (30 Å) and low (7 Å) coverage deposited on Cu(111), together with the gas-phase results are shown in 7.4.

The profile of the main line and its BE position change as a function of biphenylene thickness. The BE shift is mainly due to the different core-hole screening efficiency by the metal substrate (Cu) for increasing molecular coverage.

All the C 1s spectra of different molecular coverages show a broad low-intensity feature at about 6 eV from the main line, attributed to intra-ring (local) excitations accompanying the photoemission process [51, 75, 76]. Moreover, all the C 1s photoelectron spectra, including the gas-phase results, but with the only exception of the low coverage film, have shake-up features at about 2.7 eV from the main line, ascribed to inter-ring (non-local) excitations [77]. Such inter-ring excitations have been observed and studied for more complex molecules as for example C_{60}, and it would be caused by the charge transfer to the core-hole site from rings far away from the ring where the core-hole is located. In case of biphenylene, it would be due to the charge moved toward the core-hole site from the other ring of the molecule.

As mentioned, this shake-up feature is missing in the spectrum of the low coverage sample of biphenylene (red line in 7.4 (c)), indicating a modification of the molecular electronic structure due to the interaction with Cu(111) surface. A further sign of this interaction is the asymmetric C 1s photoemission line shape of low coverage sample as often observed for low coverage films of carbon-based molecules on metallic substrates. Such asymmetric profile is related to the molecule-substrate interaction and is usually attributed to the screening of the core-hole by the conduction electron of the metals, *i.e.* from states just below the Fermi level (E_F) to empty state just above E_F of the substrate.

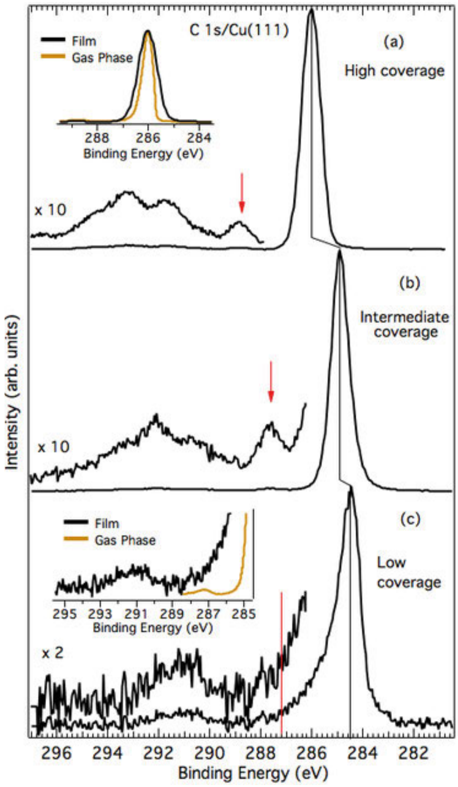

Figure 7.4. C 1s photoemission spectra of biphenylene films of (a) high (100 Å), (b) intermediate (30 Å) and (c) low (7 Å) coverage, acquired with a photon energy of 400 eV and an overall resolution of about 90 meV. Biphenylene shake-up regions have been enlarged for sake of clarity. Red arrows and line indicate the position of the shake-up peak at about 2.7 eV from the main line. Insets: (a) Comparison of C 1s spectra of high coverage film and gas-phase biphenylene; (c) comparison between the low coverage film and the gas-phase shake-up regions. The gas-phase spectrum is reprint from [78]. Figure taken from Paper II.

7.2.2 Biphenylene/Cu(111): molecular arrangement by NEXAFS

The characterizations of biphenylene molecular arrangement on Cu (111) at different coverages were also studied by C K-edge NEXAFS. The results reveal the variation of the molecular arrangement depending on the thickness of the film.

As described in Section 4.2, NEXAFS is a powerful tool to study the molecular arrangement on surfaces. In Figure 7.5 a), we display the NEXAFS results for the high coverage film taken at Normal Emission (NE) and Normal Incident (NI) geometries. For high coverage film, the first two π^* resonances at about 285.0 eV and 287.0 eV are enhanced in NI, indicating that the molecules are preferentially standing on the surface. On the other hand, for low deposition, shown in Figure 7.5 b), taken at NI and Grazing Incident (GI) geometries, an opposite polarization dependence is observed, indicating that the molecules prefer lying on the surface at such a coverage.

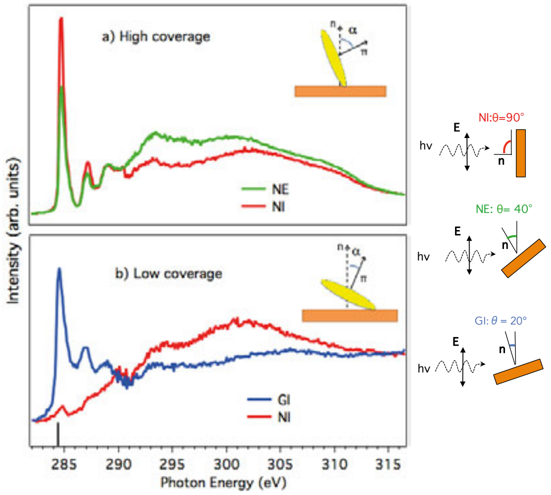

Figure 7.5. Polarization dependent NEXAFS for two film thicknesses: a) High coverage film and b) low coverage film. Each film was measured at the indicated geometry, varying the angle θ between the polarization vector $\mathbf{E}$ of the incident radiation and the surface normal of the Cu(111) sample. Figure adapted from Paper II.

7.3 Characterizations of TPA, DPTA and m-MTDATA (Paper III, IV & V)

As described in Section 2.1.2, TPA, DPTA and m-MTDATA are very promising electron donor molecules for application in optoelectronic devices. Their systematic study allows to understand the electronic structure variation from the simplest TPA building block to m-MTDATA, a more complex molecule. Moreover, we also investigated these molecules adsorbed on surfaces to fully characterize the molecule-surface interactions and get insights in their functionality when implemented in real devices. In details, we performed the following:

1. Comprehensive experimental characterizations of free TPA supported by the DFT calculations (Paper III).
2. Comprehensive experimental characterizations of free DPTA (a thiophene-analog of TPA) also with DFT supports (Paper III)
3. Comprehensive experimental characterizations of free m-MTDATA (of which TPA is the building-block) with also DFT calculations (Paper V).

4. Characterization of the electronic structure modifications due to the adsorption of TPA and m-MTDATA on an Au(111) surface (Paper VI & V).

7.3.1 Electronic structure characterization of TPA molecule (Paper III)

We recall the TPA molecular structure in Figure 7.6 (a). In Paper III, we preformed a thorough electronic structure characterizations of TPA, benefitting of the combination of core and valence level PES and NEXAFS, with DFT calculations.

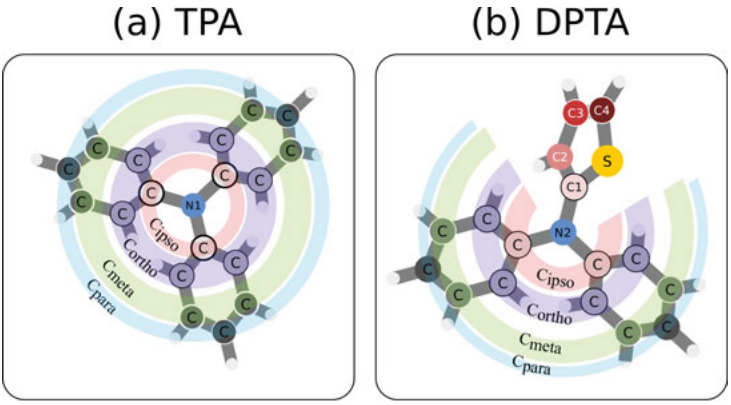

Figure 7.6. Molecular structure of (a) TPA and (b) DPTA. Figure taken from Paper III.

Evidences of lone pair electron delocalization and the donor property

The experimental C 1s PE spectrum of gas-phase TPA and the corresponding results from DFT calculations are shown in Figure 7.7 (top panel). Two peaks are observed at 289.90 eV and 290.90 eV, ascribed to the C-*ipso* and other C atoms, respectively. This is also confirmed by the fitting. The intensity ratio between peak 2 and peak 1 of the fit, is found to be 1: 4.92, very close to the expected intensity ratios between the non-equivalent C atoms of the molecule, *i.e.* 1: 5. As shown in Table 7.1, the BEs from the fit of the experimental C 1s spectrum correspond also well to the DFT calculations which give still more details about the intensity contributions and the energy positions of different C atoms of TPA.

The results show clearly that the BEs of different C atoms are in sequence:

$$BE(para) < BE(ortho) < BE(meta) < BE(ipso), \qquad (7.1)$$

where the labelling, *i.e.* C-*para*, C-*ortho*, C-*meta* and C-*ipso*, are described in Figure 7.6 (for more details refer to Section 2.1.2). The BE sequence can be well explained by the competition between the delocalization of the N lone pair electrons (introduced in Section 2.1.2) and the electronegativity of the nitrogen atom.

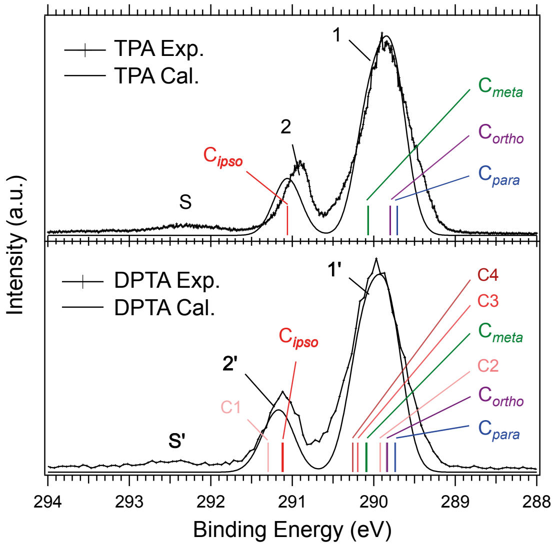

Figure 7.7. Experimental C 1s PE spectra of gas-phase TPA and DPTA measured with a photon energy of 382 eV, compared with the corresponding DFT-calculated spectra. The bars mark the calculated ionization energies of the individual carbons. Figure taken from Paper III.

C 1s of TPA				
Experimental			Theoretical	
Peak	BE (eV)	FWHM (eV)	Peak	BE (eV)
	289.64	0.58	C-*para*	289.71
1	289.76	0.53	C-*ortho*	289.80
	290.01	0.50	C-*meta*	290.07
2	290.94	0.38	C-*ipso*	291.06
S	292.32	0.80		

Table 7.1. Theoretical (right column) and experimental (left column) binding energies (BEs) of peaks 1, 2 and S for TPA obtained by a fit of the C 1s photoelectron spectrum. The right column contains the calculated C 1s BEs of the non-equivalent C atoms of TPA, shown as bars in Figure 7.7. The calculated values have been shifted by +1.09 eV to align the main peaks of the experimental and theoretical spectra. Table adapted from Paper III.

In details, C-*para* atoms are more distant from the central N atom and therefore less affected by its electronegativity, while they experience the electron-donating effect of the N lone pair which is delocalized on both *para* and *ortho* carbon atoms. The carbon atoms in the *ortho* position are at slightly higher BE because of their vicinity to the electronegative N atom. At further higher BE we found the carbon atoms in *meta* positions that do not experience the N lone pair electron donation but only the nitrogen electronegativity. Finally, the theoretical BEs underneath peak 2 are due to the carbon atoms directly bound to the central N atom, C-*ipso*, also confirming the conclusions drawn by the experimental fit.

The effect of N lone pair electron delocalization can also be found in the valence photoemission spectrum as shown in 7.8. The significant contribution from the p_z orbital of the N, C-*ortho* and C-*para* atoms to the HOMO of TPA well reflects the N lone pair delocalization.

The donor property of a molecule depends mostly on the HOMO. For example, the ionization potential (IP) of the HOMO can be roughly used to judge if a molecule is a good donor [11, 12, 79], such that a low IP energy will promote the electron donation. The N p_z (lone pair orbital) PDOS of TPA contributes mostly to the occupied states of lower BE, especially to the HOMO. Then the result shows that the electron-donating property of TPA are largely related to the lone pair electrons of N.

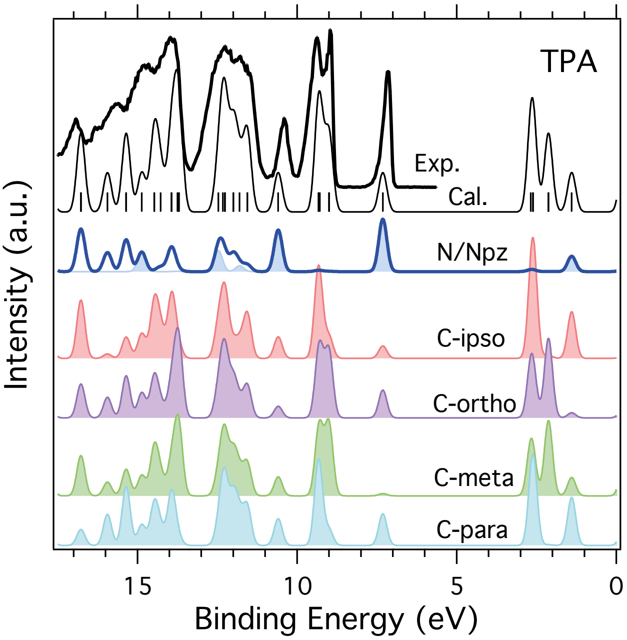

Figure 7.8. Valence PE spectra of TPA in comparison with the corresponding DFT-calculated spectra. The partial density of states (PDOS) of individual C and N are also presented. Figure adapted from Paper III.

Pre-edge of N K-edge NEXAFS of TPA

For the full characterization of TPA, we also performed NEXAFS measurements, allowing to probe the molecular empty density of states.

Figure 7.9 shows the N K-edge NEXAFS of TPA in comparison with DFT-calculated spectra, discerning the contributions from the I_z (out-of-plane orbitals) and I_{xy} (in-plane orbitals), considering the plane defined by the C-N bonds. The first π^* resonance peak is found at 403.00 eV and is ascribed to transitions to out-of-plane orbitals, LUMO+5.

As shown in Figure 7.9, by a careful analysis of the spectrum, we find a small pre-edge feature in the N K-edge NEXAFS of TPA (feature P) at about 402.20 eV, also predicted by our DFT calculation and attributed to transitions from N 1s to LUMO+1, ..., LUMO+4 for TPA. These unoccupied states contain no contribution from out-of plane molecular orbital and the intensity of this pre-edge peak is related only to in-plane components.

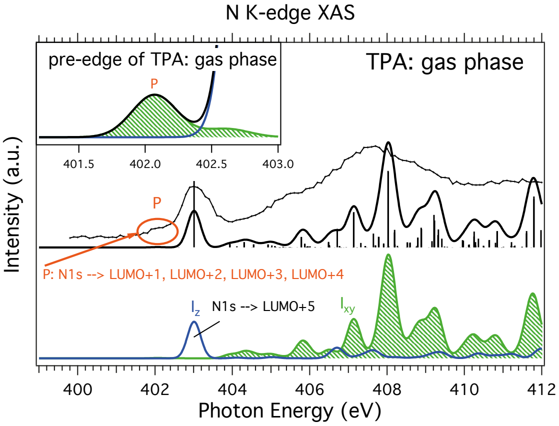

Figure 7.9. Experimental N K-edge NEXAFS of TPA and calculated contributions of I_z (out-of-plane orbital, N $2p_z$) and I_{xy} (in-plane orbital, N $2p_x$ and $2p_y$ orbitals). Inset: enlargement of the simulated pre-edge energy range (P) of the N K-edge NEXAFS spectrum of TPA. Figure adapted from Paper III.

In fact, the theoretical analysis on the molecular orbital population of the unoccupied orbitals reveals that the LUMO+5 orbital has significant nitrogen contribution, explaining the main π^* resonance intensity at 403.00 eV (due to transition to LUMO+5). On the other hand, LUMO+1, LUMO+2, LUMO+3 and LUMO+4 have negligible N character getting mainly contributions from the C atoms, and giving only a very weak intensity in the N NEXAFS spectrum, *i.e.* the pre-edge feature. Refer to Paper III for more details.

7.3.2 DPTA *vs* TPA: substitution effect (Paper III)

DPTA is another molecule which has attracted much attention due to its good electron donating properties. In fact, DPTA has been also used as the donor moiety in bigger Donor-Acceptor-Acceptor (D-A-A), since it seems to improve the charge separation and then the performance of device implementing these complexes. DPTA has a molecular structure very similar to TPA, with the difference that a phenyl is replaced by a thiophene ring. This results in a further differentiation of the C atoms (C1, C2, C3 and C4 of the thiophene ring, see Figure 7.6 (b) and Section 2.1.2), and an additional S atom which contribute to the electronic structure of the molecule. Similarly to TPA, as shown in Figure 7.7, the C 1s BEs of DPTA are also affected by the competition between the lone pair delocalization and the electronegativity of the nitrogen atom, but, additionally, they are also affected by the S lone pair delocalization over the thiophene ring. Finally, BEs of different C atoms of DPTA are in the sequence (refer to Paper III for more details):

$$BE(para) < BE(ortho) < BE(C2) < BE(meta) < BE(C3) < BE(C4) < BE(ipso). \tag{7.2}$$

New shake-up transitions

The substitution of a phenyl with a thiophene ring in DPTA brings significant modifications to the electronic structure compared to the TPA case, as it can be observed looking at the shake-up intensities in the C 1s and N 1s PE spectra.

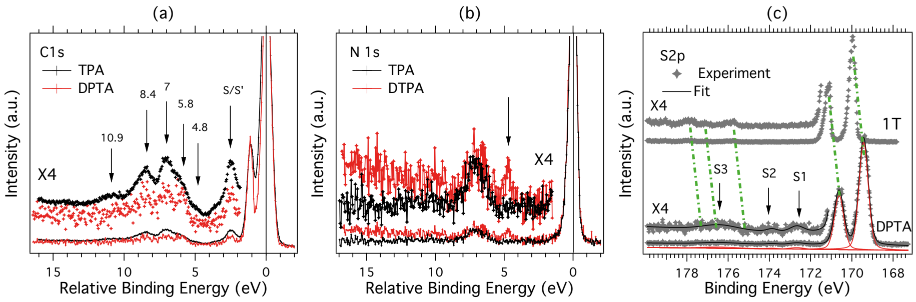

Figure 7.10. Comparison of the shake-up intensities observed in the C 1s (a) and N 1s (b) PE spectra of TPA and DPTA, and in the S 2p photoelectron spectrum of DPTA and thiophene (c). Figure adapted from Paper III.

Figure 7.10 (a) shows the C 1s shake-up spectra of TPA and DPTA displayed on a relative BE scale. The shake-up features are quite similar in the two molecular spectra with the exception of the intensity due to the different molecular structure of DPTA which has one phenyl ring less than TPA.

The N 1s spectrum of DPTA has similar shake-up as TPA at around 7 eV from the main line. However, there is an extra shake-up at 4.7 eV from the main line of DPTA (arrow in Figure 7.10 (b)), indicating that the thiophene-substitution has opened new transition channels with respect to TPA.

Moreover, as shown in Figure 7.10 (c), the S 2p PE spectrum of DPTA also shows two extra shake-up satellites (S1 and S2) with respect to the free thiophene. They are ascribed to new shake-up transitions allowed in DPTA by the modification of the electronic structure of the thiophene ring when it is part of the DPTA molecule.

C K-edge NEXAFS of DPTA: core-hole effect

As a result of the thiophene substitution, DFT calculations have to take in consideration more components than TPA, when disentangling the atomic contribution to the C K-edge NEXAFS of DPTA, *i.e.* including C1, C2, C3 and C4 contribution from the thiophene ring (for NEXAFS results of DPTA, refer to Paper III).

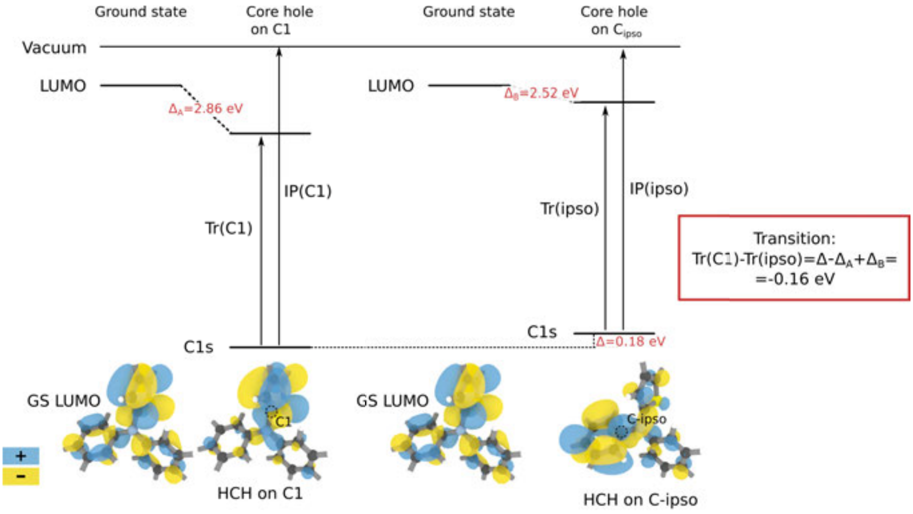

Figure 7.11. The core-hole on C1 perturbs the electronic structure of the ground state of DPTA, resulting in different transition energies compared to the core-hole in C-*ipso*, *i.e.* not following the sequence of the C 1s PES BEs of the different carbons. Figure taken from Paper III.

By a carefully analysis of the different contributions, we found that the transition energy of each C atoms is not only affected by the C 1s PES chemical shift of the non-equivalent C atoms, but instead they are also differently perturbed depending on where the core-hole is located, *i.e.* on the phenyl or thiophene rings. This means that the energies of the transitions to the empty states do not follow the sequence of the BEs shown in Equation 7.2. This is illustrated and explained in Figure 7.11, which shows how the energy position of the LUMO varies depending on either the core-hole site is on the C1 atom of the thiophene or C-*ipso* of a phenyl ring. The resulting transition energies (Tr) are affected such that $Tr(ipso) < Tr(\mathrm{C1})$, although C 1s PES BE(*ipso*) is higher than the C 1s PES BE(C1).

Moreover, as illustrated by the isosurfaces of Figure 7.11 the LUMO in the ground state is mostly localized over the thiophene moiety, with only small contributions from the phenyl rings. In presence of a core-hole on the thiophene C1, the contribution from the phenyl rings to the LUMO further decreases. When instead the core-hole is localized on the phenyl carbons C-*ipso*, the LUMO becomes mostly localized on the phenyl ring of the core-hole site, with only small contribution from the thiophene and the other phenyl rings.

Sulphur contribution to the empty density of states: enhanced acceptor property

As shown in Figure 7.12 (a), similar to TPA, the HOMO of DPTA is mainly contributed by the N p_z orbital and the C-*ortho* and C-*para* as derived from the N lone pair electron delocalization. In addition, the DPTA HOMO receives contributions from the thiophene ring, in particular from C2 and C4, as also expected by the N lone pair electron delocalization on the thiophene ring, and only little from the S atom (refer to the resonant electronic structure in Section 2.1.2).

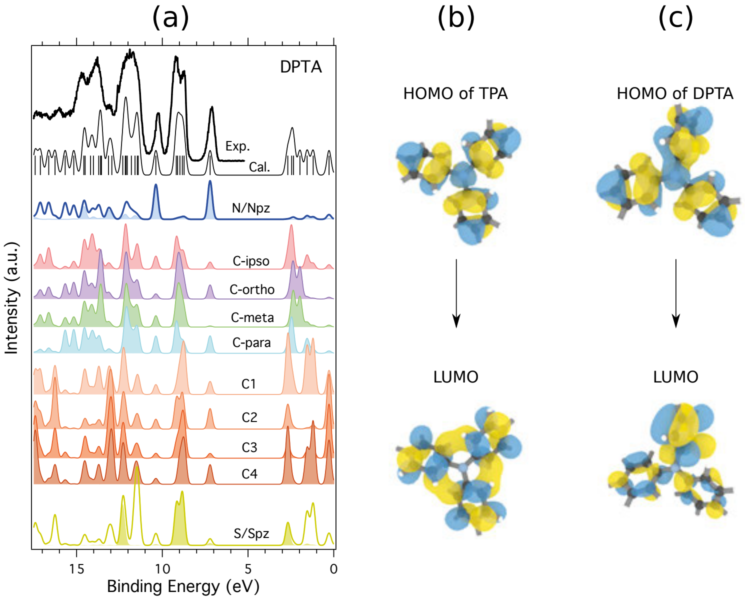

Figure 7.12. (a): Valence PE spectrum of DPTA measured with 100 eV photon energy compared with the corresponding DFT-calculated spectrum (black line). The PDOS of C, N and S are also given. (b) and (c): ground state HOMO and LUMO of TPA and DPTA. Figure adapted from Paper III.

The electron-donating properties of both TPA and DPTA are ascribe to the N lone pair electrons which strongly contribute to the HOMO level. The substitution of thiophene in DPTA decreases only slightly the HOMO ionization energy, not modifying much the electron-donating property. On the other hand, comparing with TPA, as shown in Figure 7.12 (b) and (c) the LUMO of DPTA is contributed by the S 3p orbitals and is strongly localized on the thiophene ring, indicating that the thiophene ring introduces a slight acceptor character to the molecule. This result probably explains why DPTA can be successfully used in Donor-π-Acceptor molecules. It has been shown [20] that the thiophene maintains a coplanar orientation with the acceptor part of these molecules, keeping the π-conjugation over the whole molecular backbone. In this way it behaves like a bridging unit providing a more efficient charge separation upon excitation.

7.3.3 Modification of the electronic structure due to the increased molecular complexity (Paper V)

The characterization of m-MTDATA, by gas-phase measurements and DFT calculations, are present in Paper V.

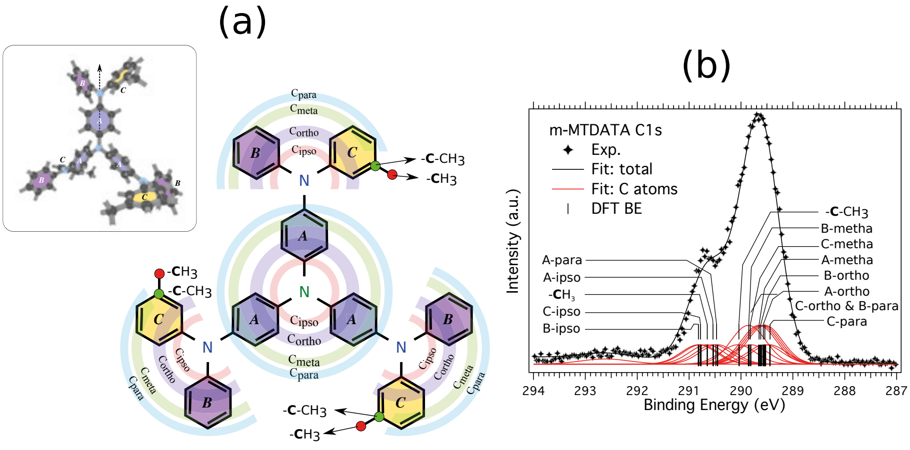

Figure 7.13. (a) Molecular structure of m-MTDADA. There are 14 kinds of carbon atoms. Following the nomenclature of benzene-derived compounds, we indicated them as C_{ipso}, C_{ortho}, C_{meta} and C_{para} in each chemically different phenyl ring (***A***, ***B*** and ***C***), getting in total 12 chemically distinct carbon atoms, then 2 other carbons related to the methyl group, *i.e.* **-C**-CH$_3$ (green circle) and -**C**H$_3$ (red circle). Inset: relaxed molecular structure of m-MTDATA: the twisting of every phenyl makes it a very complex structure. (b) C 1s PE spectrum of gas-phase m-MTDATA with 14-peak fit according to the DFT results. Figure adapted from Paper IV.

Compared to TPA, m-MTDATA has a more complex molecular structure as shown in Figure 7.13 (a) with 14 kinds of chemically non-equivalent C atoms which all contribute to the core level C 1s and C K-edge NEXAFS spectra (refer to Paper V). In Figure 7.13 (b), we show the C 1s PE spectrum fitted by using the 14 different components at the BEs suggested by our DFT calculations. Similar to TPA but more complicated, the N electronegativity and the nitrogen lone pair electron delocalization affect the C 1s PES spectrum of m-MTDATA.

Chemically non-equivalent N

The m-MTDATA N 1s PE spectrum measured in gas-phase is shown in Figure 7.14 (b), with a fit taking into account the contributions coming from the different nitrogen atoms according to our DFT calculations (Figure 7.14 (a)). Apart of the different BE (0.31 eV), the PES N 1s line of m-MTDATA is 0.1 eV broader than the N 1s peak of TPA (Figure 7.14 (c)), mainly due to the contributions from the two non-equivalent types of nitrogens of m-MTDATA: the contribution of the central N is found at lower binding energy whereas that of the three peripheral N atoms at about 0.14 eV higher binding energy according to the DFT calculations.

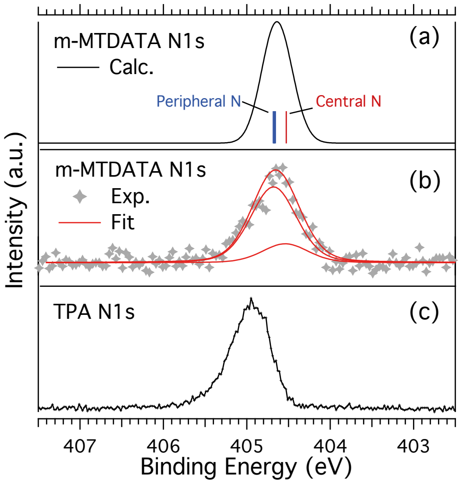

Figure 7.14. Comparison of the experimental N 1s PE spectrum of m-MTDATA measured in gas-phase (b) and the DFT calculated results (a), shifted +0.74 eV to align with the experimental spectrum. In (c) the N 1s PE spectrum of gas-phase TPA is reported. Figure taken from Paper V.

As shown in Figure 7.15 (e), the N K-edge NEXAFS of m-MTDATA resembles the spectrum of TPA. The first resonance feature of m-MTDATA seems to be broader than the corresponding feature of TPA, especially at the lower photon energy side, even if the high noise of the spectrum should also be considered. This broadening can be explained by the contributions from the chemically non-equivalent N atoms as shown by our calculations in the Figure 7.15 (a), resolving central and peripheral N contributions.

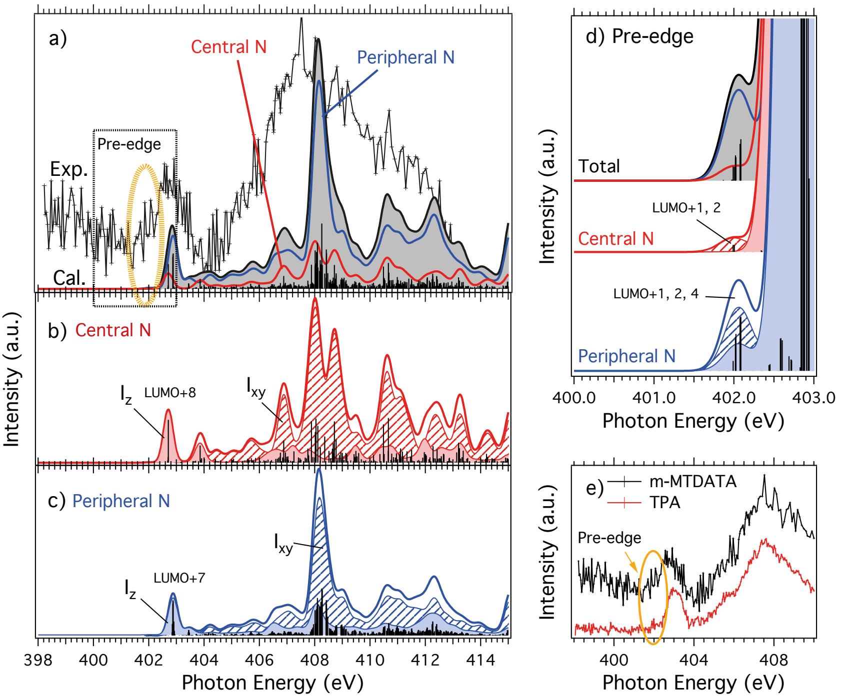

Figure 7.15. (a) Comparison between experimental (Exp., black line with markers) and calculated (Cal., solid black line with filled grey) N K-edge NEXAFS spectra, resolving the contributions from the central and peripheral N atoms. The PDOS of out-of-plane (I_z, filled) and in-plane (I_{xy}, pattern) orbitals of central (red) and peripheral N (blue) are resolved in (b) and (c), respectively, with respect to the planes defined by each N-C_3 bond. The pre-edge region (square in (a)) is enlarged in (d). (e) Comparison between the experimental N K-edge NEXAFS spectra of m-MTDATA and TPA. Figure taken from Paper V.

The calculations, presented in the Figure 7.15 (b) and (c), give the transition energies for the chemically non-equivalent N atoms. Considering the plane defined by the three N-C bonds (N-C_3), the calculations also resolve the contribution to the spectral intensity from the in-plane (I_xy) and out-of-plane (I_z) orbitals. In this way, we find that the first resonance peak would correspond to the electron transitions into out-of-plane states (I_z) from the central N 1s to LUMO+8 and peripheral N 1s to LUMO+7, whereas for TPA, the corresponding feature is due to the transition to LUMO+1, +2, ..., +4 orbitals, which are also out-of-plane orbitals.

N K-edge NEXAFS: pre-edge feature of m-MTDATA

In Figure 7.15 (e), the m-MTDATA N K-edge NEXAFS spectrum also presents a pre-edge feature like TPA. As shown in Figure 7.15 (d), most of the intensity of the pre-edge comes from the peripheral N atoms, as expected from the molecular stoichiometry ($\times 3$).

We have shown previously that the pre-edge observed in the N K-edge NEXAFS spectrum of TPA was due to the transitions to LUMO+1, +2, up to LUMO+4 orbitals including only in-plane-orbitals, whereas for m-MTDATA, as shown in Figure 7.15 (d), the transitions are different and the intensity gets also a little contribution from the out-of-plane orbitals of the peripheral N atoms. In more details, for the central N of the more complex m-MTDATA, the pre-edge is totally ascribed to the in-plane orbitals, as for TPA, but only due to the transitions towards the LUMO+1 and LUMO+2 orbitals, while for the peripheral nitrogen atoms, the pre-edge intensity is mostly due to transitions to the LUMO+1, LUMO+2 and LUMO+4 orbitals with mostly in-plane (N $2p_{xy}$) and minor out-of plane components (N $2p_z$).

The outermost valence features characteristic of m-MTDATA

Figure 7.16 a) shows the valence photoemission spectrum of m-MTDATA, characterized by a 3-peak feature at the outermost binding energy region: at 6.3 eV (HOMO), 6.9 eV (HOMO-1) and 7.5 eV (HOMO-2), to be compared with the TPA HOMO found at 7.17 eV

The calculated PDOS shows that these 3 peaks have both C and N characters. Moreover, the central N (marked CTR in Figure 7.15) and peripheral N (PPH in Figure 7.16 b)) contribute differently to these outermost valence features. The N PDOS shows that the HOMO-1 (at 6.9 eV) has only contribution from the three peripheral nitrogen atoms. On the contrary, the central N atom contributes to both HOMO and HOMO-2 features at 6.3 and 7.5 eV, to which also the three peripheral N atoms take part. Similar to TPA case, the N PDOS of the 3-peak feature has a N $2p_z$ (N lone pair) character.

In summary, the more complex m-MTDATA has a reduced ionization potential (HOMO BE energy) compared to the building block TPA, but, at the same time, it still keeps the $2p_z$ character for the outermost valence features as in TPA. Considering that the electron-donating properties of a molecule is often ascribed to the HOMO ionization potential, this result, together with its $2p_z$ character, could be of significance for the donor properties of m-MTDATA in comparison with its building block TPA.

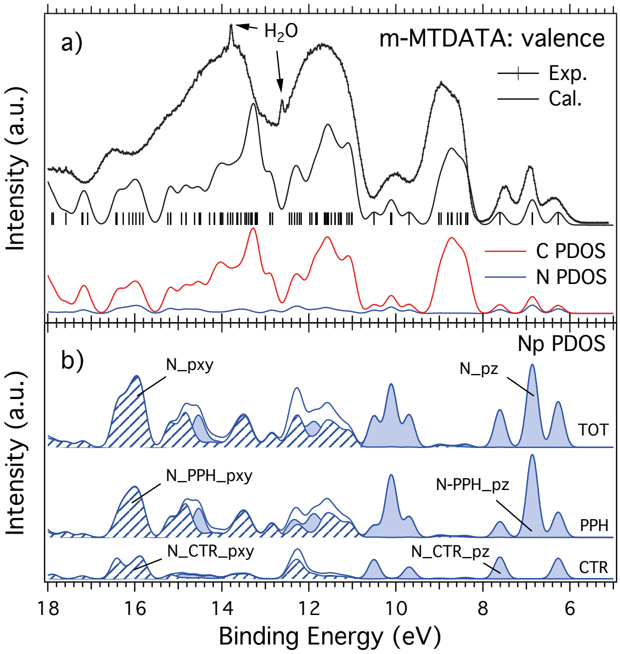

Figure 7.16. Valence photoelectron spectra of m-MTDATA in gas-phase. a): experimental spectrum obtained with a photon energy of 40 eV along with the total theoretical spectrum (black curve). The latter has been disentangled in the C (red curve) and N (light blue curve) total contributions. b): the contributions from the N peripheral (PPH) and central (CTR), as well from the N $2p_{xy}$ (pattern) and N $2p_z$ (filled) orbital are also shown. Figure adapted from Paper V.

7.3.4 Characterization of TPA and m-MTDATA molecules adsorbed on A(111) (Paper IV & V)

In Paper IV and V, thin films of TPA and m-MTDATA on an Au(111) surface are studied by PES and NEXAFS. The comparison with the gas-phase shows the modification of the electronic structure of molecules due to their interactions with the surface.

First of all, we noted that it was not possible to deposit a thick film of TPA at room temperature, indicating only a weak interaction between TPA and the gold surface. Differently, it was possible to deposit a multilayer of m-MTDATA on Au(111) at room temperature, indicated a more significant interaction between the molecules and the surface.

Molecular arrangement of TPA and m-MTDATA on Au(111) surface

The C K-edge NEXAFS spectra of both TPA and m-MTDATA 1 ML/Au(111) do not show much intensity variation depending on different measuring geometry (not shown here, refer to Paper IV & V). This is however expected since the phenyl rings of both the molecules are twisted giving the molecules a non-planar structure and then contributing at different measuring angles when the the molecules are adsorbed on the Au surface.

However, this is different for the N K-edge NEXAFS. At 1 ML coverage, both TPA and m-MTDATA absorption spectra show significant polarization dependence. In Figure 7.17 (a), the results of TPA show that, although the molecule itself is not flat, the plane defined by the (N-C_3) bonds of the TPA molecule is parallel to the Au(111) surface. This is also valid for m-MTDATA as shown in Figure 7.17 (b). Even if m-MTDADA is a quite large molecule with phenyl rings and methyl group twisted and forming a complex molecular structure, all four planes defined by the N-C bonds are parallel to the surface.

Figure 7.17 (b) also shows that the m-MTDATA molecules are arranged more disordered with increasing thickness. The similarity of this N K-edge NEXAFS of m-MTDATA/Au(111) of 3 ML with the gas-phase results, confirms that the film at such coverage is already molecular like.

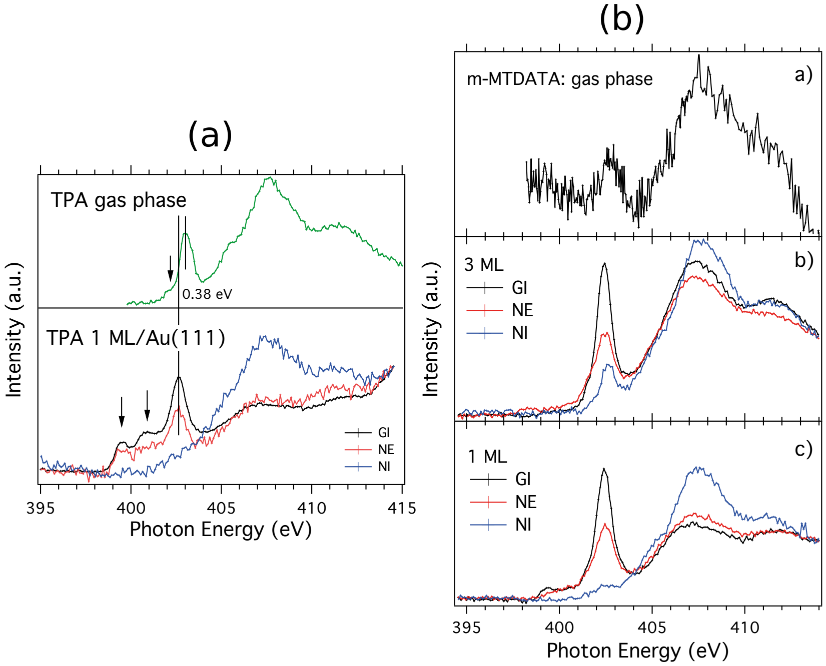

Figure 7.17. (a) N K-edge NEXAFS of 1 ML of TPA/Au(111) (bottom) compared with gas-phase measurements (top). (b) N K-edge NEXAFS of film of 1ML and 3 ML films of MTDATA /Au(111), measured at different geometries, compared to the gas-phase results (top). Figure adapted from Paper VI and V.

Strong electronic structure modification due to molecule-substrate interaction

As shown in Figure 7.17 (a), for TPA N K-edge NEXAFS, compared to gas-phase, one significant change is that we observe a pre-edge feature of quite significant intensity, starting from photon energy of 398.7 eV. This pre-edge feature is only enhanced at GI and disappears at NI, showing to have a π (out-of-plane) character whereas the gas-phase pre-edge feature of TPA, starting from higher photon energy, was assigned to transition into in-plane orbitals (see Section 7.3.1). Therefore, having a different character and covering a wider photon energy range than the gas-phase, the pre-edge feature appearing in the NEXAFS spectrum of adsorbed TPA is ascribed to the molecule-surface interaction, probably due to a charge redistribution between the molecule and the gold substrate.

Similar results are also observed for m-MTDATA at 1 ML coverage on Au(111) as seen in Figure 7.17 (c). Also, in this case, the pre-edge intensity is ascribed to the out-of-plane orbitals. With increasing thickness (3 ML) the pre-edge intensity is strongly reduced further confirming that it is due to the molecular-surface interaction.

However, for both studied systems, considering that the interaction between the molecules and the surface has been described as quite weak also by our calculations, we think that the increased interaction resulting in the pre-edge feature of the NEXAFS spectra, can be attributed to a core-hole final state effect.

7.4 Results of melamine (Paper VI)

The molecular structure of melamine is shown in Figure 7.18. As mentioned in Section 2.2.2 and in Paper VI, it has been predicted that the important photocalytic process of water splitting in H and O by cabon nitride materials would occur via the H-bonding of water to the lone pair electrons of the N of the melem unit [80, 81]. However, to date, only extensive scanning tunneling microscopy (STM) and theoretical investigations have been focused on such materials but no detailed spectroscopic characterizations have been performed. Previous STM study of melamine/Au(111) showed that the surface promotes flat adsorption and formation of honeycomb structures [82], where the nitrogen functional groups are involved in intermolecular H-bonds.

In Paper VI, by comparing gas-phase and solid-state measurements and with the help of DFT calculations, an accurate study of the effect of the H-bonds formed between amino- and pyridine-like nitrogen atoms of melamine molecules adsorbed on Au (111) is presented.

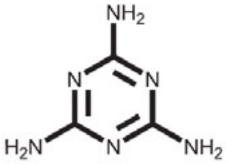

Figure 7.18. Molecular structure of melamine.

7.4.1 Evidences of H-bonding interactions in N 1s PE spectra

As shown in Figure 7.19, the most significant difference between gas-phase and solid-state N 1s spectra of melamine adsorbed on a Au(111) surface, is the reduced chemical shift between the N 1s lines of the two non-equivalent nitrogen atoms, *i.e.* the nitrogen of the amino group (-NH_2) and the nitrogen inside the triazine ring (N=C). The chemical shift is reduced from about 1.5 eV in gas-phase, to less than 1.0 eV for the adsorbed molecule, ascribed to the intermolecular H-bonding (HB) interactions on the surface.

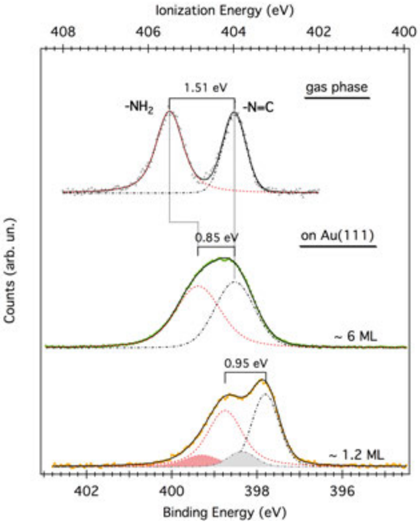

Figure 7.19. N 1s PE spectra for melamine molecule in the gas-phase and adsorbed on Au(111) at two different coverages, ∼6 ML and ∼1.2 ML. The gas-phase spectrum has been displayed *vs* top axis (Ionization Energy scale) while the solid-state spectra *vs* bottom axis (Binding Energy). Figure taken from Paper VI.

To relate the hydrogen-bonding to the chemical shift observed in the N 1s PE spectra, we used a theoretical modelling of systematic increased complexity to simulate the BEs of -NH_2 and N=C from gas-phase to H-bonded network, *i.e.* a monomer, a dimer, a trimer and a periodic hexagonal arrangement. The results are shown in Figure 7.20.

The N 1s photoelectron spectrum simulated by considering a monomer is very similar to the experimental spectrum acquired for gaseous melamine, with a chemical shift, between the two spectral features, of 1.67 eV (theory) *vs* 1.51 eV (experiment). The intermolecular interaction, which is present when the molecules are adsorbed on the Au(111) surface, have been simulated by considering an increasing number of melamine units. For a dimer, the -NH_2 component, experiencing the H-bond shifts closer to N=C, resulting, in the theoretical spectrum, in a new feature in between -NH_2 and N=C components. For a trimer, more -NH_2 components are shifted. For the hexagonal arrangement, where all -NH_2 groups are involved in H-bonding interactions with the the N=C functionalities of neighbouring melamine molecules, only two N 1s features, with reduced chemical shift compared to a monomer, are observed.

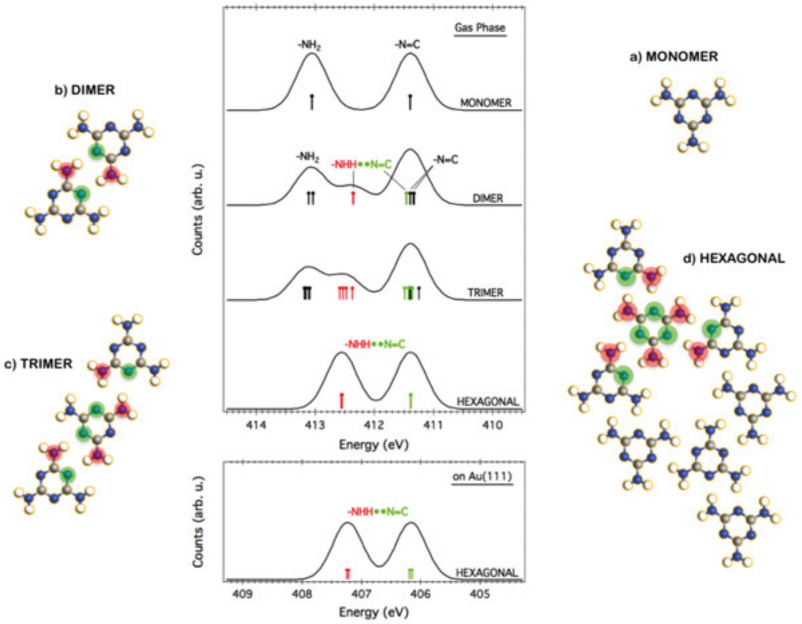

Figure 7.20. (Top graph) Simulated N 1s PE spectra for a) melamine monomer, b) dimer, c) trimer and d) a “floating” periodic hexagonal structure. (Bottom graph) Simulated PE N 1s spectrum for the hexagonal structure on top of a Au(111) surface. Figure taken from Paper VI.

Finally, the theoretical N 1s photoelectron spectrum for the hexagonal structure on top of the Au(111) surface (Figure 7.20 (bottom)) does not show any big change with respect to spectrum of the hexagonal structure of a floating layer indicating that there is no strong N-Au interaction for the adsorbed melamine molecules. However, by considering such hexagonal structure on top of the Au(111) surface, a further little shift of the spectral components is observed, resulting in a better agreement of the theoretical and experimental results.

7.4.2 Evidences of H-bonding interactions in N K-edge NEXAFS spectra

As shown in Figure 7.21, the π^* energy region of the N K-edge NEXAFS spectrum of free melamine shows three main resonances (a, b and c), whereas for the adsorbate sample, the feature b is shifted to lower photon energy, forming a shoulder aside the 1^{st} resonant peak. The shift of the peak b correlates well to the reduction of the amino N 1s binding energy, as observed in the analysis of the N 1s photoemission data for gas and adsorbed samples.

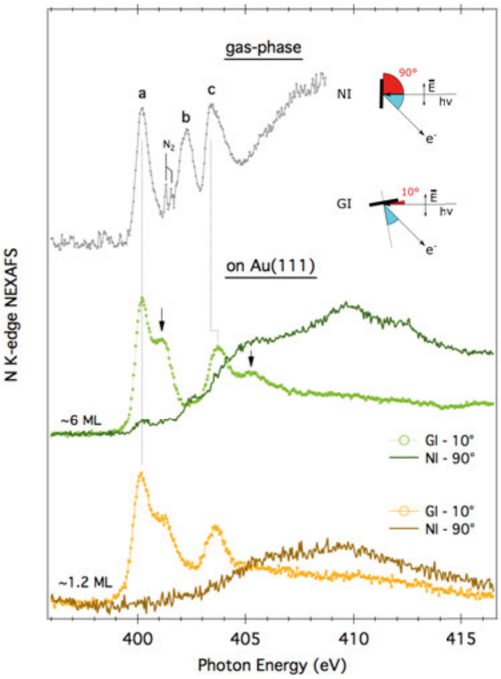

Figure 7.21. N K-edge NEXAFS spectra of melamine in the gas-phase and adsorbed on Au(111) with coverage of ∼6 ML and and ∼1.2 ML. A schematic of the measurements geometry is shown in the inset. Figure taken from Paper VI.

To model the N K-edge NEXAFS results of the adsorbed melamine, we used a model consisting of four H-bonded molecules extracted from the hexagonal structure on top of the Au(111) surface (HB model).

In Figure 7.22 the theoretical spectrum is shown to be in very good agreement with the experimental results. In the Figure, the theoretical out-of-plane and in-plane components are, respectively, compared with the GI and NI experimental spectra of the 6 ML sample (right graph of Figure 7.22). Moreover, also the triazine (N=C) and amino (-NH_3) N contributions are given separately. By comparing the in-plane and out-of-plane contributions of each N atom for the monomer and the HB model we can identify the effect of the HB interactions on the unoccupied density of states of the melamine molecule. Many peaks in the solid-state spectrum can be directly related to the same kind of transitions as identified in the gas-phase, even if at different photon energies due to the chemical shift already discuss for the photoemission data.

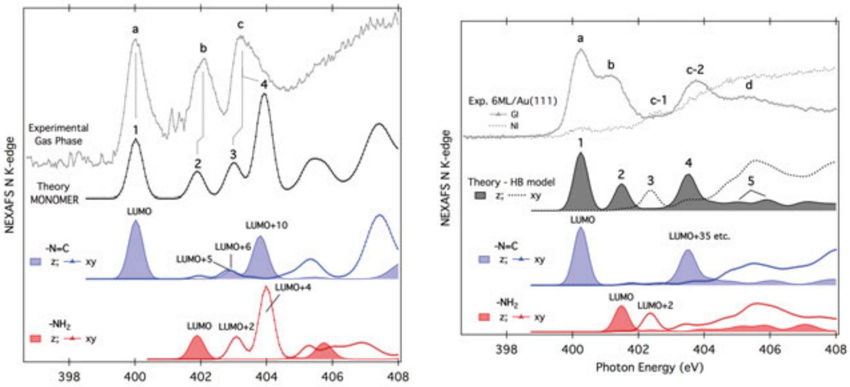

Figure 7.22. (Left Graph) Comparison between the experimental and theoretical N K-edge NEXAFS spectrum for isolated melamine. The theoretical spectrum has been decomposed in the contribution deriving from each N atom as well as from out-of-plane (z) and in-plane (xy) components. (Right graph) Comparison between the experimental N K-edge spectra taken at GI and NI for the 6 ML sample and the out-of-plane and in-plane N K-edge spectra simulated for the H-bonded (HB) model. Figure adapted from Paper VI.

8. Summary in Swedish - Svensk sammanfattning

Sedan urminnes tider har man i mänskliga samhällen tillverkat verktyg av material som finns i naturen. Sådana material är fortfarande av vital betydelse för att upprätthålla våra liv. Vi kan exempelvis nämna olje- och gasutvinning för energiändamål, och även produktion av högrent monokristallint kisel för att tillverka halvledarkomponenter. Det senare är förstås av vital betydelse för teknikbaserad industri m.m.

I framtiden måste samhällena i ökad omfattning använda sig av nya material för energiproduktion och även av nya material av betydelse för informationsteknologin (IT). Vi är alla medvetna om de nuvarande materialens begränsningar och vilka materialegenskaper som behövs för den framtida energiproduktionen och IT-utvecklingen. Exempelvis har sedan 2016 många länder beslutat sig för att avveckla eller på sikt förbjuda fordon drivna av fossila bränslen - allt i syfte att minska miljöförgiftning och för att minska hälsoriskerna. Till dessa länder hör Norge, Storbritannien, Frankrike, Nederländerna, Indien, Kina m.fl. Emellertid är utvecklingen av elektriska fordon för närvarande begränsad av batteriernas egenskaper. Kapacitet, och laddnings/urladdningshastighet och livslängd. Därför konkurrerar elektriska fordon ännu inte helt med de fossildrivna.

Å andra sidan, för att bli verkligt miljövänliga måste elektriska fordon även laddas med ren energi. Exempelvis vindenergi, hydroelektrisk energi och solenergi. Den sistnämnda har en mycket stor potential. Emellertid producerades globalt år 2015 enbart ca 1.05 % av världens elektriska energi av solceller [1]. Detta till stor del beroende begränsningar i form av otillräckliga energiomvandlingsegenskaper och för höga kostnader.

De innovationer som informationsteknologin framställt har omformat våra samhällen genom att vi kan utnyttja och processa stora datamängder och att vi omges i allt högre grad av smarta apparater. Kisel har spelat en avgörande roll i halvledarindustrin alltsedan 1940 då Russell Ohl upptäckte p-n övergången och därmed möjligheten att tillverka fotodioder. Men nu mer än ett halvsekel senare håller produktionen av kiselbaserad elektronik på att nå sina fysiska gränser: I april 2018 meddelade TSMCTM att man nu kan rapportera en hög produktion av 7nm chips. Emellertid kommer transistorer mindre än så att uppvisa tunneleffekter genom oxidlagren och därmed kommer chipsens funktion att störas. Då måste man finna nya 2D material (som exempelvis grafén). Dessa material är nu av stort intresse för forskare som hoppas kunna utveckla snabbare, mindre, billigare och mer effektiva elektroniska komponenter.

I min avhandling har jag studerat elektronstrukturen i två grupper av molekylära byggstenar som har tillämpningar för i) Energikonversionsmaterial: CoPc, TPA, DPTA och m-MTDATA och ii) 2D matrial: Bifenylen och melamin.

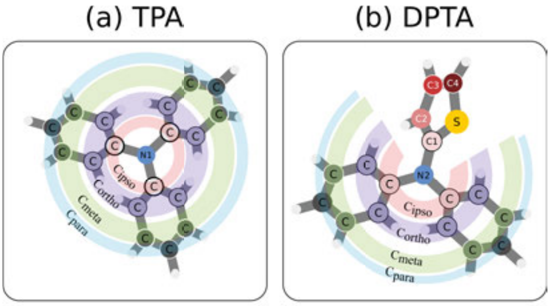

(c) m-MTDATA

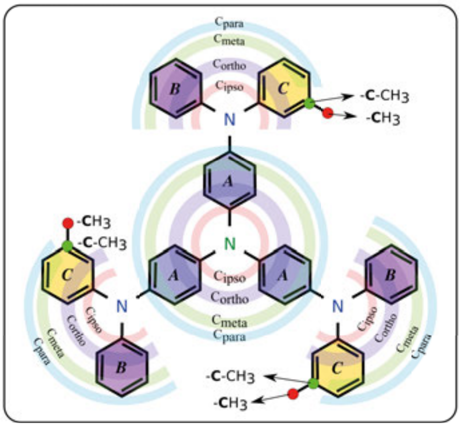

Figure 8.1. (a) TPA, (b) DPTA och (c) m-MTDATA molekyler som jag har studerat i avhandlingen.

Mina studier syftar till att på en fundamental nivå förstå byggstenarnas funktionssätt. Och att försöka på så sätt underlätta utveckling och design av nya material. Jag har utnyttjat fotoelektronspektroskopi (PES) och röntgenabsorptionsexperiment (NEXAFS). Mina experiment har utförts på synkrotronljusanläggningar. Dessa är mycket kraftfulla källor för UV- och Röntgenstrålning som möjliggör de kvalificerade undersökningar av materialen som är nödvändiga.

Jag har även studerat molekyler adsorberade på ytor, och som fria gasformiga system. De senare experimenten kan tolkas med så kallade DFT beräkningar och vi får en mycket detaljerad bild av elektronstrukturen. Denna detaljerade kunskap kan vi sedan använda när vi undersöker de mycket mer komplexa system som vi sammansätter av de molekylära byggstenarna.

Funktionella material tillverkas och studeras nu ända ner till nanoskalan. Detta görs för att maximera yta/Interface egenskaperna och för att minimera storleken av de framställda komponenterna. På denna skala uppträder materialen ofta väldigt annorlunda än vad avser bulkmaterialet. Egenskaperna domineras ofta av sina interface- och ytegenskaper. Detta har mycket långtgående effekter när dessa nanomaterial används för heterogen katalys, eller tillverkning av halvledarkomponenter, solceller och molekylära komponenter som tillverkas via självorganisation i “bottom-up" processer.

Detta är anledningen till att en annan viktig aspekt som jag tar upp i min avhandling, rör växelverkan mellan adsorberade molekyler och ytor. Jag har studerat tunna filmer av byggstensmolekyler och mer komplexa molekyler som används för energiomvandling. Jag har också studerat 2D material som framställts mycket omsorgsfullt. Genom att studera elektronstrukturen för både fria molekyler och adsorbat har vi även kunnat se hur elektronstrukturen ändras genom växelverkan med ytan.

Acknowledgements

Only when I started writing this last part of the thesis, I realized it would soon be the end of my PhD studies. Looking back to the last four years (1620 days, to be precise if counting from the start to now), there were so many exciting things happened. I still remember that I joined my 1^{st} beamtime at gas-phase beamline at ELETTRA only 2 weeks after I landed in Sweden. Since then I took a lot of hardworking but fruitful beamtimes. I think I will for sure miss this PhD student period, for which I should first of all thank my supervisors: Carla, Nils, Svante and Valeria.

Thank you, Carla, for all the support and caring during my whole PhD period. Actually, I should count from the very first MAX-lab beamtime I had with you during my master time, where I knew you would be the best supervisor if I got chance to have. It turned out I was totally right. You are always positive and encouraging, which has made me progress. Although you have many duties, you always put me on the 1^{st} place. My research will never be worked out without your ideas and guidance. There are so many more that I want to learn from you.

Thank you, Nils and Svante, for involving me into the ArTOF project. The half-year experience working fully at BESSY II synchrotron helping building up CoESCA and commissioning the LowDosePES endstations was very precious. It was a great chance to be working as a beamline scientist instead of a user. And it is also very exciting to build an endstation from scratch. I also got the chance to working closely with Ruslan, Erika, Torsten, Ieva and Yasmine, making the possibility to extend my research field with ARPES and pump-probe experiments. Also, I would like to thank you for the individual course started after my licentiate. The discussions always gave me new insights into physics and extending the limit of my knowledge. I believe there were more things you passed on from the course than what I can learn from the books.

Thank you, Valeria, for being my supervisor. You became my supervisor just after my licentiate, but your help was always there since you arrived in Uppsala. My real surface investigations started by making the new evaporators with you. By the hardworking from you and Cesare, I got to "own" the ELEPHANT lab for a period, making me to feel like a king for the first time, which is a completely different feeling than synchrotron experiments. And I am grateful that you pushed me for the UV-Vis and fluorescence experiments, which I would hardly have linked to our projects. I am also thankful for your teaching on running the experiments, manuscript writing, chemistry, and much more.

Through my supervisors I also got the chance to know all of the great collaborators, experimentalists and theoreticians, as listed (but not limited) as co-authors in the papers. I would like to thank all of you and your great help in my research. Among them, my special thanks to Cesare, Ambra, Ieva, Roberta, Fredrik, Ruslan, Erika, Monica and Marcello, for the hardworking times we had at synchrotrons and labs, and Iulia, Johann, Barbara for the reliable and strong support from the theoretical side. Also, I would like to thank Nadine and Petra for the very warm hosting in Paris and Groningen, respectively. I can hardly imagine a thesis without any of you.

I would like to thank all of my colleges of Molecular and Condensed Matter Physics division, especially to Somnath, Minjie, Dibya, and Yevgen, with whom I shared the office for more than four years. I would also like to thank all of my friends I met in Uppsala and conferences, especially Dou and Wenxing, being my 1^{st} and 2^{nd} met Chinese friends in Uppsala.

I also would like to express my gratitude to the Vice-Chancellor of Uppsala University for the financial support for my PhD position through the U4 collaboration.

Finally but most importantly, I would like to give my special thanks to my family.

References

[1] "Bp statistical review of world energy," June 2016.

[2] J. E. Hutchison, T. A. Postlethwaite, and R. W. Murray, "Molecular Films of Thiol-Derivatized Tetraphenylporphyrins on Gold: Film Formation and Electrocatalytic Dioxygen Reduction," *Langmuir*, vol. 9, pp. 3277–3283, 1993.

[3] S. Berner, H. Lidbaum, G. Ledung, J. Åhlund, K. Nilson, J. Schiessling, U. Gelius, J.-E. Bäckvall, C. Puglia, and S. Oscarsson, "Electronic and structural studies of immobilized thiol-derivatized cobalt porphyrins on gold surfaces," *Applied Surface Science*, vol. 253, pp. 7540–7548, Jul. 2007.

[4] S. Berner, S. Biela, G. Ledung, A. Gogoll, J. Backvall, C. Puglia, and S. Oscarsson, "Activity boost of a biomimetic oxidation catalyst by immobilization onto a gold surface," *Journal of Catalysis*, vol. 244, pp. 86–91, Nov. 2006.

[5] S. Boudet, "Auto-assemblage moléculaire de bisphtalocyanines de lutétium: organisation, structure et propriétés optiques," 2011.

[6] M. Bouvet, A. Leroy, J. Simon, F. Tournilhac, G. Guillaud, P. Lessnick, A. Maillard, S. Spirkovitch, M. Debliquy, A. De Haan, and A. Decroly, "Detection and titration of ozone using metallophthalocyanine based field effect transistors," *Sensors and Actuators, B: Chemical*, vol. 72, no. 1, pp. 86–93, 2001.

[7] J. Bartolomé, F. Luis, and J. F. Fernández, eds., *Molecular Magnets*. NanoScience and Technology, Berlin, Heidelberg: Springer Berlin Heidelberg, 2014.

[8] S. Sanvito, "Molecular spintronics," *Chemical Society Reviews*, vol. 40, no. 6, p. 3336, 2011.

[9] P. Agarwala and D. Kabra, "A review on triphenylamine (TPA) based organic hole transport materials (HTMs) for dye sensitized solar cells (DSSCs) and perovskite solar cells (PSCs): evolution and molecular engineering," *J. Mater. Chem. A*, vol. 5, no. 4, pp. 1348–1373, 2017.

[10] V. Merz and W. Weith, "Vermischte Mittheilungen," *Berichte der deutschen chemischen Gesellschaft*, vol. 6, pp. 1511–1520, Jul. 1873.

[11] J. Wang, K. Liu, L. Ma, and X. Zhan, "Triarylamine: Versatile Platform for Organic, Dye-Sensitized, and Perovskite Solar Cells," *Chemical Reviews*, vol. 116, no. 23, pp. 14675–14725, 2016.

[12] K. Zhang, L. Wang, Y. Liang, S. Yang, J. Liang, F. Cheng, and J. Chen, "A thermally and electrochemically stable organic hole-transporting material with an adamantane central core and triarylamine moieties," *Synthetic Metals*, vol. 162, pp. 490–496, Apr. 2012.

[13] H. Choi, S. Paek, N. Lim, Y. H. Lee, M. K. Nazeeruddin, and J. Ko, "Efficient Perovskite Solar Cells with 13.63 % Efficiency Based on Planar Triphenylamine Hole Conductors," *Chemistry - A European Journal*, vol. 20, pp. 10894–10899, Aug. 2014.

[14] Z. Ning and H. Tian, "Triarylamine: a promising core unit for efficient photovoltaic materials," *Chemical Communications*, no. 37, p. 5483, 2009.

[15] A. Mahmood, "Triphenylamine based dyes for dye sensitized solar cells: A review," *Solar Energy*, vol. 123, pp. 127–144, Jan. 2016.

[16] F. Zhang, X. Zhao, C. Yi, D. Bi, X. Bi, P. Wei, X. Liu, S. Wang, X. Li, S. M. Zakeeruddin, and M. Grätzel, "Dopant-free star-shaped hole-transport materials for efficient and stable perovskite solar cells," *Dyes and Pigments*, vol. 136, pp. 273–277, 2017.

[17] T. Kitamura, M. Ikeda, K. Shigaki, T. Inoue, N. A. Anderson, X. Ai, T. Lian, and S. Yanagida, "Phenyl-Conjugated Oligoene Sensitizers for TiO2 Solar Cells," *Chemistry of Materials*, vol. 16, no. 9, pp. 1806–1812, 2004.

[18] Y. Cao, Y. Saygili, A. Ummadisingu, J. Teuscher, J. Luo, N. Pellet, F. Giordano, S. M. Zakeeruddin, J. E. Moser, M. Freitag, A. Hagfeldt, and M. Grätzel, "11% efficiency solid-state dye-sensitized solar cells with copper(II/I) hole transport materials," *Nature Communications*, vol. 8, p. 15390, Jun. 2017.

[19] A. Y. Chang, Y.-h. Chen, H.-W. Lin, L.-y. Lin, K.-t. Wong, and R. D. Schaller, "Charge Carrier Dynamics of Vapor-Deposited Small-Molecule/Fullerene Organic Solar Cells," *Journal of the American Chemical Society*, vol. 135, pp. 8790–8793, Jun. 2013.

[20] L. Y. Lin, Y. H. Chen, Z. Y. Huang, H. W. Lin, S. H. Chou, F. Lin, C. W. Chen, Y. H. Liu, and K. T. Wong, "A low-energy-gap organic dye for high-performance small-molecule organic solar cells," *Journal of the American Chemical Society*, vol. 133, no. 40, pp. 15822–15825, 2011.

[21] Y. H. Chen, L. Y. Lin, C. W. Lu, F. Lin, Z. Y. Huang, H. W. Lin, P. H. Wang, Y. H. Liu, K. T. Wong, J. Wen, D. J. Miller, and S. B. Darling, "Vacuum-deposited small-molecule organic solar cells with high power conversion efficiencies by judicious molecular design and device optimization," *Journal of the American Chemical Society*, vol. 134, no. 33, pp. 13616–13623, 2012.

[22] Y. Shirota, T. Kobata, and N. Noma, "Starburst molecules for amorphous molecular materials. 4,4',4"-Tris(N,N-diphenylamino)triphenylamine and 4,4',4"-tris[N-(3-methylphenyl)-N-phenylamino]triphenylamine.," 1989.

[23] W. C. Lothrop, "Biphenylene," *Journal of the American Chemical Society*, vol. 63, pp. 1187–1191, May 1941.

[24] J. Waser and C.-S. Lu, "The Crystal Structure of Biphenylene," *Journal of the American Chemical Society*, vol. 66, pp. 2035–2042, Dec. 1944.

[25] M. De La Pierre, P. Karamanis, J. Baima, R. Orlando, C. Pouchan, and R. Dovesi, "Ab Initio Periodic Simulation of the Spectroscopic and Optical Properties of Novel Porous Graphene Phases," *The Journal of Physical Chemistry C*, vol. 117, pp. 2222–2229, Feb. 2013.

[26] A. T. Balaban, C. C. Rentea, and E. Ciupitu, "Chemical graphs. VI. Estimation of the relative stability of several planar and tridimensional lattices for elementary carbon," *Revue Roumaine de Chimie*, vol. 13, pp. 231–247, 1968.

[27] J. Lüder, C. Puglia, H. Ottosson, O. Eriksson, B. Sanyal, and B. Brena, "Many-body effects and excitonic features in 2D biphenylene carbon," *Journal of Chemical Physics*, vol. 144, no. 2, 2016.

[28] G. Brunetto, P. A. S. Autreto, L. D. Machado, B. I. Santos, R. P. B. dos Santos, and D. S. Galvão, “Nonzero Gap Two-Dimensional Carbon Allotrope from Porous Graphene,” *The Journal of Physical Chemistry C*, vol. 116, pp. 12810–12813, Jun. 2012.

[29] J. Björk, F. Hanke, and S. Stafström, “Mechanisms of Halogen-Based Covalent Self-Assembly on Metal Surfaces,” *Journal of the American Chemical Society*, vol. 135, pp. 5768–5775, Apr. 2013.

[30] X. Wang, K. Maeda, A. Thomas, K. Takanabe, G. Xin, J. M. Carlsson, K. Domen, and M. Antonietti, “A metal-free polymeric photocatalyst for hydrogen production from water under visible light,” *Nature Materials*, vol. 8, no. 1, pp. 76–80, 2008.

[31] B. Streetman and S. Banerjee, *Solid State Electronic Devices*. Prentice Hall, 1999.

[32] Y. Wang, X. Wang, and M. Antonietti, “Polymeric graphitic carbon nitride as a heterogeneous organocatalyst: From photochemistry to multipurpose catalysis to sustainable chemistry,” *Angewandte Chemie - International Edition*, vol. 51, no. 1, pp. 68–89, 2012.

[33] J. Wirth, R. Neumann, M. Antonietti, and P. Saalfrank, “Adsorption and photocatalytic splitting of water on graphitic carbon nitride: a combined first principles and semiempirical study,” *Phys. Chem. Chem. Phys.*, vol. 16, no. 30, pp. 15917–15926, 2014.

[34] H.-Z. Wu, L.-M. Liu, and S.-J. Zhao, “The effect of water on the structural, electronic and photocatalytic properties of graphitic carbon nitride,” *Physical Chemistry Chemical Physics*, vol. 16, no. 7, p. 3299, 2014.

[35] J. Ehrmaier, T. N. Karsili, A. L. Sobolewski, and W. Domcke, “Mechanism of Photocatalytic Water Splitting with Graphitic Carbon Nitride: Photochemistry of the Heptazine-Water Complex,” *Journal of Physical Chemistry A*, vol. 121, no. 25, pp. 4754–4764, 2017.

[36] H. Hertz, “Uiber den Einfluß des ultravioletten Lichtes auf die elektrische Entladung,” *Ann. Physik*, vol. 33, p. 983, 1887.

[37] A. Einstein, “Uiber einen die Erzeugung und Verwandlung des Lichtes betreffenden heuristischen Gesichtspunkt,” *Ann. Physik*, vol. 17, p. 132, 1905.

[38] S. Hüfner, *Photoelectron Spectroscopy Principles and Applications*. Springer, 2003.

[39] J. Yeh and I. Lindau, “Atomic subshell photoionization cross sections and asymmetry parameters: $1 \leq Z \leq 103$,” *Atomic Data and Nuclear Data Tables*, vol. 32, pp. 1–155, Jan. 1985.

[40] I. Bidermane, J. Lüder, R. Totani, C. Grazioli, M. de Simone, M. Coreno, A. Kivimäki, J. Åhlund, L. Lozzi, B. Brena, and C. Puglia, “Characterization of gas phase iron phthalocyanine with X-ray photoelectron and absorption spectroscopies,” *physica status solidi (b)*, vol. 252, pp. 1259–1265, Jun. 2015.

[41] I. Bidermane, I. Brumboiu, R. Totani, C. Grazioli, M. Shariati-Nilsson, H. Herper, O. Eriksson, B. Sanyal, B. Ressel, M. de Simone, L. Lozzi, B. Brena, and C. Puglia, “Atomic contributions to the valence band photoelectron spectra of metal-free, iron and manganese phthalocyanines,” *Journal of Electron Spectroscopy and Related Phenomena*, vol. 205, pp. 92–97, Nov. 2015.

[42] B. Brena, C. Puglia, M. de Simone, M. Coreno, K. Tarafder, V. Feyer, R. Banerjee, E. Gothelid, B. Sanyal, P. M. Oppeneer, and O. Eriksson, “Valence-band electronic structure of iron phthalocyanine: An experimental and theoretical photoelectron spectroscopy study,” *The Journal of Chemical Physics*, vol. 134, no. 7, p. 74312, 2011.

[43] K. Siegbahn, C. Nording, A. Fahlman, R. Nordberg, K. Hamrin, J. Hedman, G. Johansson, T. Bergmark, S.-E. Karlsson, I. Lindgren, and B. Lindberg, *ESCA; atomic, molecular and solid state structure studied by means of electron spectroscopy*. Almqvist & Wiksells, Uppsala, 1967.

[44] K. Siegbahn, C. Nordling, G. Johansson, J. Hedman, P. Hedén, K. Hamrin, U. Gelius, T. Bergmark, L. Werme, R. Manne, and Y. Baer, *ESCA Applied to Free Molecules*. Amsterdam: North-Holland Pub. Co., 1969.

[45] N. Mårtensson, P. Baltzer, P. Brühwiler, J.-O. Forsell, A. Nilsson, A. Stenborg, and B. Wannberg, “A very high resolution electron spectrometer,” *Journal of Electron Spectroscopy and Related Phenomena*, vol. 70, pp. 117–128, dec 1994.

[46] R. Ovsyannikov, P. Karlsson, M. Lundqvist, C. Lupulescu, W. Eberhardt, A. Föhlisch, S. Svensson, and N. Mårtensson, “Principles and operation of a new type of electron spectrometer - ArTOF,” *Journal of Electron Spectroscopy and Related Phenomena*, vol. 191, pp. 92–103, Dec. 2013.

[47] E. Giangrisostomi, R. Ovsyannikov, F. Sorgenfrei, T. Zhang, A. Lindblad, Y. Sassa, U. B. Cappel, T. Leitner, R. Mitzner, S. Svensson, N. Mårtensson, and A. Föhlisch, “Low Dose Photoelectron Spectroscopy at BESSY II: Electronic structure of matter in its native state,” *Journal of Electron Spectroscopy and Related Phenomena*, vol. 224, pp. 68–78, Apr. 2018.

[48] M. Klasson, A. Berndtsson, J. Hedman, R. Nilsson, R. Nyholm, and C. Nordling, “Electron escape depth in silicon,” *Journal of Electron Spectroscopy and Related Phenomena*, vol. 3, no. 6, pp. 427–434, 1974.

[49] O. Travnikova, K. J. Borve, M. Patanen, J. Söderström, C. Miron, L. J. Sæthre, N. Mårtensson, and S. Svensson, “The ESCA molecule - Historical remarks and new results,” *Journal of Electron Spectroscopy and Related Phenomena*, vol. 185, no. 8-9, pp. 191–197, 2012.

[50] T. Karlsen, K. J. Børve, L. J. Sæthre, K. Wiesner, M. Bässler, and S. Svensson, “Toward the Spectrum of Free Polyethylene: Linear Alkanes Studied by Carbon 1s Photoelectron Spectroscopy and Theory,” *Journal of the American Chemical Society*, vol. 124, pp. 7866–7873, Jul. 2002.

[51] C. Enkvist, S. Lunell, B. Sjögren, S. Svensson, P. A. Brühwiler, A. Nilsson, A. J. Maxwell, and N. Mårtensson, “C_{1s} shakeup spectrum of C_{60}: Global charge-transfer satellites and their relation to the x-ray threshold singularities in macroscopic systems,” *Physical Review B*, vol. 48, pp. 14629–14637, Nov. 1993.

[52] S. Doniach and M. Sunjic, “Many-electron singularity in X-ray photoemission and X-ray line spectra from metals,” *Journal of Physics C: Solid State Physics*, vol. 3, no. 2, pp. 285–291, 1970.

[53] W. Eberhardt, A. Bradshaw, H. Freund, F. Hoffmann, H. Kuhlenbeck, N. Mårtensson, D. Menzel, A. Nilsson, G. Williams, D. Woodruff, *et al.*, *Applications of Synchrotron Radiation: High-Resolution Studies of Molecules and Molecular Adsorbates on Surfaces*. Springer Series in Surface Sciences,

Springer Berlin Heidelberg, 1994.

[54] G. Hähner, “Near edge X-ray absorption fine structure spectroscopy as a tool to probe electronic and structural properties of thin organic films and liquids,” *Chem. Soc. Rev.*, vol. 35, no. 12, pp. 1244–1255, 2006.

[55] J. Stöhr, *NEXAFS Spectroscopy*. Springer-Verlag, 1992.

[56] S. Elke and C. J. Carlos, *Molecular Electronics: An Introduction To Theory And Experiment*. World Scientific Series In Nanoscience And Nanotechnology, World Scientific Publishing Company, 2010.

[57] A. D. Becke, “Density-functional thermochemistry III The role of exact exchange,” *The Journal of Chemical Physics*, vol. 98, no. 7, pp. 5648–5652, 1993.

[58] M. J. Frisch, G. W. Trucks, H. B. Schlegel, G. E. Scuseria, M. A. Robb, J. R. Cheeseman, G. Scalmani, V. Barone, G. A. Petersson, H. Nakatsuji, X. Li, M. Caricato, A. V. Marenich, J. Bloino, B. G. Janesko, R. Gomperts, B. Mennucci, H. P. Hratchian, J. V. Ortiz, A. F. Izmaylov, J. L. Sonnenberg, D. Williams-Young, F. Ding, F. Lipparini, F. Egidi, J. Goings, B. Peng, A. Petrone, T. Henderson, D. Ranasinghe, V. G. Zakrzewski, J. Gao, N. Rega, G. Zheng, W. Liang, M. Hada, M. Ehara, K. Toyota, R. Fukuda, J. Hasegawa, M. Ishida, T. Nakajima, Y. Honda, O. Kitao, H. Nakai, T. Vreven, K. Throssell, J. A. Montgomery Jr., J. E. Peralta, F. Ogliaro, M. J. Bearpark, J. J. Heyd, E. N. Brothers, K. N. Kudin, V. N. Staroverov, T. A. Keith, R. Kobayashi, J. Normand, K. Raghavachari, A. P. Rendell, J. C. Burant, S. S. Iyengar, J. Tomasi, M. Cossi, J. M. Millam, M. Klene, C. Adamo, R. Cammi, J. W. Ochterski, R. L. Martin, K. Morokuma, O. Farkas, J. B. Foresman, and D. J. Fox, “Gaussian 16 Revision A.03,” 2016.

[59] V. A. Rassolov, J. A. Pople, M. A. Ratner, and T. L. Windus, “6-31G* basis set for atoms K through Zn,” *The Journal of Chemical Physics*, vol. 109, pp. 1223–1229, Jul. 1998.

[60] G. Schaftenaar, E. Vlieg, and G. Vriend, “Molden 2.0: quantum chemistry meets proteins,” *Journal of Computer-Aided Molecular Design*, vol. 31, pp. 789–800, Sep 2017.

[61] O. Plekan, V. Feyer, R. Richter, M. Coreno, M. de Simone, and K. C. Prince, “Photofragmentation of guanine, cytosine, leucine and methionine,” *Chemical Physics*, vol. 334, no. 1-3, pp. 53–63, 2007.

[62] R. Nyholm, J. N. Andersen, U. Johansson, B. N. Jensen, and I. Lindau, “Beamline I311 at MAX-LAB: A VUV/soft X-ray undulator beamline for high resolution electron spectroscopy,” *Nuclear Instruments and Methods in Physics Research, Section A: Accelerators, Spectrometers, Detectors and Associated Equipment*, vol. 467-468, pp. 520–524, 2001.

[63] D. F. Förster, B. Lindenau, M. Leyendecker, F. Janssen, C. Winkler, F. O. Schumann, J. Kirschner, K. Holldack, and A. Föhlisch, “Phase-locked MHz pulse selector for x-ray sources,” *Optics Letters*, vol. 40, no. 10, p. 2265, 2015.

[64] J. Berkowitz, “Photoelectron spectroscopy of phthalocyanine vapors,” *The Journal of Chemical Physics*, vol. 70, no. 6, p. 2819, 1979.

[65] P. Gargiani, G. Rossi, R. Biagi, V. Corradini, M. Pedio, S. Fortuna, A. Calzolari, S. Fabris, J. C. Cezar, N. B. Brookes, and M. G. Betti, “Spin and orbital configuration of metal phthalocyanine chains assembled on the Au(110)

surface," *Physical Review B - Condensed Matter and Materials Physics*, vol. 87, no. 16, pp. 1–11, 2013.

[66] T. Kroll, V. Y. Aristov, O. V. Molodtsova, Y. A. Ossipyan, D. V. Vyalikh, B. Büchner, and M. Knupfer, "Spin and Orbital Ground State of Co in Cobalt Phthalocyanine," *The Journal of Physical Chemistry A*, vol. 113, no. 31, pp. 8917–8922, 2009.

[67] S. Stepanow, P. S. Miedema, A. Mugarza, G. Ceballos, P. Moras, J. C. Cezar, C. Carbone, F. M. F. De Groot, and P. Gambardella, "Mixed-valence behavior and strong correlation effects of metal phthalocyanines adsorbed on metals," *Physical Review B - Condensed Matter and Materials Physics*, vol. 83, no. 22, pp. 4–7, 2011.

[68] J. Zhou, L. Zhang, Z. Hu, C. Kuo, H. Liu, X. Lin, Y. Wang, T.-W. Pi, J. Wang, and S. Zhang, "The significant role of covalency in determining the ground state of cobalt phthalocyanines molecule," *AIP Advances*, vol. 6, p. 035306, Mar. 2016.

[69] M. S. Liao and S. Scheiner, "Electronic structure and bonding in metal phthalocyanines, metal=Fe, Co, Ni, Cu, Zn, Mg," *Journal of Chemical Physics*, vol. 114, no. 22, pp. 9780–9791, 2001.

[70] F. Petraki, H. Peisert, F. Latteyer, U. Aygül, A. Vollmer, and T. Chassé, "Impact of the 3d Electronic States of Cobalt and Manganese Phthalocyanines on the Electronic Structure at the Interface to Ag(111)," *The Journal of Physical Chemistry C*, vol. 115, pp. 21334–21340, Nov. 2011.

[71] M. Grobosch, V. Y. Aristov, O. V. Molodtsova, C. Schmidt, B. P. Doyle, S. Nannarone, and M. Knupfer, "Engineering of the energy level alignment at organic semiconductor interfaces by intramolecular degrees of freedom: Transition metal phthalocyanines," *Journal of Physical Chemistry C*, vol. 113, no. 30, pp. 13219–13222, 2009.

[72] S. Bhattacharjee, B. Brena, R. Banerjee, H. Wende, O. Eriksson, and B. Sanyal, "Electronic structure of Co-phthalocyanine calculated by GGA+U and hybrid functional methods," *Chemical Physics*, vol. 377, no. 1-3, pp. 96–99, 2010.

[73] M. G. Betti, P. Gargiani, R. Frisenda, R. Biagi, A. Cossaro, A. Verdini, L. Floreano, and C. Mariani, "Localized and dispersive electronic states at ordered FePc and CoPc chains on Au(110)," *Journal of Physical Chemistry C*, vol. 114, no. 49, pp. 21638–21644, 2010.

[74] F. Petraki, H. Peisert, I. Biswas, and T. Chassé, "Electronic structure of Co-phthalocyanine on gold investigated by photoexcited electron spectroscopies: Indication of Co ion-metal interaction," *Journal of Physical Chemistry C*, vol. 114, no. 41, pp. 17638–17643, 2010.

[75] C. Enkvist, S. Lunell, B. Sjögren, P. A. Brühwiler, and S. Svensson, "The C1s shakeup spectra of Buckminsterfullerene, acenaphthylene, and naphthalene, studied by high resolution x-ray photoelectron spectroscopy and quantum mechanical calculations," *The Journal of Chemical Physics*, vol. 103, no. 15, p. 6333, 1995.

[76] M. P. Keane, A. Naves De Brito, N. Correia, S. Svensson, L. Karlsson, B. Wannberg, U. Gelius, S. Lunell, W. R. Salaneck, M. Lögdlund, D. B. Swanson, and A. G. MacDiarmid, "Valence and core-shakeup photoelectron spectra of solid polyacetylene and related free model molecules," *Physical*

Review B, vol. 45, no. 12, pp. 6390–6399, 1992.

[77] C. Enkvist, S. Lunell, and S. Svensson, “Experimental and theoretical study of the Cls shakeup spectra from biphenyl and p-terphenyl,” *Chemical Physics*, vol. 214, pp. 123–130, Jan. 1997.

[78] J. Lüder, M. De Simone, R. Totani, M. Coreno, C. Grazioli, B. Sanyal, O. Eriksson, B. Brena, and C. Puglia, “The electronic characterization of biphenylene-Experimental and theoretical insights from core and valence level spectroscopy,” *Journal of Chemical Physics*, vol. 142, no. 7, 2015.

[79] H. M. Senn, D. V. Deubel, P. E. Blöchl, A. Togni, and G. Frenking, “Phosphane lone-pair energies as a measure of ligand donor strengths and relation to activation energies,” *Journal of Molecular Structure: THEOCHEM*, vol. 506, pp. 233–242, 2000.

[80] B. V. Lotsch, M. Döblinger, J. Sehnert, L. Seyfarth, J. Senker, O. Oeckler, and W. Schnick, “Unmasking melon by a complementary approach employing electron diffraction, solid-state NMR spectroscopy, and theoretical calculations - Structural characterization of a carbon nitride polymer,” *Chemistry - A European Journal*, vol. 13, no. 17, pp. 4969–4980, 2007.

[81] M. Döblinger, B. V. Lotsch, J. Wack, J. Thun, J. Senker, and W. Schnick, “Structure elucidation of polyheptazine imide by electron diffraction-a templated 2D carbon nitride network,” *Chemical Communications*, no. 12, p. 1541, 2009.

[82] F. Silly, A. Q. Shaw, M. R. Castell, G. A. D. Briggs, M. Mura, N. Martsinovich, and L. Kantorovich, “Melamine Structures on the Au (111) Surface,” *Journal of Physical Chemistry C*, vol. 112, no. 30, pp. 11476–11480, 2008.

Acta Universitatis Upsaliensis

Digital Comprehensive Summaries of Uppsala Dissertations from the Faculty of Science and Technology 1693

Editor: The Dean of the Faculty of Science and Technology

Distribution: publications.uu.se
urn:nbn:se:uu:diva-354766

ACTA
UNIVERSITATIS
UPSALIENSIS
UPPSALA
2018